Turbulence Characteristics

of

Counter Flowing Free Jets

Seyed Fazlolah Saghravani

A Thesis

in

The Department

of

Building, Civil, and Environmental Engineering

Presented in Partial Fulfillment of the Requirements
for the Degree of Doctor of Philosophy at
Concordia University

Montreal, Quebec, Canada

September 2002

Abstract

Turbulence Characteristics of Counter Flowing Free Jets

Seyed Fazlolah Saghravani, Ph.D.

Concordia University, 2002

Jets are used in several engineering applications including dilution and mixing. The counter flowing free jet was investigated to find the penetration length and geometry of the expanded jet. The turbulence characteristics of the counter flowing free jets have been determined.

Several jet nozzles with different diameters were used to form the jet located at the center of a closed conduit that had a square cross section. The results show that the penetration length varies linearly with the ratio of the jet velocity to the main flow velocity that is denoted by R.

Axial and radial velocity components were measured simultaneously using a 2-D laser velocity probe. The raw data was processed and several characteristics of the counter flowing free jets such as the decay rate of the jet and the turbulence behavior of the jet along the jet axis are reported.

The turbulent kinetic energy of the counter flowing free jets was studied. Several profiles were chosen and the turbulent kinetic energy was balanced along the

radial direction of the jet. The terms including pressure component were used as the closure, since the pressure was not measured.

Another major part of the study was to find the wake mixing characteristics of the counter flowing free jets. Several tests with different R values were performed and for each test, the concentration of the tracer injected by the jet to the main flow was measured at several points at different cross sections in the near wake region of the jet. The results show that the mixing between the tracer and the main flow improves with larger jet diameter and bigger velocity ratios.

A small part of the study was devoted to numerical test using the software code, Phoenics. Three sets of tests using different turbulence models were performed and the results were compared with the measurement. In comparison, for the case of turbulent jets in counter flow, the k–ε model gave a better result than k-ω and mixing length models.

The results can be applied directly to the control of stream pollution, as the counter flowing free jet is a very effective device to dilute the effluents injected in a stream.

Acknowledgement

I would like to express my sincere gratitude to my supervisor Dr. Amruthur S. Ramamurthy for his encouragement, knowledgeable suggestions, and invaluable support in the course of my research.

Iranian Ministry of Science, Research, and Technology sponsored me during my Ph.D. program in Canada. Here, I would like to acknowledge their helps and support.

Also, I would like to thank Mr. L. Vo, Mr. A. Checiwski, and Mr. D. Roy for their help in conducting the laboratory work. In addition, I profited Mr. R. Parisella's experience and knowledge during the tests in the Environmental Lab. I appreciate the precision and all the effort that the machine shop staff put towards the construction of the test equipment.

Table of contents

List of Figures

List of tables

Chapter 1

Introduction

1.1 General remarks

1.1.1 Jet flows

Jets traditionally have served as efficient devices to disperse effluents in a receiving body of water. More recently, jets in counter flow have been the subject of study to understand their flow characteristics. Jets are also used in afterburners or turbojet engines as stabilizers (Lam 1997). In a turbojet engine, where the velocity is very high, the injected fuel should be completely mixed with the incoming air. Counter flowing fuel jet can provide such a mixing but injecting it in any other direction has a risk of incomplete reaction. This application is linked to the counter jet's ability to spread very fast and form a homogenous mixture of fuel and air. This suggests that they may also be used to obtain rapid dilution of the industrial and municipal effluent discharged to a stream. This direct

application in environmental engineering encouraged researchers to study the counter flowing jet flow characteristics. The applications include dilution of wastewater into a river or a river carrying effluent into an ocean. In the latter case, the surging ocean flow towards the land serves as the main flow. The use of a counter jet to dispose a disinfectant such as chlorine to water in a conduit carrying filtered water has been stated as an application for counter flowing jets. The importance of counter flowing jet flows in fluid mechanics in general, and in environmental engineering in particular, is discussed in the following sections. The following section deals with the general characteristics of counter flowing free jets. The last section of this chapter is allocated to describe the organization of the thesis.

1.1.2 Counter flowing jet flow in fluid mechanics

The turbulence mixing characteristics of counter flowing jet is quite complex and as such the information about its flow characteristics is very limited. Barring the study of mean flow characteristics of the counter flowing jet, there is little information related to the turbulence characteristics of counter flowing jets. The jet turbulence characteristics influence the jet penetration length, the geometry of the return flow zone, for both two dimensional and axisymmetric jet flow systems.

The only attempt to get the turbulence characteristics of counter flowing free jet is related to the limited study of Lam (1991) who obtained the turbulent fluctuation

data in the axial direction for a counter flowing jet set in an open channel. As the jet study was in an open channel, understandably, the jet velocity relative to the main flow was very moderate.

In the present study, the turbulent characteristics of counter flowing free jets were studied in a closed conduit. Besides mean flow characteristics, the normal and the shear stresses of turbulence were also measured. The latter enables the determination of the scales of velocity and turbulence of the counter flowing free jet that are related to the mixing characteristics in the effluent dispersion process.

1.1.3 Counter flowing jet flow in chemical and environmental engineering

One of the most important aspects of the counter jet flow is the large scale mixing which it provides to ensure efficient dilution of the effluent in a very short reach. This property renders the counter flowing free jet to be an ideal device in many waste disposal sites. The counter flowing jet needs only a short mixing distance and this qualifies it to be very suitable as a mixing device to dispose the industrial or municipal effluent in a pipe or an open channel carrying water. There are also some limitations to their use. For instance, from a practical point of view, counter flowing jets, unlike cross-flowing jets, are not ideally suited for use as an effluent disposing unit in rivers because it needs additional facilities to locate the wastewater injection devices in the middle of a receiving stream. It also interferes with navigation facilities. If these devices are located close to the banks (cross

jet) the possibility of scouring and erosion could also be reduced significantly, unlike jet on the river floor (wall jets), cross jets also reduce the potential for bed scour. However, the scales of mixing in counter flowing free jet are expected to be large compared to cross jets.

1.2 Objectives of the present study

In the present study attention was focussed on an axisymmetric free counter flowing jet located in a closed square conduit that also carried the main flow.

A. The mean jet flow characteristics determination included the following:

   i. Mean jet penetration length

   ii. The flow structure

   iii. Turbulent characteristics of the jet flow

   iv. Numerical test

B. The turbulent characteristic studies of the jet will include the record of the following:

   i. Normal and shear stresses

   ii. Kinetic energy balance and the energy balance based on the individual energy components

C. Studies were conducted to know the mechanics of mass transport using a water - salt - dye dispersion system that directly yields data related to the effectiveness of the jet as an injecting device for pollution control.

1.3 Organization of the thesis

This thesis is organized in eight chapters. In each chapter an introduction is followed by a literature review. The results and discussion on the subject finishes the chapter. An overall conclusion discuses the obtained results. The sequence and the concepts of the chapters are briefly explained below:

a. Chapter 1 is a general introduction to the counter jet phenomena and the aim of the present research.

b. Chapter 2 presents the experimental setup and instrumentation. This chapter also includes the limitations of the measuring instruments used. Dimensional analysis is also presented in this chapter.

c. Chapter 3 is allocated to determine the penetration length of the counter flowing free jet. In this chapter the process used to validate the test procedure is also presented.

d. Chapter 4 contains the other mean flow properties and turbulence measurements of the counter flowing free jets.

e. Chapter 5 is devoted to the structure of turbulence for this kind of flow in both the jet and the mixing layer region.

f. Chapter 6 deals with numerical experiments and the comparison between some turbulence models.

g. In Chapter 7 the investigation on mixing properties of counter flowing free jets is presented.

h. Chapter 8 summarizes the thesis and also mentions the original contributions of the present study to enhance knowledge. Some suggestions for further studies are also given at the end of the chapter.

References are provided at the end of the thesis.

Chapter 2

Experimental setup, instrumentation, and dimensional analysis

2.1 General remarks

This chapter is allocated to describe the test setup and the instruments that were used in the experiment.

The first part of the study deals with the flow profiles and the turbulence measurements in the counter flowing free jet region.

The second part is devoted to the collection of data related to the mixing characteristic of counter flowing free jet. To this end, the concentration distribution of a salt-water solution is determined at various locations in the wake of the jet field.

The energy balance and other theoretical considerations are discussed in the next part of the study.

To provide a contribution to the numerical modeling of the counter flowing free jets, a computer code, namely Phoenics was used to study some aspects of the jet flow in the last part of the study.

2.2 Experimental arrangements

2.2.1 General

The experimental setup and instrumentation are discussed in this section. The main flow and jet flow were obtained from the laboratory's sump. Different pumps were used to supply the jet and the main flow. To avoid any irregularity in the pumping process, both pumps were operated up to 80% of the maximum output. A calibrated venturi meter was placed in the supply pipes that carried the main flow. In the pipeline supplying the jet flow, a calibrated orifice-meter was located to measure the jet flow. The combined flow including both the main flow and jet flow was measured periodically by a 30° V-notch to provide a check on the flow measurement. The inlet pipe preceding the jet nozzle had a diameter of 38.5 mm and this provides a large area ratio for the jet nozzle. A transition was used to convert the circular cross section of the 305 mm diameter supply pipe to a square cross section (305 mm x 305 mm) of the test section pipe. Two

honeycomb meshes with 6.35 mm hexagonal cells were placed in this approach pipe. These meshes reduce the relative turbulence of the incoming main flow. Measurement of velocity in the potential core region of the jet provided another check on the jet flow rate. Other details of the setup and procedure are given in the following sub sections (Figure 2-1).

2.2.2 The test section

The conduit of the main flow and the combined flow is made of 12.7 mm thick Plexiglas plates. The conduit has a square cross section of sides W= 305 mm. The conduit has 5 individual panels and each panel is 940 mm long. At the top of the conduit, along the X axis, several pressure tips are installed to measure the pressure. The 38.1 mm pipe carrying the jet flow enters the test section from the top and is set at the center of the panel [Figure 2-2].

2.2.3 The jet

The counter flowing jet flow is carried to the test section by a brass nozzle. The details of the jet nozzle are shown in Figure 2-3. Four brass nozzles with different diameters used in the tests (Table 2-1), were made in a very precise way to convert flow from a 38.1 mm brass pipe to the desired diameter to have a completely circular, smooth and uniform jet flow. The test results show that the contracted flow at the start of the jet has a uniform velocity distribution.

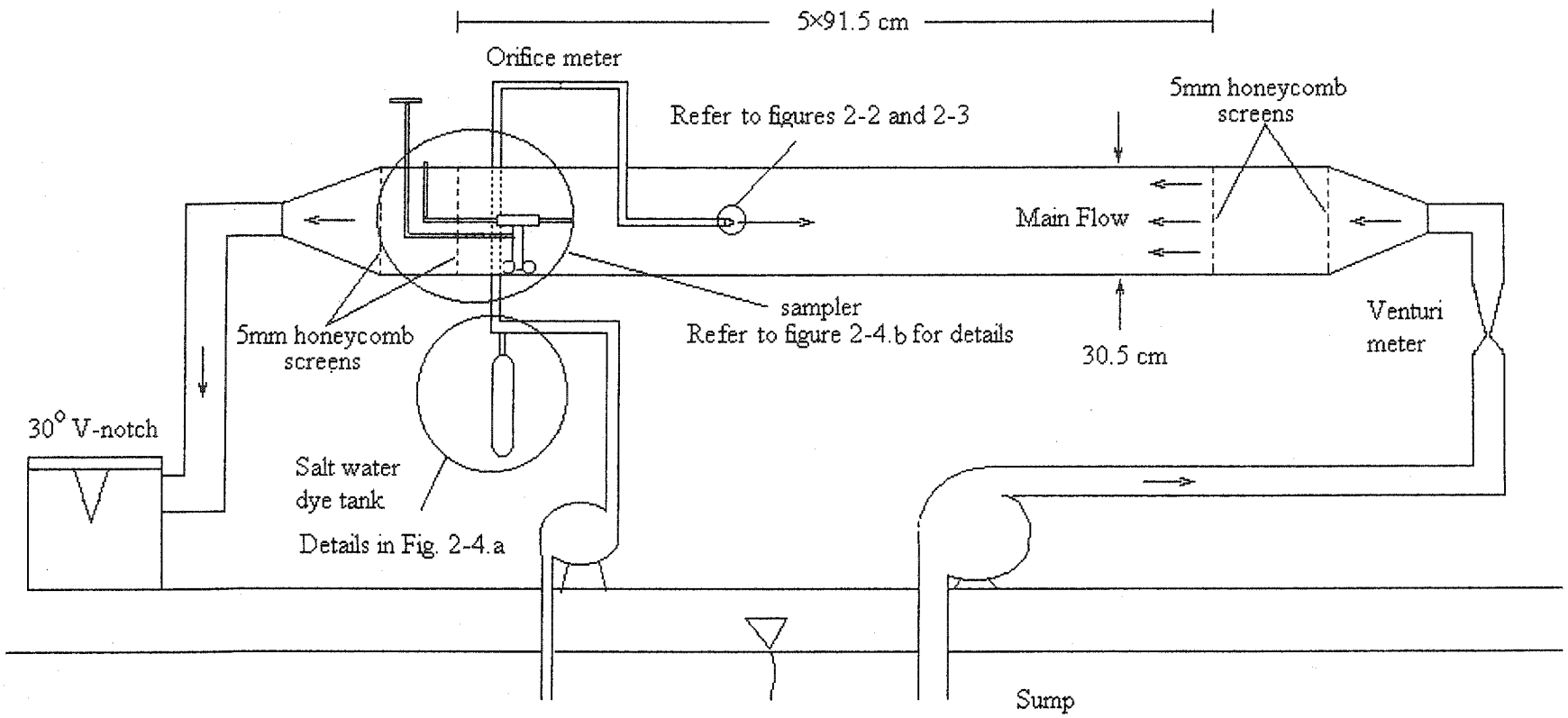

Figure 2-1 Schematic view of the test setup

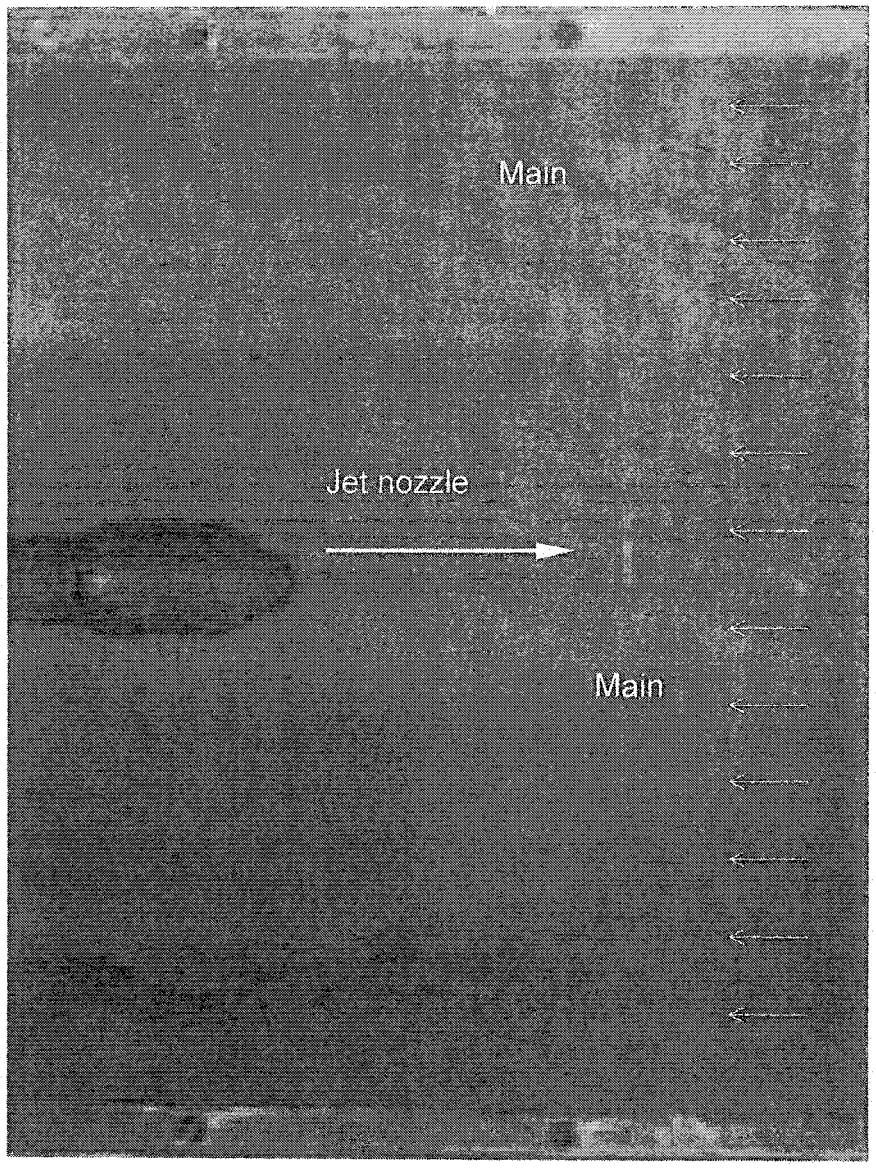

Figure 2-2. Position of jet in the flow.

As mentioned earlier, an orifice meter measures the jet flow. This orifice meter was calibrated by the gravimetric method. Since the velocity profile at the jet exit (core) is uniform, it can also be periodically used to check the laser equipment calibration data.

Table2-1 Jet diameters and their properties (W=300 mm)

Jet Diameter (mm)	1.588	3.175	6.350	9.575	12.700
W/D	192.126	96.063	48.031	31.854	24.016
Contraction ratio (Ajet / Apipe)	0.002	0.007	0.028	0.063	0.111

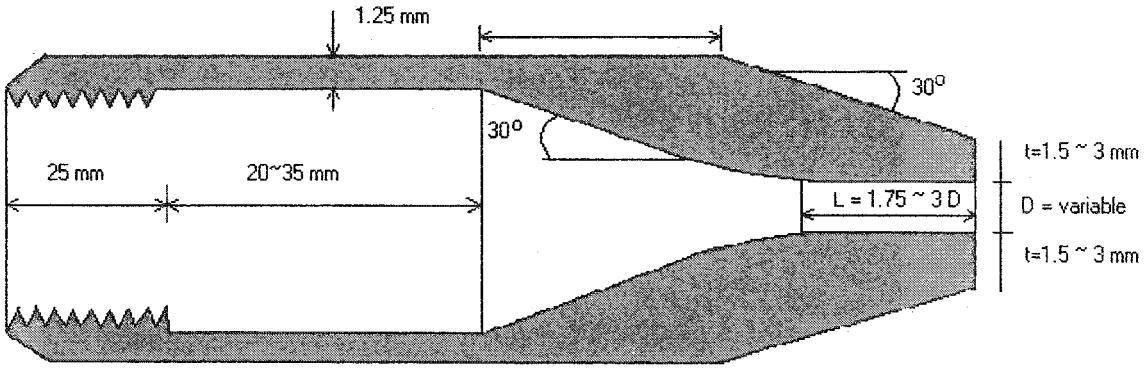

Figure 2-3. The cross section of the jet exit

2.2.4 The dye and salt injection system and sampler

An injection tank system was used to inject salt solution tracer into the pipe carrying the water for the jet (Fig. 2-4.a). An air intake pipe placed at the injection tank top and the solution exit at the tank bottom. A big pipe allows refilling the tank with solution. The solution outlet was connected to the jet water supply pipe. The washing outlet was used for maintenance and cleaning proposes.

The salt solution was colored by a food color to visualize the flow. Although the salt concentration was 75 g/L, because of variation in the jet flow, for each test a blank and a jet sample were taken.

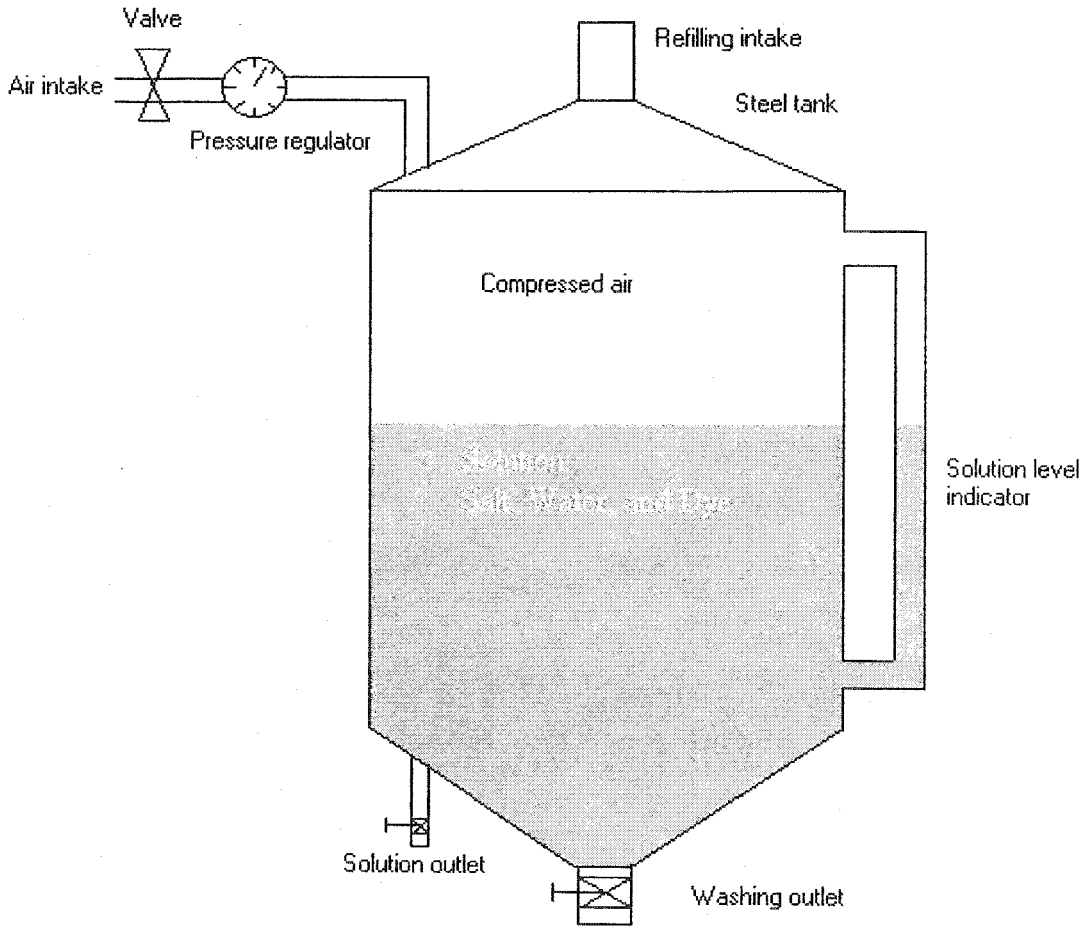

Figure 2-4.a. The pressure tank for water-salt injection to the jet.

The sampler (Fig. 2-4.b) assembly includes eleven equally spaced narrow copper tubes (1.25 mm in diameter and 100 mm long) in a horizontal row. The tubes can be moved along the centerline of the test section. The samples were collected in a bank of sampler tubes position periodically after the steady conditions were established.

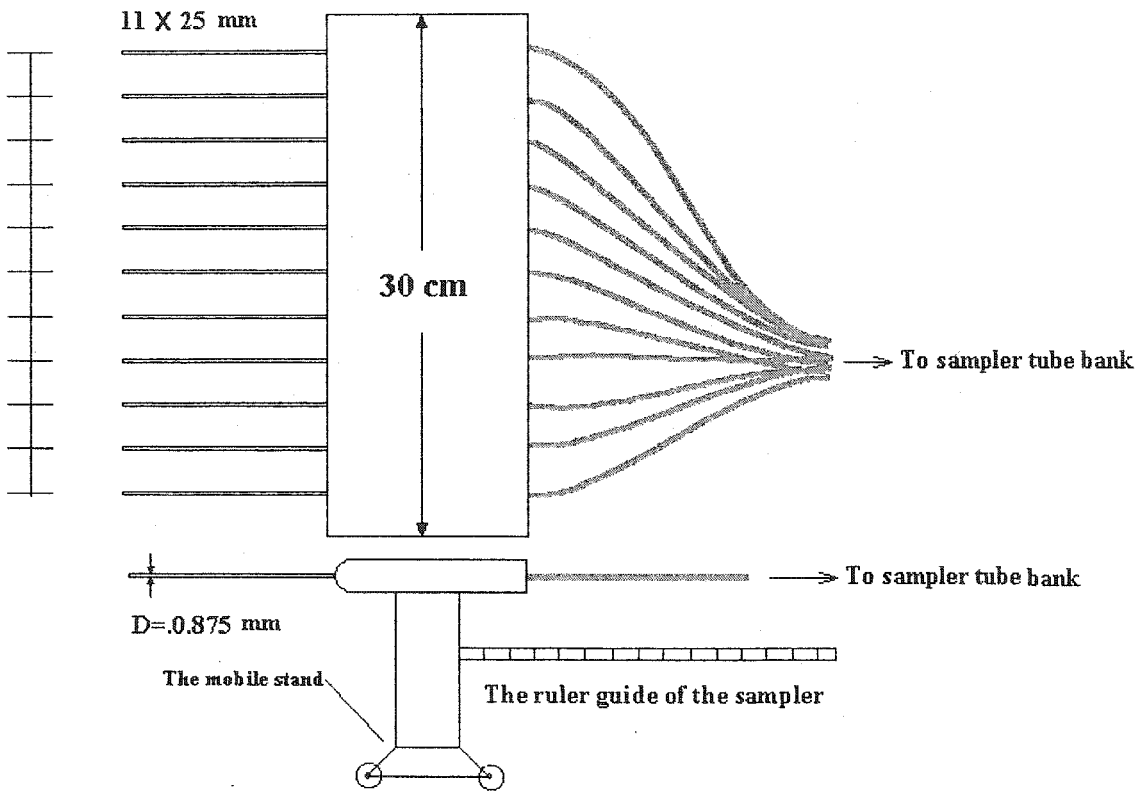

Figure 2-4.b. The sampler, plan (up), and side (down)

2.2.5 The water supply system: pumps and pipes

A pump is used to supply water for the main flow directly from a huge sump. This pump can steadily feed the test section with a maximum pressure of 355 kPa at the delivery end when the bypass valve is completely closed. The pump with the current piping system can supply a maximum flow of 35 liters per second to the test section at the gage pressure of 0.3 m of water. At the maximum discharge the maximum main flow velocity in the center of the test section was noted to be 0.616 m/s.

The jet flow supplier is a high-pressure pump (200 psi = 1379 kPa) that provides enough pressure to form a very high velocity jet flow. The maximum jet velocity at the jet exit with the current piping system was 24 m/s.

2.3 Measurement instruments

2.3.1 General remarks

In this section the measurement equipment and the related software are described following the details provided by the LDA manufacturer. A brief review of the principle on which each instrument is based is provided. This is followed by the general description of the related software used for data reduction. Laser Doppler Anemometry and conductivity meter device is covered in this section.

2.3.2 Laser Doppler Anemometry (LDA)

The velocity is measured by a 2-dimensional Dantec Particle Dynamics Analyzer (PDA) system. All the data from the signal processor (Dantec 58N10) comes to an internal computer card, which can process and save data and display it in several ways.

The laser beam comes from a 750-mw Argon-Ion laser beam generator (Fig. 2-5.a). The laser beam enters the photomultiplier and produces two pairs of beams with different wavelengths: the blue beam and the green beam. The green beam

(514 nm) was used for vertical velocity and the blue one (480 nm) was used for axial velocity. Each beam pair converges at the selected measurement volume. The laser beams are 1 mm diameter and were 38 mm apart. The beam divergence can be calculated using equation [2-1].

$$\alpha = \frac{4\lambda}{\pi d_0} \qquad [2\text{-}1]$$

Where:

α : the divergence.

λ : the wavelength of the laser

d_0 : the initial beam diameter

Since the wavelength is very small, the beam divergence is also very small.

A convex 160-mm focal length lens converges the beams into the point of measurement. This point, in fact, is a volume since the beam is a cylinder of 1mm diameter. From now on, this point will be called measurement volume. If d_f is the entering beam diameter and θ is the angle between two similar beams, the entire overlap volume is the volume of measurement and can be found by the following equations.

$d_x = \frac{d_f}{\cos(\theta/2)}$ is the volume width in the similar beam plane. [2-2]

$d_y = d_f$ is the volume depth that is perpendicular to the beams plane. [2-3]

$d_z = \frac{d_f}{\sin(\theta/2)}$ is the volume length. [2-4]

The probe can be used for one or two velocity components. If the third component is needed, another 1-D probe will be used. Figure 2-5.a shows the application of 2-D measurement in another study on spray nozzle.

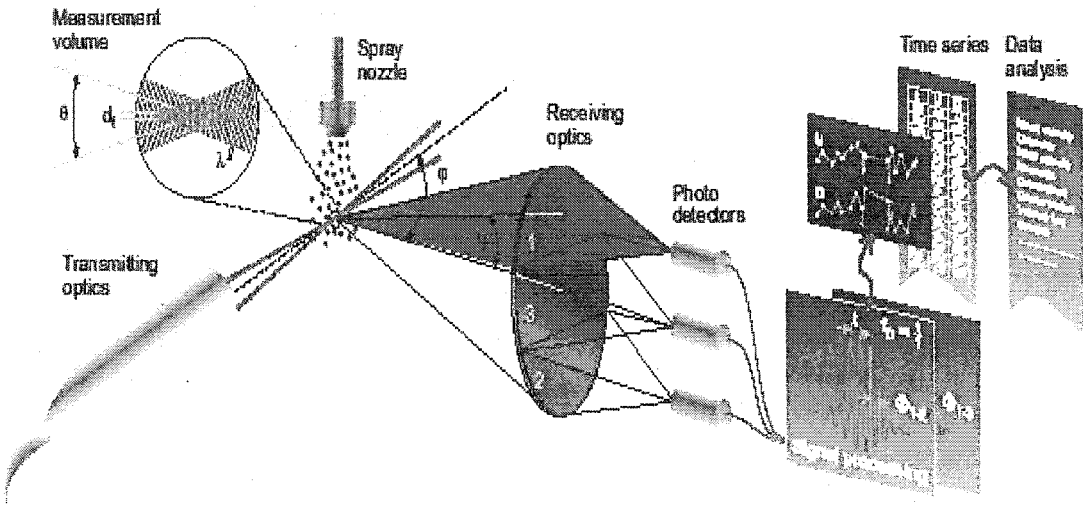

Figure 2-5-a Dantec's schematic overview of PDA and LDA techniques as applied for jet spray studies. [Adapted from Dantec documents]

When a particle passes through the measurement volume the laser beam reflects and refracts (Fig. 2-5.b). The reflected wave is captured by the receiver and the signal processor measures the incoming wavelength. The beat frequency or Doppler frequency is much lower than the laser frequency and therefore it is measured by the fluctuation in the intensity of the laser light which is reflected or refracted from the particle. If the Doppler frequency is f_D, the particle velocity, U, can be calculated by:

$$U = \frac{\lambda}{2\sin\theta} f_D \qquad [2\text{-}5]$$

The other parameters are as defined before.

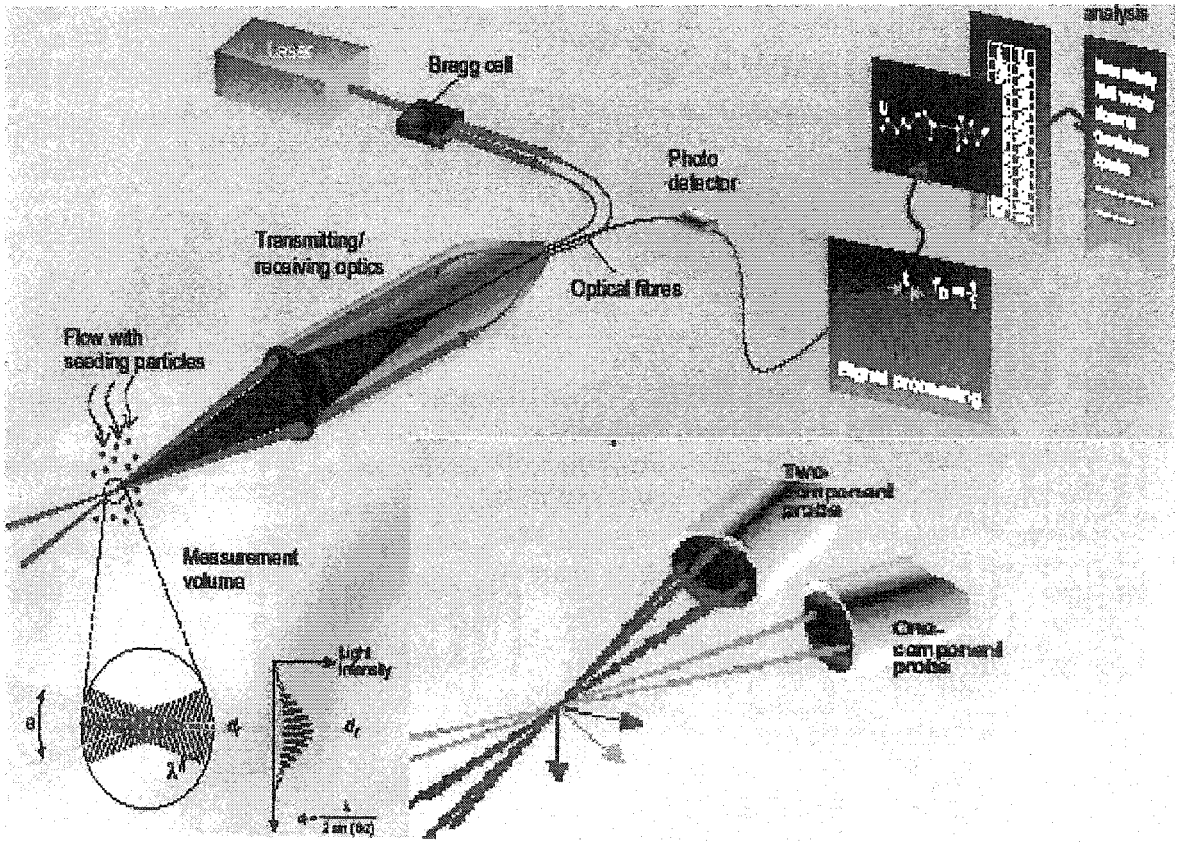

Figure 2-5-b One, two, and three dimensional LDA system. [Adapted from Dantec documents]

This processing simultaneously can be done for numerous particles at a time. Since particles at each instance pass through the measurement volume [Fig. 2-5], which is made of two pairs of beams, two velocities U and V, are measured at the same time. The measurement device can read velocities in time steps as short as 1/1000000 second and therefore if the period of measurement for each

point is long enough, the average velocity as well as other turbulence quantities such as u and v can be measured [Table 2-2 and Table 2-3].

2.3.3 Particle Dynamic Analyser (PDA) software

The process described above is very complicated and therefore choosing the right value for the setting the hardware of the system is very important. The roll of PDA is to set up such parameters and also to display and save the results in a proper way.

The software has been written in the C++ language and works in the Windows environment. Before starting the measurement, the positions of the points to be read are entered as the input by a program application. This application numbers the points and it is possible to define several regions for each set of measurement. Each region can have its special set up and therefore a more accurate measurement is possible. One of the applications shows the results of measurement at each point whenever 8 particles are validated. This data contains the number of detected particle, arrival and transit times for each particle, and horizontal and vertical velocities of the particle [Table 2-1].

Another application exports this data to a file whose name refers to the point number. By activation of another application, the software calculates the

turbulence parameters and displays the chosen parameters on the screen [Table 2-2 and Figure 2-6].

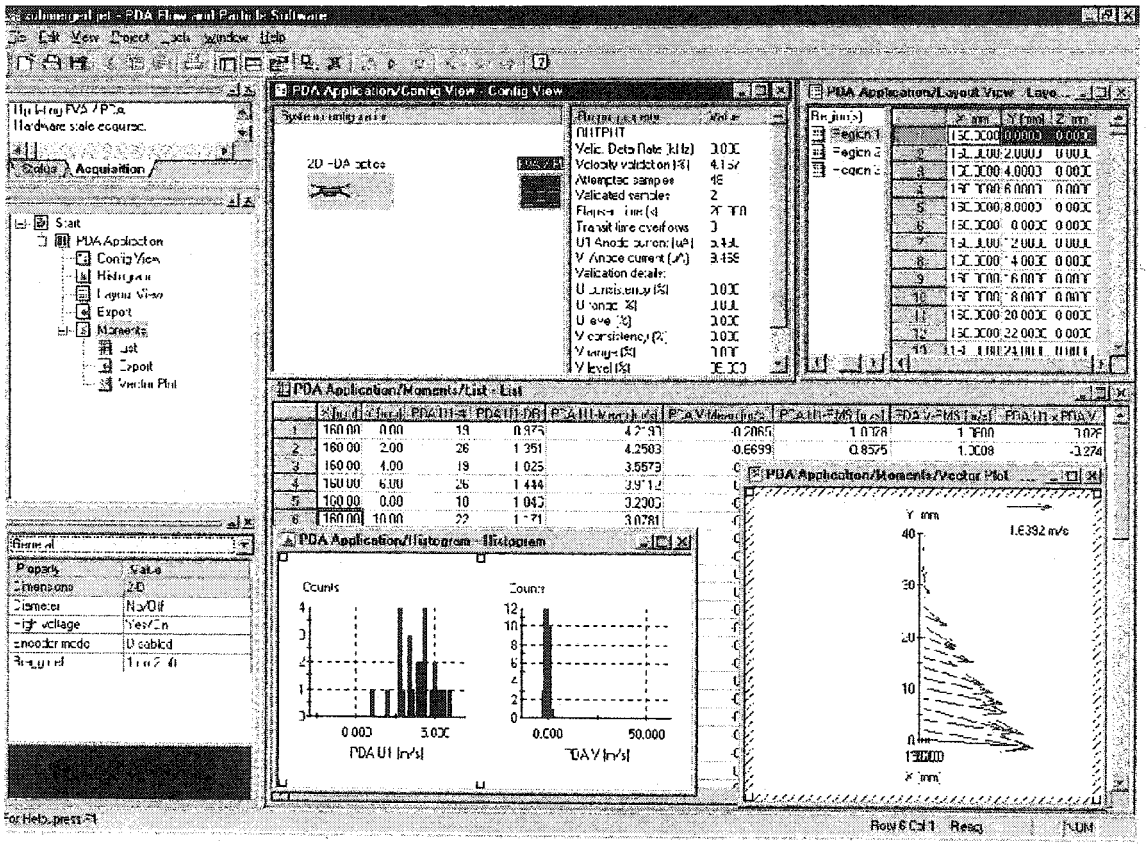

Figure 2-6 Typical screen of PDA software during turbulent measurement for a free submerged jet.

The position of the measurement volume, number of particles, data rate, average velocities, root mean square of u and v and finally the product of u and v or the turbulence shear stress related terms are shown by this application and can be saved by another application. The operator monitors the distribution of velocities by activation of the histogram window [Fig 2-6]. Histogram shows the distribution

of velocities of particles passing through the measurement volume. The vectors show the velocities along the cross section during this run. Some applications are not active or they are hidden.

Table (2-2) shows selected data of a typical data file obtained from an LDA measurement for a point whose position is given in the first row. The first column is the number of detected particle. The second column shows the status of measurement. It is zero when the particle dimension is not to be measured. Column 3, AT, shows the arrival time in 1/1000000 second where TT in column 4 is the transit time in the same scale. U and V are axial and radial velocities respectively that are shown in the next two columns (columns 5 and 6).

Tabe (2-3) is typical output file obtained from a LDA measurement.The first column shows the order of the point in the test. X, Y, and Z are columns 2,3, and 4 are the position of the measurement volume. Number of detected particle(NP) is given in column 4 and data rate incolumn 5. U and V, mean vevocities in x and y direction respectively are shown in columns 6 and seven. The root mean square of the summation of the unsteady part of those velocities are presented in the columns 8 and 9. The last column contains the shear stress data.

Table 2-2 A part of file contaning an LDA data. Definitions are presented in the text. POSX, POSY, POSZ, represent position of the measurement volume in x, y, and z direcrtion respectively.

POSX=0.00 mm;POSY=0.00 mm;POSZ=0.00 mm; PROJECT=C:\WINDOWS\TEMP\jet1-4-1-pen.lda					
Row 1	Status 2	At (μs) 3	TT(μs) 4	U (m/s) 5	V (m/s) 6
1	0	53.953	0.017	3.23	-0.03
2	0	71.298	0.011	3.12	-0.05
3	0	121.382	0.017	3.16	-0.04
4	0	172.29	0.022	3.23	-0.06
5	0	174.641	0.017	3.19	-0.04
6	0	179.934	0.022	3.12	-0.02
7	0	183.198	0.017	3.19	-0.05
8	0	216.751	0.022	3.19	-0.06
9	0	232.402	0.017	3.23	0.03
10	0	233.775	0.039	3.23	-0.01
11	0	295.975	0.017	3.23	-0.03
12	0	299.431	0.011	3.3	0.04
13	0	314.783	0.011	3.23	-0.05
14	0	321.257	0.017	3.19	0.01
221	0	6645.79	0.017	3.01	-0.03
222	0	6653.338	0.017	3.08	-0.04
223	0	6662.159	0.017	3.05	-0.06
224	0	6662.816	0.006	3.08	0
225	0	6771.971	0.017	3.12	-0.05
226	0	6800.91	0.022	3.16	-0.06
227	0	6921.643	0.017	3.23	-0.05
228	0	6925.765	0.017	3.19	-0.04
678	0	18074.92	0.017	3.01	-0.05
680	0	18082.69	0.011	3.01	-0.05
681	0	18100.44	0.017	3.01	-0.06
682	0	18106.57	0.006	3.08	-0.05
683	0	18215.1	0.011	3.3	-0.04
684	0	18224.43	0.017	3.19	-0.03

Table 2-3 **The averaged turbulence data. POSX, POSY, POSZ, represent the position of the starting point in x, y, and z direcrtion respectively. Project refferes to the LDA file name for the data aqusition.**

POSX=0.00mm; POSY=0.00mm;POSZ=0.00mm; PROJECT=C:\WINDOWS\TEMP\jet1-4-1-Pen.lda										
Row	X	Y	Z	N P	D R (Hz)	U-Mean (m/s)	V-Mean (m/s)	u-RMS (m/s)	v-RMS (m/s)	U x V $(m/s)^2$
	1	2	3	4	5	6	7	8	9	10
1	0	0	0	684	37.532	3.08	-0.02	0.11	0.04	0
2	1	0	0	537	28.819	3.11	-0.02	0.11	0.04	0
3	2	0	0	670	36.497	3.15	-0.02	0.13	0.04	0
4	3	0	0	871	47.094	3.16	-0.02	0.12	0.04	0
5	4	0	0	905	49.356	3.14	-0.02	0.12	0.05	0
6	5	0	0	1024	52.374	3.14	-0.02	0.1	0.04	0
7	6	0	0	930	49.993	3.14	-0.02	0.11	0.04	0
8	7	0	0	823	44.479	3.12	-0.02	0.12	0.04	0.001
9	8	0	0	892	48.282	3.13	-0.01	0.12	0.04	0
10	9	0	0	766	41.821	3.13	-0.01	0.11	0.05	0
11	10	0	0	840	45.604	3.16	-0.01	0.14	0.05	0
12	11	0	0	970	52.805	3.15	-0.01	0.13	0.05	0
13	12	0	0	943	51.115	3.13	0	0.15	0.05	0.001
14	13	0	0	1024	54.174	3.15	0	0.15	0.05	0
15	14	0	0	1024	56.192	3.15	0	0.14	0.05	-0.001
16	15	0	0	860	46.766	3.15	0	0.15	0.05	0
17	16	0	0	1024	56.678	3.14	0	0.17	0.05	0
18	17	0	0	1024	55.417	3.12	0.01	0.22	0.06	0
19	18	0	0	1024	59.897	3.12	0.02	0.18	0.06	-0.001
20	19	0	0	1024	53.868	3.11	0.02	0.21	0.06	-0.001
21	20	0	0	1024	55.503	3.09	0.02	0.24	0.06	-0.001

2.3.4 Conductivity meter

A conductivity meter was used to measure the concentration of salt in each sample taken by the sampler through their conductivity. The conductivity meter used in this study is a Fisher-Scientists® brand and reads the conductivity of a fluid as small as 1 micromho or micro S (1 Simon equals to 1/ohm). To read a sample, both two electrodes should be completely entering the fluid. The controller sets the reading type (conductivity or total dissolved solids) and range (Figure 2-7).

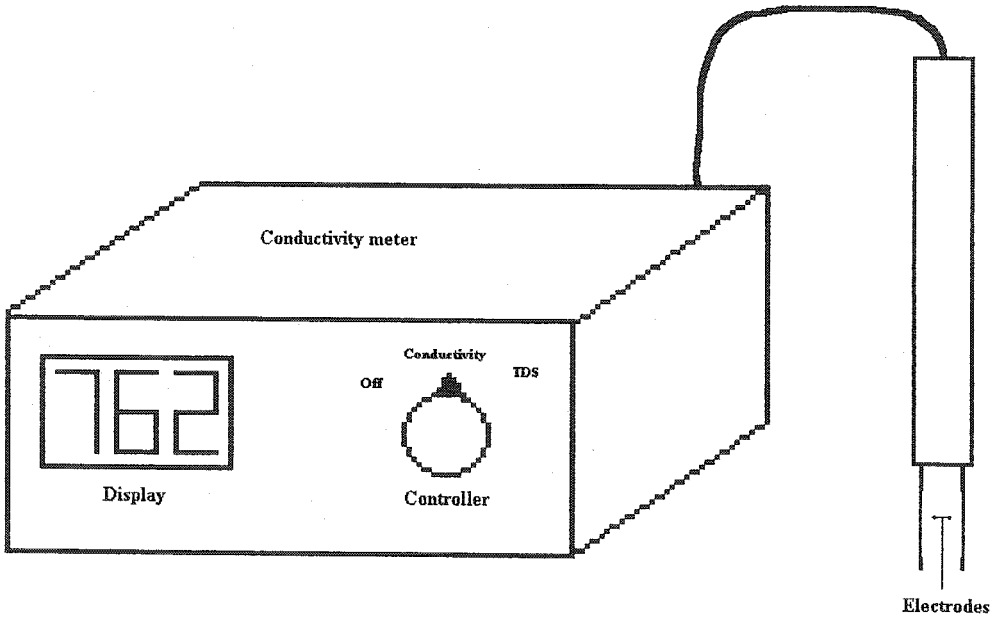

Figure 2-7 Conductivity meter

2.4 Numerical tests (Phoenics)

Phoenics is a computational fluid dynamics software that has the ability to work on a PC. The software was developed by CHAM, a British company. The software originally created by Professor D. Brian Spalding in 1974. Phoenics uses finite volume technique to solve Reynolds equations by the predefined turbulence models such as mixing length, k-ω, and k-ε, etc.. The software has the ability to compute velocities, pressure, and turbulent kinetic energy. It also has a graphical application to show the results by vector plot, contour lines, or color grading pattern.

The test process starts with providing geometrical data of boundary conditions and also initial values. A 150x 30x30 cm^3 test section was set as the test section. The jet and the pipe carrying the jet were also defined for the model by their equivalents in the software library. Since the model does not accept a circular inlet, the jet exit was defined as a square inlet.

A non-homogeneus grid mesh was defined with a denser joints close to jet and wider grids towards the walls. Because the test section is made of plexyglass, the roughness was set to zero but the boundary layer effect still existed in the calculations.

2.5 Dimensional analysis

Figure 2-8 shows the parameters used for the dimensional analysis.

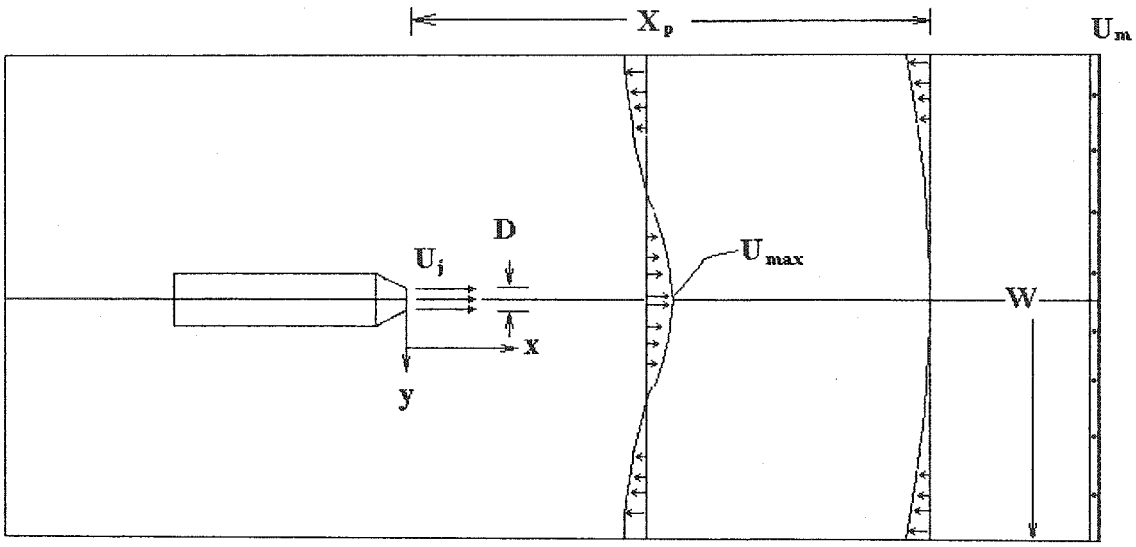

Figure 2-8 Parameters used in dimensional analysis

Now, the parameters can be collected in one equation:

$$f(U_j, U, U_m, V, u_{rms}, v_{rms}, D, W, x, X_p) = 0 \qquad [2\text{-}6]$$

using U_j and X_p as the primary dimensions, the π terms are calculated:

$$\pi_1 = \frac{U_m}{U_j} \qquad [2\text{-}7]$$

$$\pi_2 = \frac{U}{U_j} \qquad [2\text{-}8]$$

$$\pi_3 = \frac{u_{rms}}{U_j} \qquad [2\text{-}9]$$

$$\pi_4 = \frac{v_{rms}}{U_j} \qquad [2\text{-}10]$$

$$\pi_5 = \frac{W}{X_p} \qquad [2\text{-}11]$$

$$\pi_6 = \frac{D}{X_p} \qquad [2\text{-}12]$$

and also:

$$\pi_7 = \frac{\pi_6}{\pi_1 \times \pi_5} = \frac{U_j D}{U_m W} \qquad [2\text{-}13]$$

Some reduced parameters may be used occasionally but the main dimensionless parameters are as listed above.

Chapter 3

Study of penetration length

3.1 General remarks

Jets are known to be efficient devices for disposal of liquid wastes into a water body. Probably, the first attention to jets was related to the application of Bernoulli's equation on exit velocity of a fluid from a tank under pressure (Torricelli's theorem). If a jet of fluid freely enters another fluid body that is still or moving, it is called a free jet. Free jets are usually classified according to their shape (plane or round jets) or in the sense of flow direction (co-flowing, cross-flowing, and counter-flowing jets).

Abramovich (1936) published his text on jets " Theory of Turbulent Jet". The recent edition of this text appeared in 1963. The latter was translated to English during the same year (Abramovich 1963). This text covers almost all kinds of jets. An important aspect of this book is the large number of references in the

Russian language. Fortunately, the English version of the book provides us most of the results of the previous studies up to 1963. Rajaratnam (1976) published the text titled "Turbulent jets" and in it, he reviewed the existing literature related to jets. Reviewing the literature published during 1970s and 1980s shows, one notices that almost all studies on jets during these years were concerned with cross-flowing jets because of their importance to air pollution and river bank effluent. Subsequently, a number of experimental jet studies based on laser technology have been published. A very important fact is that in most of the recent studies, the main flow is restricted to open channel flow or wind tunnel studies. The next section presents more details on some selected major research results on counter flowing free jets.

3.2 Literature review

3.2.1 General

When counter flowing free jets appeared independently in scientific literature in the middle of the last century (Arendt 1956), it drew the attention of several investigators in the field of fluid mechanics and hydraulics. In earlier literature, the main goal was to predict the penetration length of the counter flowing free jet. The early results are still valid, but improvements in velocity measurement technology increased the measurement accuracy and also provided a wider range of knowledge about this phenomenon.

In the earlier studies, the counter flowing free jet was considered as a fundamental problem in fluid mechanics with no particular applications in engineering (Arendt 1956). Later, some engineers paid special attention to this kind of jet as an aerodynamic stabilizer for afterburner or turbojet engines (Sekundov 1969).

During the 1970s, when the environmental problems became a major concern in engineering projects, counter flowing free jets gained an important role as a means of disposing industrial effluents. Beltaos (1973) and Robillard (1974) mentioned the possibility of using counter flowing free jet for dilution of the wastewater effluent into a river. Morgan (1976) made another contribution to the subject using several jet and pipe diameters.

During the 1990s, Lam (1991, 1995,1997) and Konig (1991) published new results related to the counter flowing jets. Lam indicated that counter flowing free jet can be used as an aerodynamics stabilizer too (Lam 1991). Yoda (1996) reported the results of study on counter flowing free jet using visualizing techniques.

In the next section, a detailed review of the experimental approach to solve the counter flowing counter jet will be presented. It should be added that the scope of the review of the previous major studies is limited to counter flowing free circular jets only.

3.2.2 Counter flowing free jet studies

One of the first available published paper on circular counter flowing free jet is probably the one that was published half a century ago by Arendt et al. (1956). The paper cited only one reference: a paper by Albertson et al. (1950). They defined two dimensionless functions based on the jet system geometry and momentum. The velocities were measured by a pitot tube. The result showed a linear relation between the penetration length and the velocity ratio as indicated in the following simple equation (Fig. 2-1):

$$\frac{X_p}{D} = 2.7\sqrt{\frac{\pi}{4}} \times \frac{U_{jet}}{U_{main}} = 2.4\frac{U_{jet}}{U_{main}} \qquad [3\text{-}1]$$

where

X_p: The penetration length

D: Jet diameter

U_{jet}: Jet velocity

U_{main}: Stream velocity.

Later studies (Beltaos 1973, Konig 1991, and Lam 1995) show that the results are not valid for all jet velocities although the equation can be used for the velocity ratio (jet velocity / stream velocity) less than 10. Apparently, the error shows up from the assumption that the penetration length is linearly proportional to the product of velocity ratio and the jet diameter. The later observations (Konig 1991, Lam 1991 and 1995) showed such an assumption is not correct, especially for velocity ratio greater than 10.

Beltaos and Rajaratnam (1973) tried to find functions and length scales to predict the penetration length. They used a wind tunnel as the test section with a nozzle mounted in the center to provide the counter flowing jet. They used their result and those stated in the original Russian literature to form the following relation to denote the penetration distance:

$$\frac{X_p}{D} = 2.6\frac{U_j}{U_0} \qquad [3\text{-}2]$$

Equation [3-2] gives 10% longer penetration length than that recommended by Arendt et al. (1956) and has a better agreement with the test results published later. Since Beltaos and Rajaratnam (1973) used the pitot tube to measure velocities, they did not record turbulence data. The other investigators support the recommended equation, equation 3-2 (Lam 1991, 1995, and 1997, Konig 1991, Yoda 1996).

Using several jets with various diameters in different pipes, Morgan et al. (1976) presented a comprehensive study on penetration length. The measurement of jet velocity was done through conductivity measurement of the injecting tank. Their results show a logarithmic relation between $\frac{U_j D}{U_m W}$, and $\frac{X_p}{D}$ the momentum factor ratio of jet to main flow, the dimensionless penetration length. On a log-log graph, the results show three regions: a line, a curve and another line.

Lam (1991) made a contribution to the study of the counter flowing free jet set in an open channel. In the study, using the one dimensional Laser Doppler

Anemometry (LDA), he measured some of the turbulence characteristics of jets in a water flume (width = 30 cm and depth = 24 cm). The jet exit diameter was 1 cm. The jet was installed in the center of the main flow. They also recorded the axial and Radial turbulent velocity components. No turbulent shear data was measured, as they used a one-dimensional laser probe. In that study, they presented a set of graphs resulting from the measurements along the jet centerline for velocity ratios up to10. One test was also done for the velocity ratio of 20. This study confirmed the validity of equation [3-2] for velocity ratios less than 10.

Lam (1995 and 1997) also used the Laser Induced Fluorescence (or LIF) technology to investigate the counter flowing free jet phenomena. These studies were also done in a 30-cm width flume with a water depth of 40 cm. The jet was installed at the center of the cross section of the flow. In the first experiment, a monochromic frame grabber was used to catch the video recording of the test data onto a computer. The first experiment (Lam 1995) had little new information because of the poor quality of the pictures (512 pixel by 512 pixel and an 8-bit resolution per pixel). However, it was actually a good base for the next experiment (Lam 1998). In the second experiment, Lam used a charged-coupled device (CCD) camera with the speed of one image per second and took 100 images per test. The range of Reynolds number of the jet flow was 1000 to 8000, while the velocity ratio range was 2.5 to 15. To avoid any secondary flow and to provide higher velocity ratio, the main velocity was kept at 5 cm/s and jet exit

velocity was changed from 12.5 to 75 cm/s. Lam (1991) also for the first time obtained turbulence measurements for the counter flowing free round jet.

Konig and Fiedler (1991) presented a paper on the structure of the counter flowing jet flow based on flow visualization. They used a high intensity flashing light to illuminate the jet region (volumetric lighting) and a laser light sheet to visualize the flow phenomena in a vertical plane passing through the jet centerline. In LIF method, a laser sheet is radiated from a partial sphere lens while the fluorescence particles enter into the region of study through the jet flow. The laser induces the fluorescence material to radiate light. In the next few moments all lights including the laser light are turned off to let a camera capture the action in the illuminated area. Since the only source of light is from the radiating fluorescence material, the result is a picture of the plane in which the laser radiated. They were able to recognize two different cases of the jet phenomena:

a. the stable case when $R \leq 1$ and

b. the unstable case when $R > 1.4$

where '$R=U_j/U_m$'. They showed that the penetration length can be calculated from equation [3-2] when $R<9$. In summary, one can say that all the studies indicated that the penetration length of counter flowing free jet is linearly varies with the velocity ratio.

Later Yoda and Fiedler (1996) verified the results using several jet diameters in a flow visualization study.

3.3 Validation of results

In this section, the results of the validation tests on penetration length are presented. In this manner, a set of experiments on a round jet in the still water, or a submerged jet has been completed to validate the test procedure by comparing the collected data with the existing data. Another set of experiments was also performed on the counter flowing free round jet. The results are presented and discussed in the next sections.

3.3.1 Axisymmetric free jet

To validate the procedure, an experiment was designed and performed. In this step, the characteristics of the free jet in still water were studied and compared with existing data (Abramovich 1963, Daily 1966).

Figure 3-1 shows the axial velocity distribution in an axisymmetric free jet compared to existing data (Abramovich 1963). In the present study, different values for x were chosen to measure the centerline velocities along the axis of the test section. In Figure 3-1, the lateral distance, $y_{½}$, denotes the location

where the axial velocity is 50% of the centerline velocity, U_{max}. U_{max} and $y_{½}$ were used to non-dimonsionalize the parameters U and y respectively.

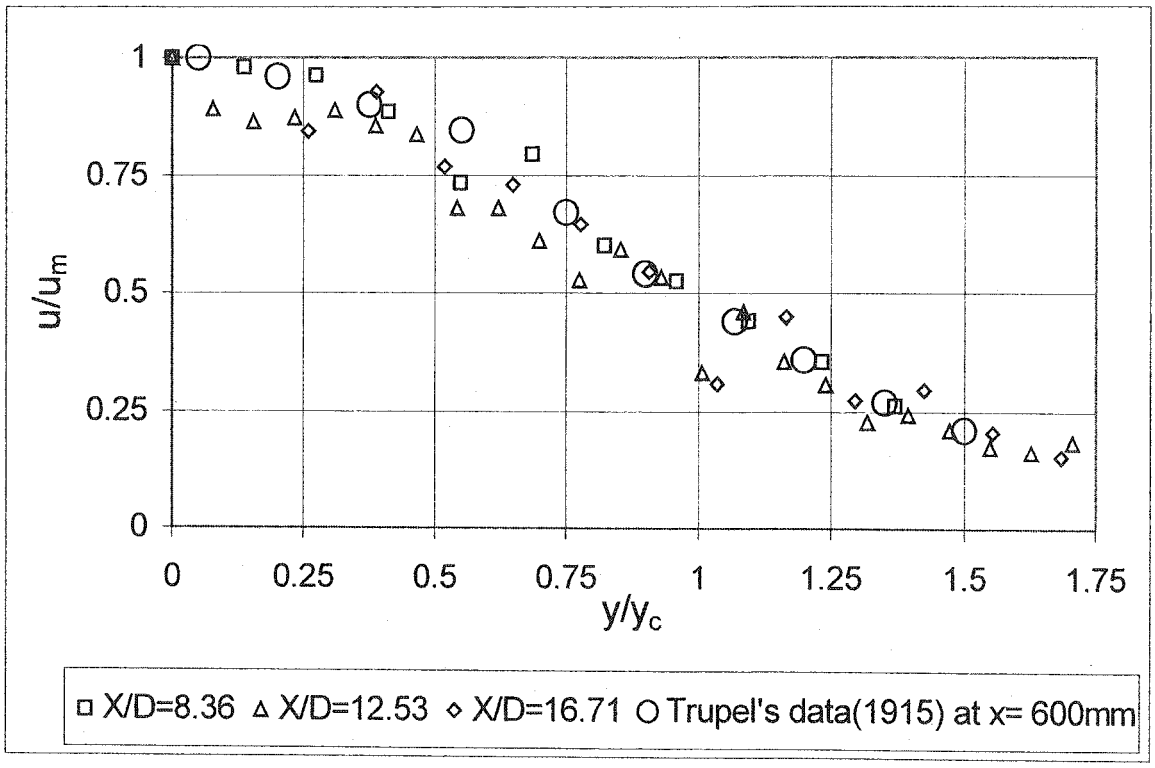

Figure 3-1 **Variation of the axial velocity at various radial locations. Trupel's data were obtained from Abramovich (1963).**

Figure 3-2 shows the comparison between the results of this study and the one given equation by Daily and Harleman (1966) for the free unconfined jet. They also suggested the following equation for the mean axial velocity variation along the vertical direction:

$$\frac{U}{U_{max}} = \frac{1}{[1+\frac{x^2}{0.016y^2}]^2} \qquad [3\text{-}1]$$

Here, x is axial distance from jet, y is radial distance to the centerline, U is the velocity at the point, and U_{max} is the maximum velocity at the centerline. It also should be noted that the given equation is for a jet with no boundary effects. In the present study, the boundary has an effect on the jet behavior and these effects will be discussed latter.

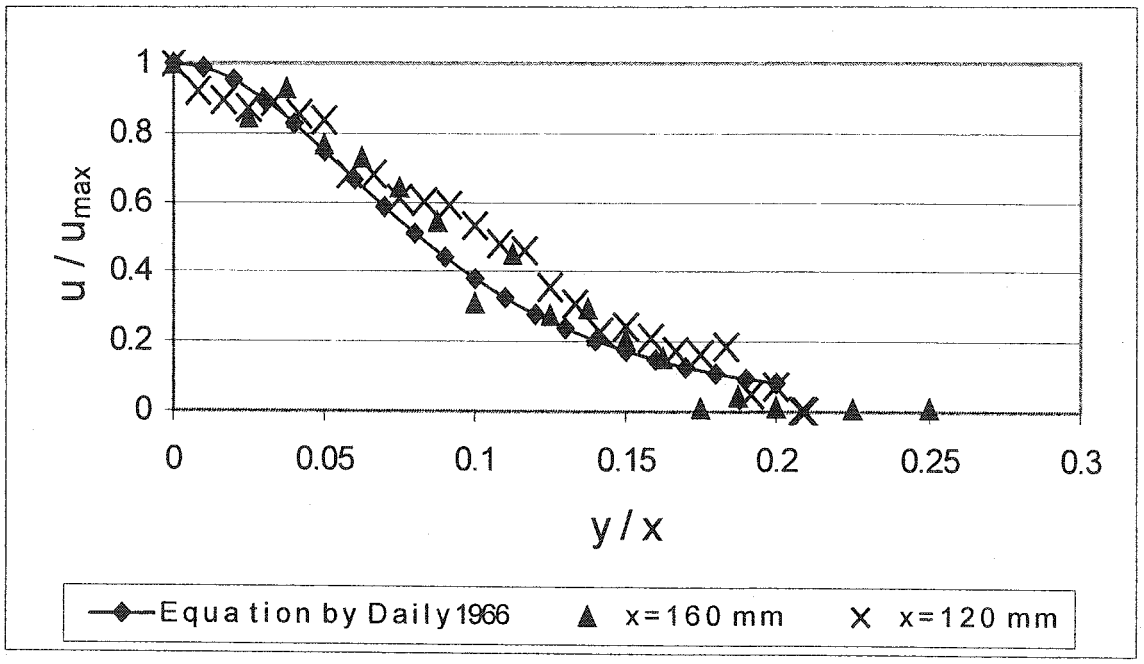

Figure 3-2 Radial velocity distribution in the round jet.

3.3.2 Counter flowing free jet

Penetration length, flow pattern, and turbulence intensities are the important characteristics of the turbulent counter flowing free jet. To compare the results of the present study with some previous studies, three graphs are presented in this

section. Since there are slightly varying results from different investigators for the penetration length, a comparative graph can illustrate the agreement between these data.

The measurement of penetration length in a wide range of low velocity ratio is shown in Figure 3-3. The present results shown in Figure 3-3 fall in the range reported by Lam (1997).

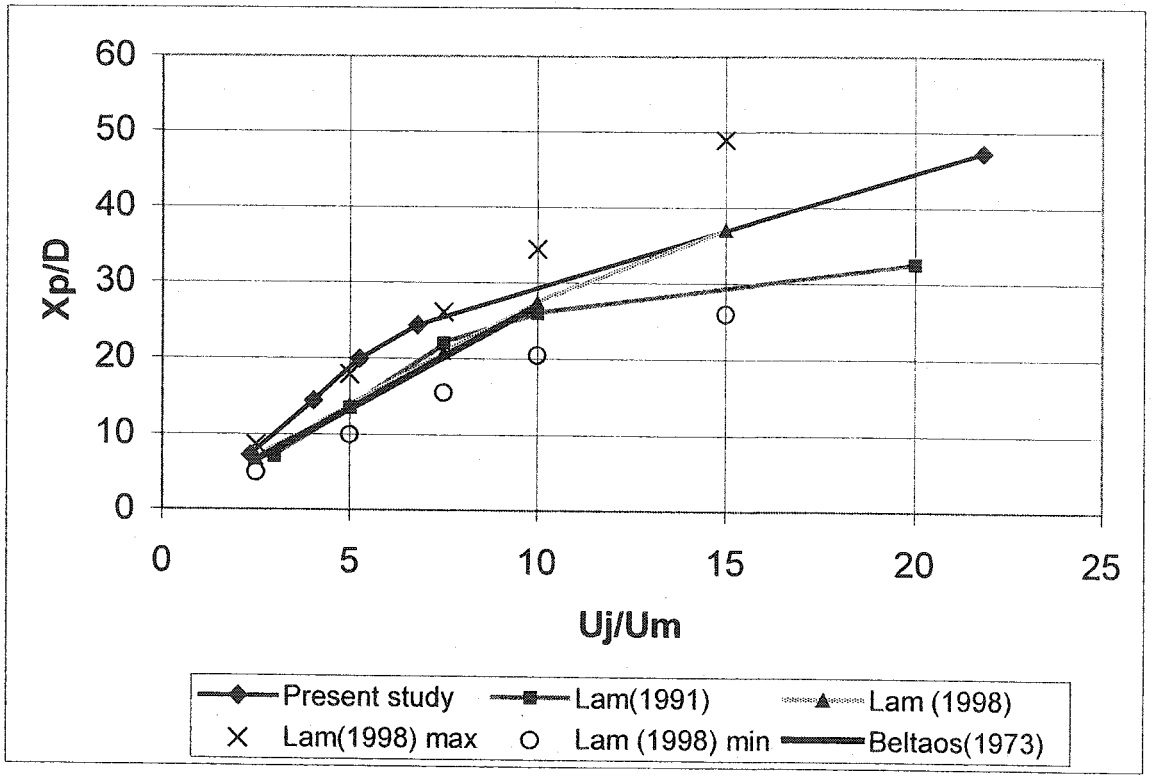

Figure 3-3 Penetration length of a counter flowing round jet.

3.4 Results and discussion

3.4.1 General

All previous researchers agree that the jet penetration length varies linearly with the velocity ratio (R= $U_j/U_{m)}$. Those tests that were performed with larger test sections of width and depth; W/D or H/D did not point out any limitation for this general rule. Studies by Lam and Konig conducted tests where R is as high as 9 or 10. Table (3-1) provides a brief summary of earlier studies related to counter flowing free jets.

Table 3-1. Counter flowing free jet studies: parameter ranges and other details.

Researcher	Jet D (mm)	Width W (mm)	Height H (mm)	W/D	H/D	Fluid	Method of finding X_p
Arendt (1956)	4.572	914.4	914.4	200	200	Air	Pitot tube
Beltaos (1973)	5.08	609.6	609.6	120	120	Air	Pitot tube
Lam (1991)	10	300	240	30	10	Water	LDA
Konig(1991)	25	NA	NA	NA	NA	Air	Flow Visualization
Lam (1995)	10	300	400	30	40	Water	Flow Visualization
Lam (1997)	10	300	400	30	40	Water	Flow Visualization

To find out the effect of the parameters W/D and H/D on the jet characteristics, several jet diameters were used in the square shaped test section. The results are presented in the following sections.

3.4.2 Penetration length (X_p)

The tests were performed with several jet diameters: 1.587 mm, 3.175 mm, 6.350 mm, 9.525 mm, and 12.700 mm (figure 2-3, table 2-1). In the tests, the velocity of the main flow was kept constant while the jet velocity was varied. The maximum possible range is dictated by the available facilities such as the pump and the pipeline.

To find the penetration length, the laser probe was moved upstream horizontally along the jet axis on the centerline of the test section, starting from the jet exit. Since the software used provides real time data of the velocities, the average axial velocity of the centerline could be read at any time. The definitions in figure 2-8 were given to the software to read the jet velocity as a positive value and main flow as a negative value. The position of zero axial velocity denotes the stagnation point. Its distance of this point from the jet exit denotes the penetration length X_p. It is not possible to find the exact place during the test as the stagnation point varies with time. Whenever the axial velocity recorded a negative value, the test was considered done. To be on the safe side, the

reading was continued up to the region where the detected particles did not have positive velocity.

Figure 3-4 shows the variation of penetration length with the velocity ratio for a 1.587-mm jet diameter. The main flow velocity varied between 0.407 m/s to 0.465 m/s while the jet velocity varied between 3.774 m/s and 52.937 m/s.

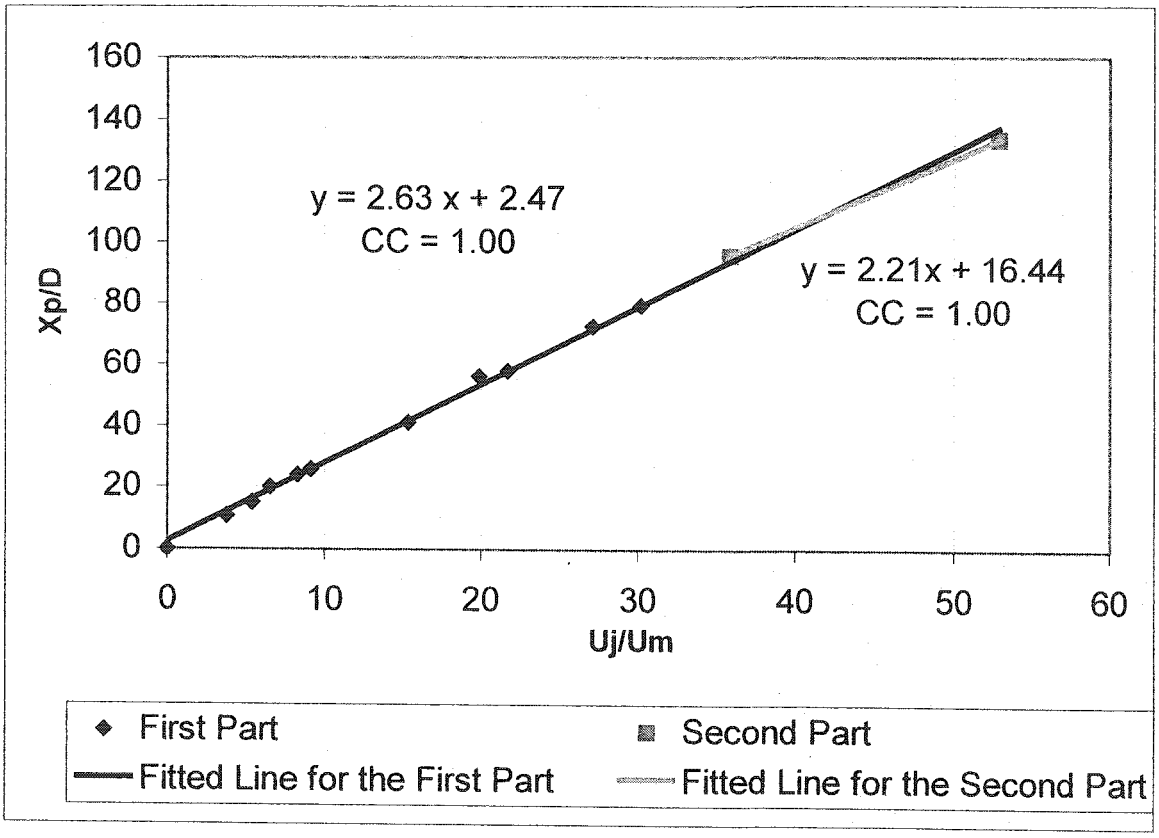

Figure 3-4 Dimensionless penetration length (X_p/D) for a 1.587-mm jet.

To follow the pattern of the available data, the graph can be divided to two parts. The first part means the points which can be categorized into a group with the

same ratio of Uj/Um to Xp/D. The second part includes the point with higher Uj/Um than the first part. The best fit line for R= Uj/Um = 37.5 is slightly steeper than the line fitted to the rest of the data. The slope is 2.63 and confirms the results that are provided by the previous researchers (Beltaos 1973, Lam 1991, 1995, and 1997, Konig 1991, Yoda 1995) in the range R≤ 37.5. R=37.5 denoted the critical velocity ratio R_c.

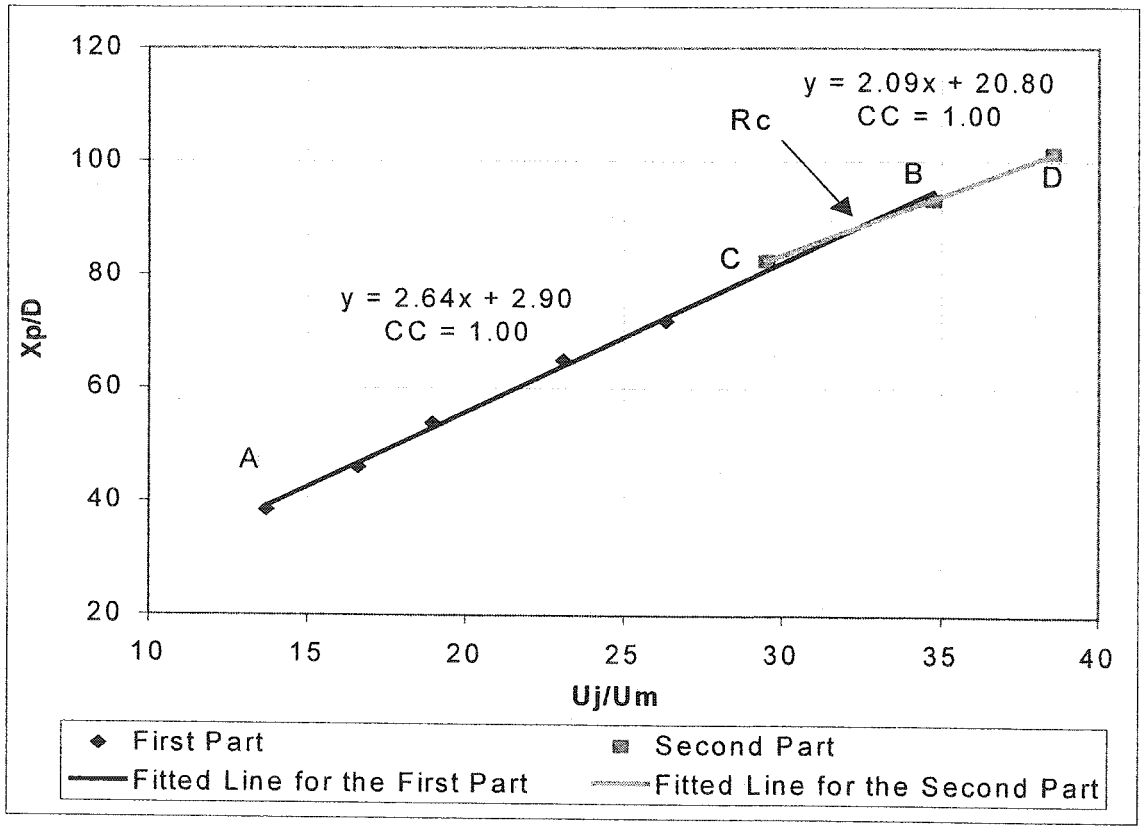

Figure 3-5. Penetration length of a 3.175 mm jet in a counter flow.

Another set of tests was performed with a 3.175mm diameter jet. The results of that test are shown in Figure 3-5. Here, the two regions AB and CD separated by R_c are clearly seen. The slope of the fitted line for the first region remains at 2.64

while the slope of the fitted line for the second region drops to 2.09. In this test R_c=32.5 that show a drop from 37.5 for the D=1.5875 mm.

A test was performed with the jet diameter increased to 6.35 mm whose results are shown in Figure 3-6.

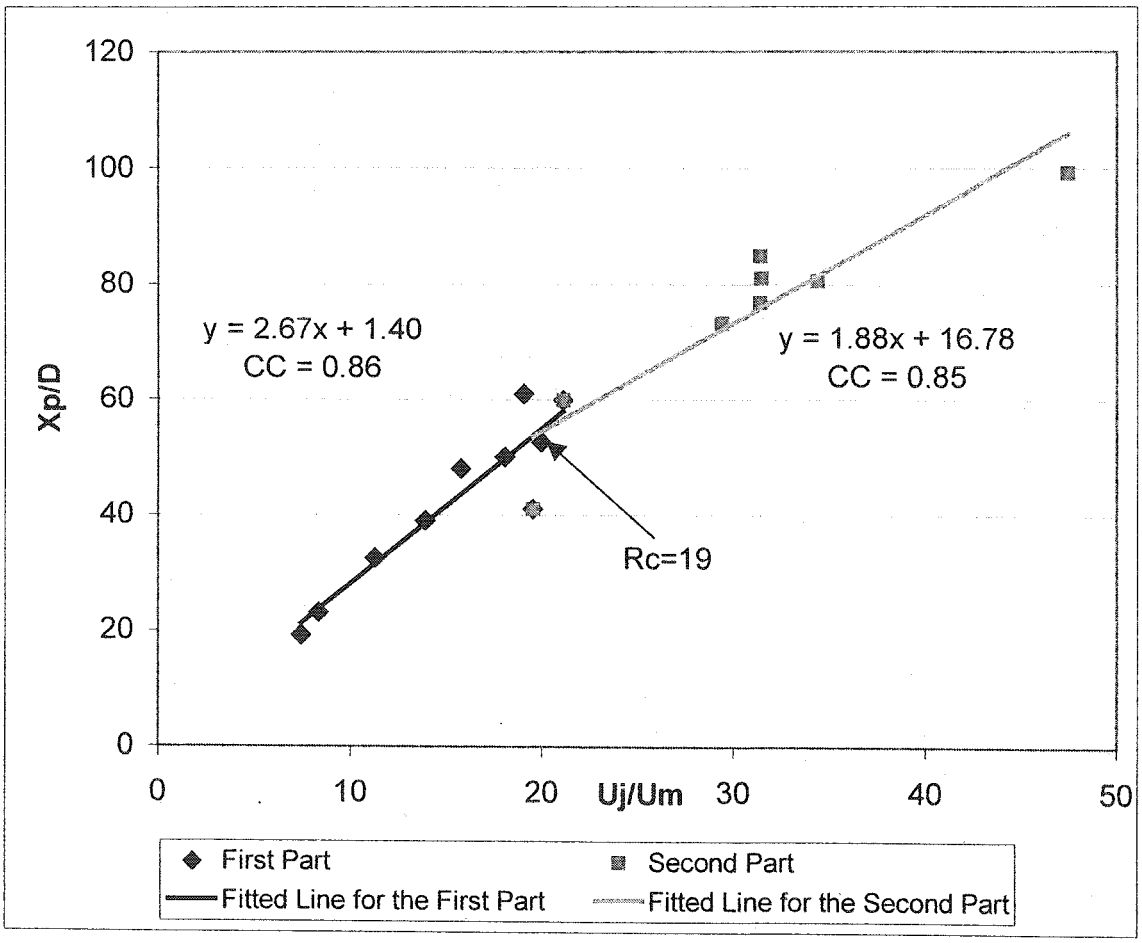

Figure 3-6. Penetration length of a 6.35 mm jet in a counter flow.

In this test the slope of the line fitted to the points with R<Rc=19, or the first part of the data, is 2.67 and for the second part, R>Rc, it drops to 1.88. A comparison

between above three graphs shows the increasing of the jet diameter reduces of Rc and slope of the second part while it increases the slope of the first part. This test shows that although there is at least one R at which the slope of the line fitted to the test data falls, but this value changes from one jet diameter to another.

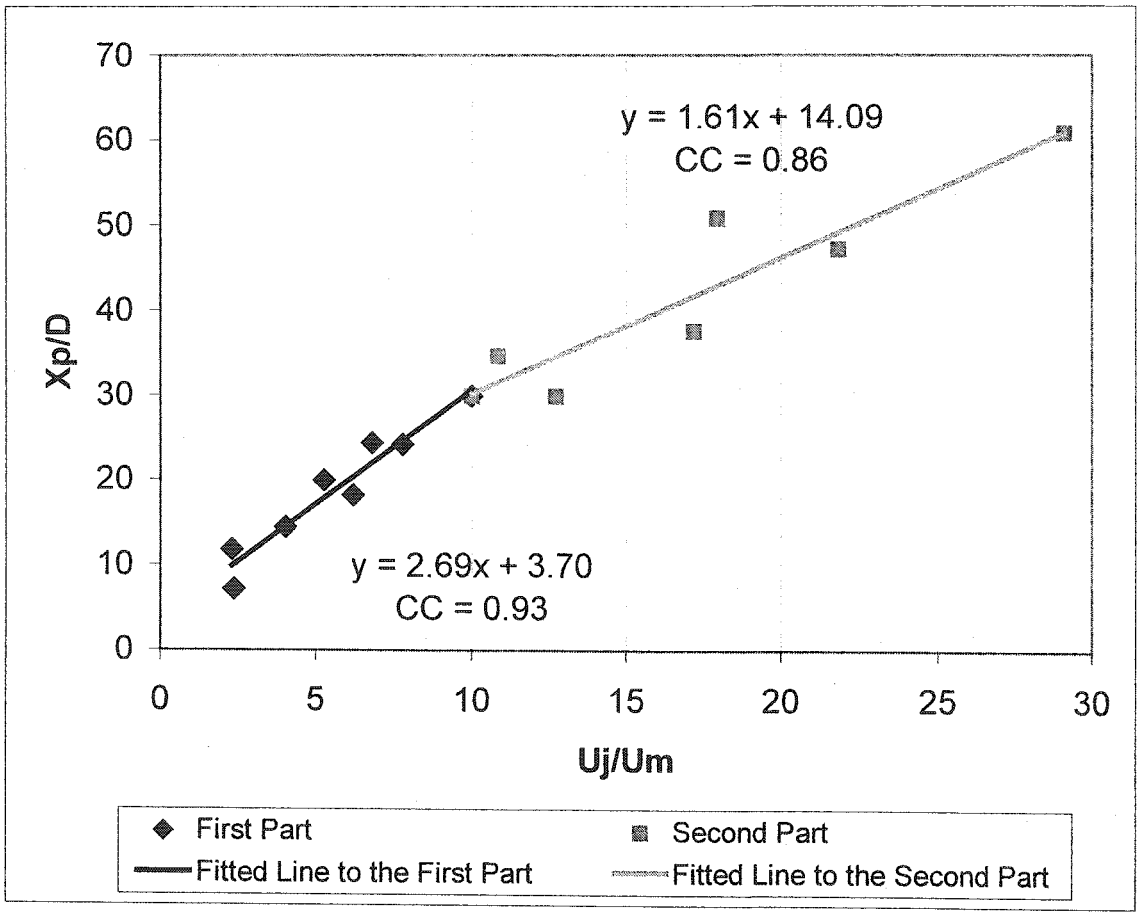

Figure 3-7. Penetration length of a 9.575 mm jet in a counter flow.

To have a criteria for the first value of R, some more tests have been performed. The two next graphs show the results of test with jets of D= 9.525 mm and

D=12.7 mm (figures 3-7 and 3-8). Both graphs support the idea of the effect of W/D on penetration length.

In Figure 3-8, one immediately notices that the better fitting for the whole data will be a curve. A curve is fitted to the data and shows a high correlation coefficient, or CC, very close to 1.00 (Figure 3-9).

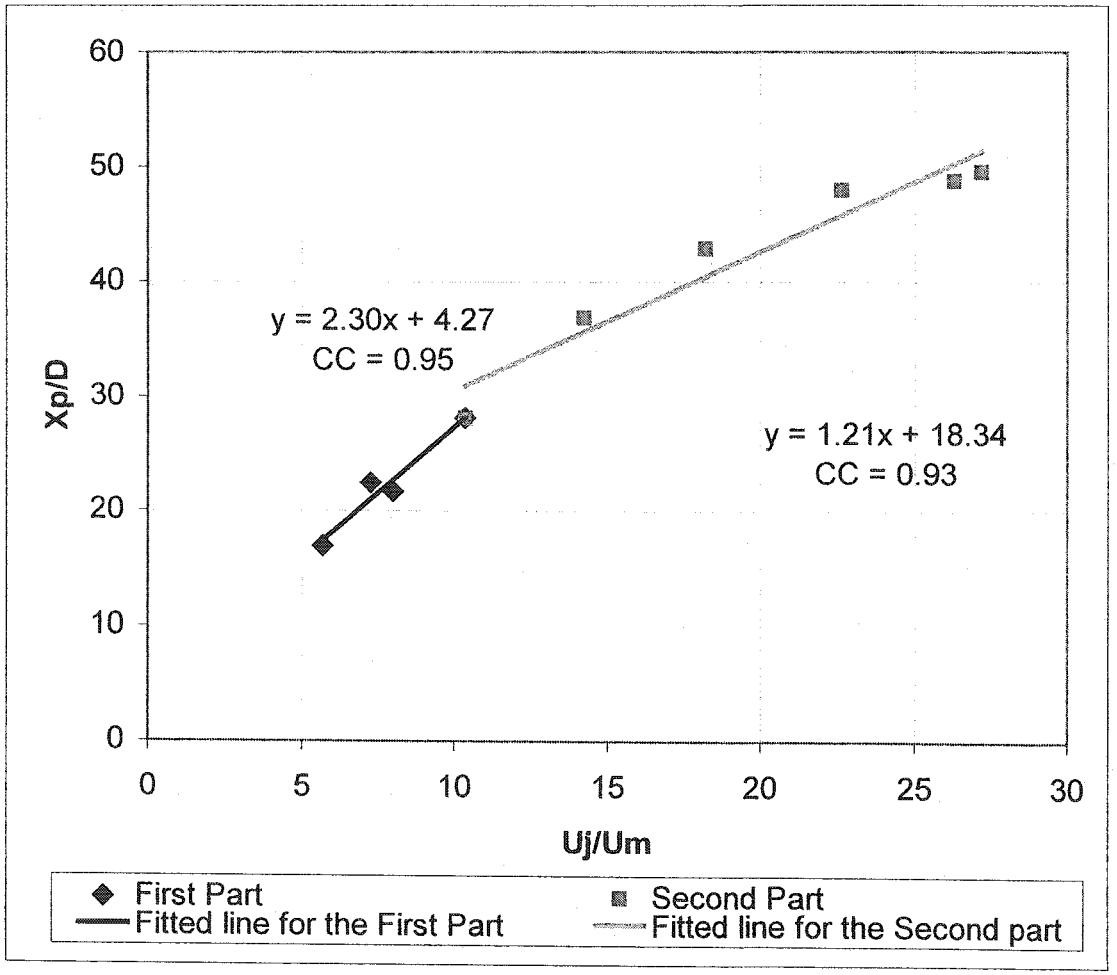

Figure 3-8. Penetration length of a 12.7 mm jet in a counter flow.

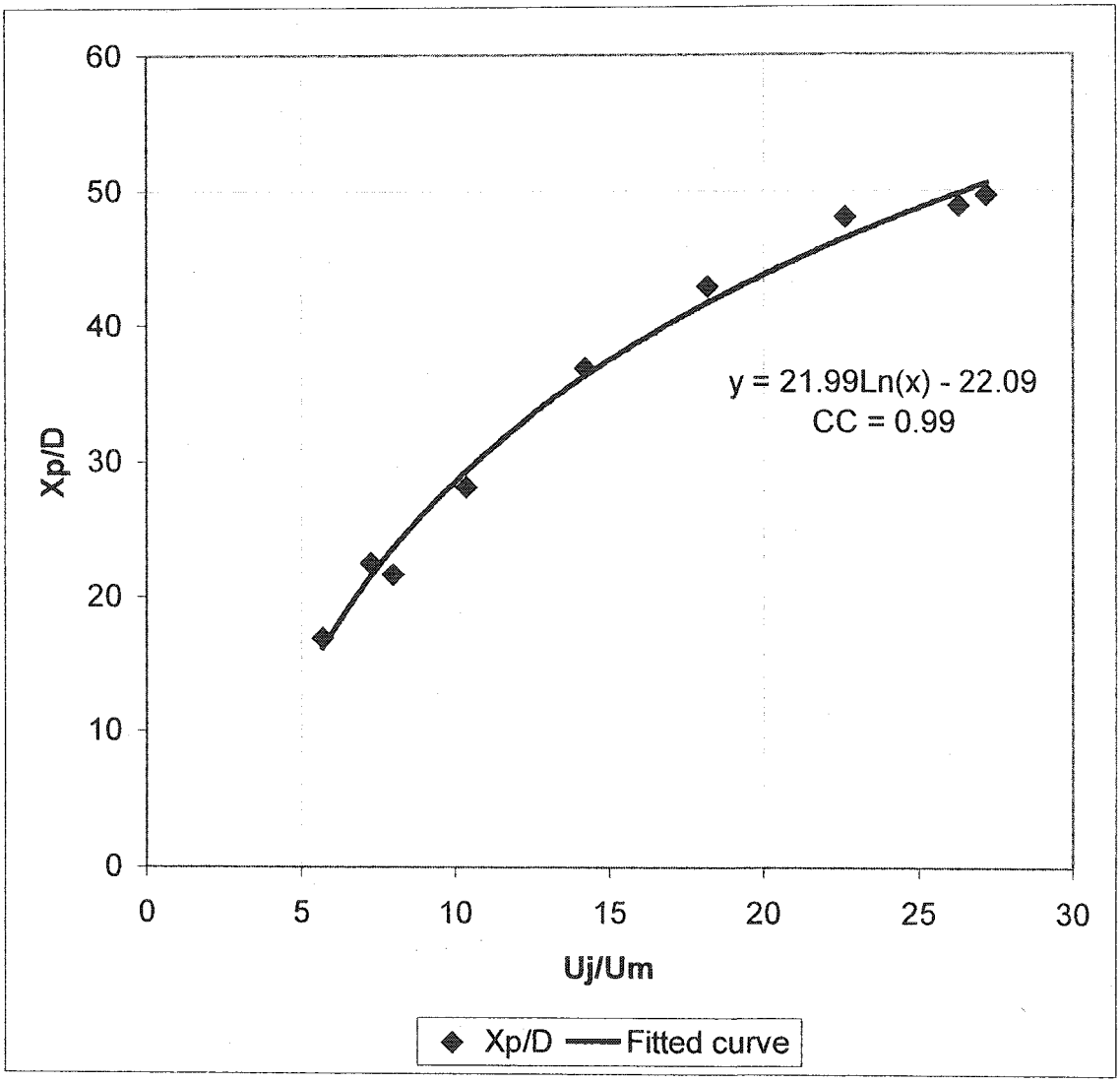

Figure 3-9. Penetration length of a 12.7 mm jet in a counter flow. A curve is fitted to the data.

The next step is to find the criteria for variation of Rc and the jet diameter. The next section is allocated to achieve this goal.

3.4.3. Critical Uj/Um ratio (Rc)

The ratio of Rc at the changing slope point versus the ratio W/D is plotted and a logarithmic curve has been fitted to the data (Figure 3-10).

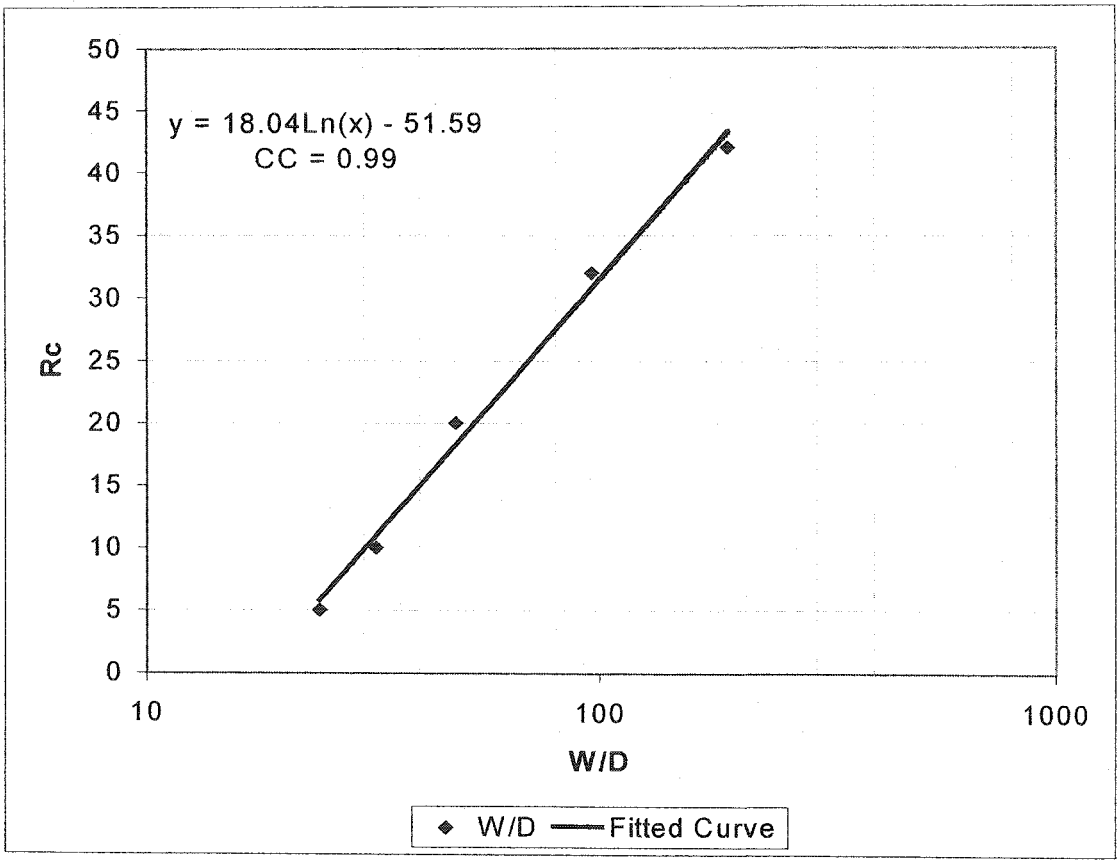

Figure 3-10. The critical Uj/Um ratio versus W/D.

To find the minimum W/D that happens for Rc=0, the fitted equation was solved for y=0. The answer is 17.46 which means for the W > 17.46 D, the jet will be critical regardless what its velocity is.

Since the change in the behavior of penetration length is a function of the W/D, it can be interpreted as the effect of the confining boundaries on the penetration length. The present jet is classified as a confined jet. Thus, R_c can also be called the entrance of confinement for jets.

Chapter 4

Structure of flow and turbulence

4.1 General remarks

The structure of counter flowing free jet turbulent flow is the subject of this chapter. As the jet flow penetrates the main flow, all its characteristics such as centerline velocity, lateral or radial velocity, and turbulence intensity change. In the following sections, all the processed raw data and also the reduced data are presented along with analysis of data.

The variation of the centerline velocity, the turbulent intensities, the relations between the Radial and the axial turbulence intensities, and also the reduced data of these parameters are shown in this chapter. As a general rule, in all the figures of this chapter, the numbers in the legend of each graph, R indicates the ratio of jet exit velocity to the main flow velocity or U_j/U_m.

4.2 Centerline velocity

4.2.1 General remarks on the background

Since the measurement of the centerline velocity of the jet needs special devices, only few of the investigators provided information on this issue. Abramovich (1963) mentions that for a submerged jet, axial velocity, U, at any distance, X, along the centerline of a round free jet can be described by:

$$U = \frac{\text{const.}}{X} \qquad [4\text{-}1]$$

Rajaratnam (1976), using dimensional analysis approach presents an explanation for this equation.

Lam (1991) presented five graphs related to the axial velocity resulting from his investigations. Each single curve shows the behavior of the parameter U/Ux with X/D with no discussion of results.

4.2.2 Present study

In figures 4-1.a to 4-1.e results of several tests on the centerline velocity decay are shown. A very obvious observation is that at higher jet velocity ratios R, the velocity decays more smoothly. However, the centerline velocity abruptly drops in the domain X/Xp<0.2. When R increases and approaches to infinity, a

submerged jet approximates the free jet. Figure 4-1.f shows this approximation is in agreement with the obtained data. In this figure, the velocity decay rate of submerged jet, $\frac{U}{U_j} = \frac{5.4}{\frac{X}{D}}$, is completely fitted to the curves of R=35 and R=54. According to figure 4-1.a to 4-1.e, for a smaller R, decay rate becomes more linear and can be approximated by a line.

A small horizontal part of curves in figures 4-1.4 to 4-1.e denotes the core at which the velocity of a jet is constant and equal to the jet velocity at the exit. For the bigger R this part is not considerable since the penetration length is much longer than the core while for the small R, length of the core is comparable to the penetration length.

In the region close to the stagnation, regardless the value of R, the velocity changes linearly and after this points all curves become horizontal as expected since $\frac{U_m}{U_j}$ is constant for each case.

Beltaos (1973) recommended for the radial expansion of the jet:

$$y = 0.26\,x \qquad [4\text{-}2]$$

If the velocity distribution of the jet across its axis assumed to be in the form of second degree parabola with maximum U at the centerline:

$$U_y = U_i\left(1 - \frac{y^2}{y_0^2}\right) \qquad [4\text{-}3]$$

where:

U_y = axial velocity in radial distance of y from the centerline,

U_i = centerline axial velocity that has the maximum value in the section i,

y = radial distance from the centerline,

y_0 = maximum expansion of the jet in the section where the axial velocity is zero.

If the discharge issued by the jet at a section 1 upstream of the jet is Q_1 and in a section 2 upstream of the section 1 is Q_2, because of the enteranment of jet to the main flow, one can assume:

$$Q_1 = KQ_2 \qquad [4\text{-}4]$$

K is a constant that indicates the jet discharge decay rate.

$$Q_i = \int U_y \, dA = \int_0^{y_1} U_1 (1 - \frac{y^2}{y_0^2}) = \frac{\pi}{2} U_1 y_1^2 \qquad [4\text{-}5]$$

and similarly:

$$Q_2 = \frac{\pi}{2} U_2 y_2^2 \qquad [4\text{-}6]$$

Using equations 4-4, 4-5, and 4-6, K can be found.

$$K = \frac{Q_1}{Q_2} = \frac{\frac{\pi}{2} U_1 y_1^2}{\frac{\pi}{2} U_2 y_2^2} = \frac{U_1 y_1^2}{U_2 y_2^2} \qquad [4\text{-}7]$$

$$\text{or } \frac{U_1}{U_2} = K \frac{y_2^2}{y_1^2} \qquad [4\text{-}8]$$

On the other hand it is found previously (Beltaos 1999) and verified by the present study:

$$\frac{U_1}{U_j} = \frac{C}{\frac{x_1}{D}} \qquad [4\text{-}9]$$

and $$\frac{U_2}{U_j} = \frac{C}{\frac{x_2}{D}}. \qquad [4\text{-}10]$$

Dividing equation 4-9 by equation 4-10 gives:

$$\frac{U_1}{U_2} = \frac{x_2}{x_1} \qquad [4\text{-}11]$$

Equalizing equation 4-8 and 4-11, K will be found:

$$\frac{U_1}{U_2} = \frac{x_2}{x_1} = K\frac{y_2^2}{y_1^2}$$

or

$$\frac{x_2}{x_1} = K\frac{y_2^2}{y_1^2} \qquad [4\text{-}12]$$

If equation 4-2 is used,

$$\frac{x_2}{x_1} = \frac{0.26y_2}{0.26y_1} = K\frac{y_2^2}{y_1^2} \qquad [4\text{-}13]$$

from there:

$$K = \frac{x_2}{x_1} \text{ and } \text{Length of the core} \le x_1, x_2 \le 0.8x_p \qquad [4\text{-}14]$$

can be introduced as the discharge decay rate. The above calculation shows that the discharge linearly decays along the centerline.

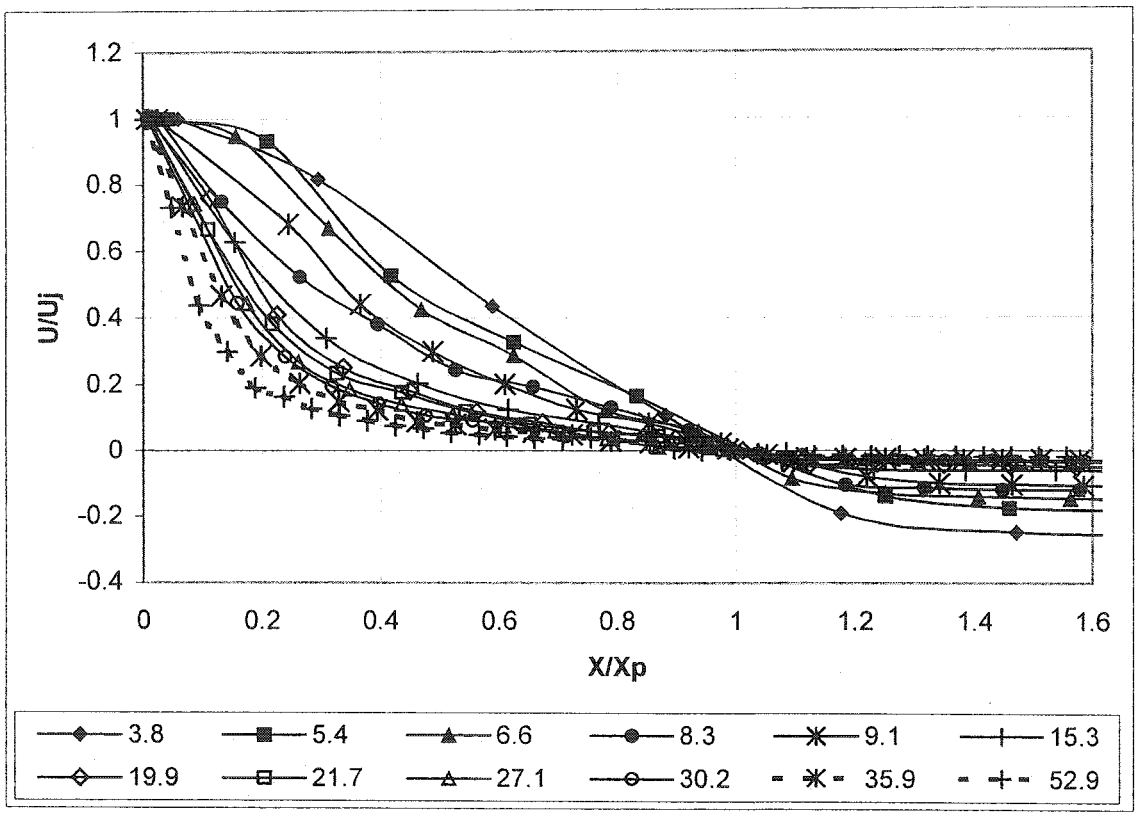

Figure 4-1.a The velocity decay rate along the centerline (D=1.587 mm)

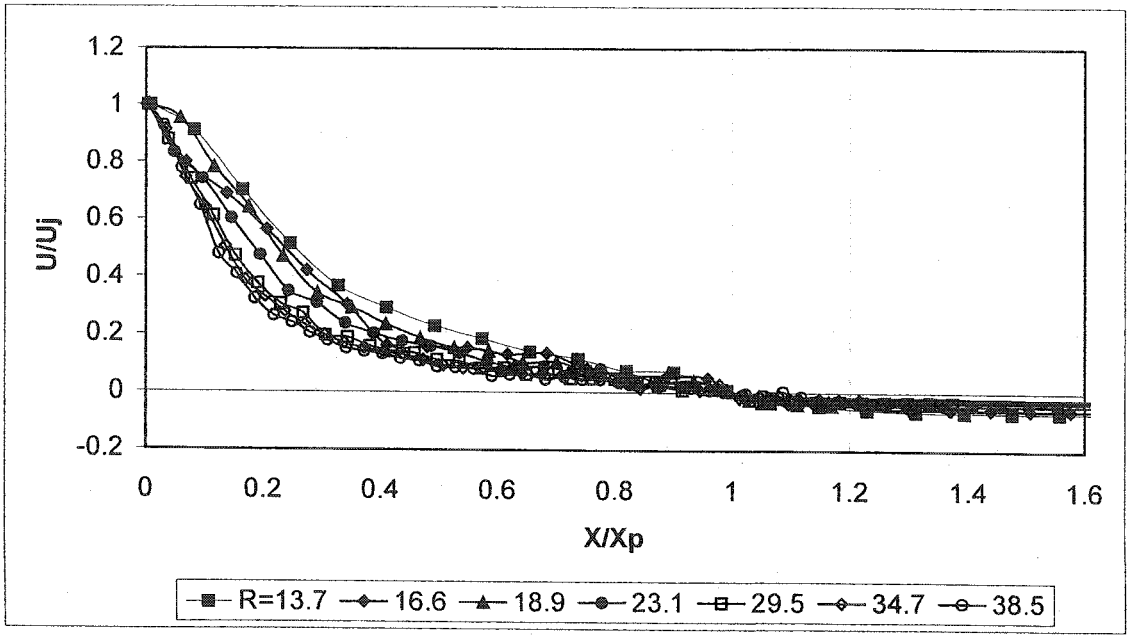

Figure 4-1.b The velocity decay rate along the centerline (D=3.175 mm)

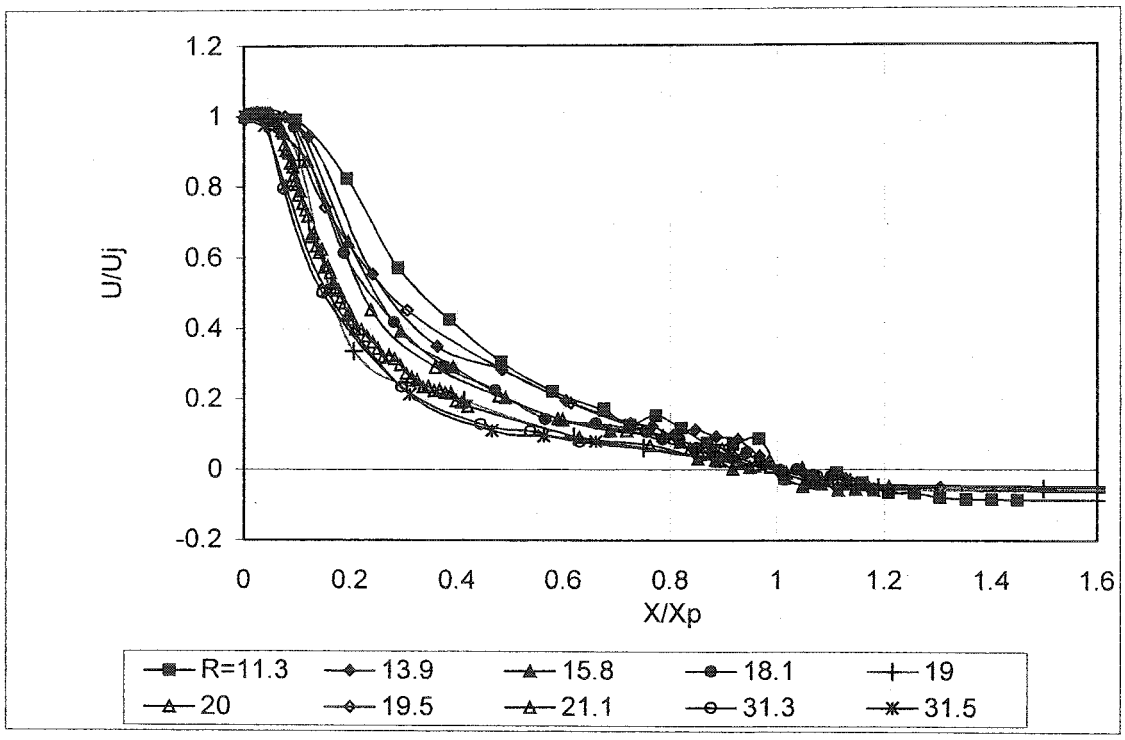

Figure 4-1.c The velocity decay rate along the centerline (D=6.35 mm)

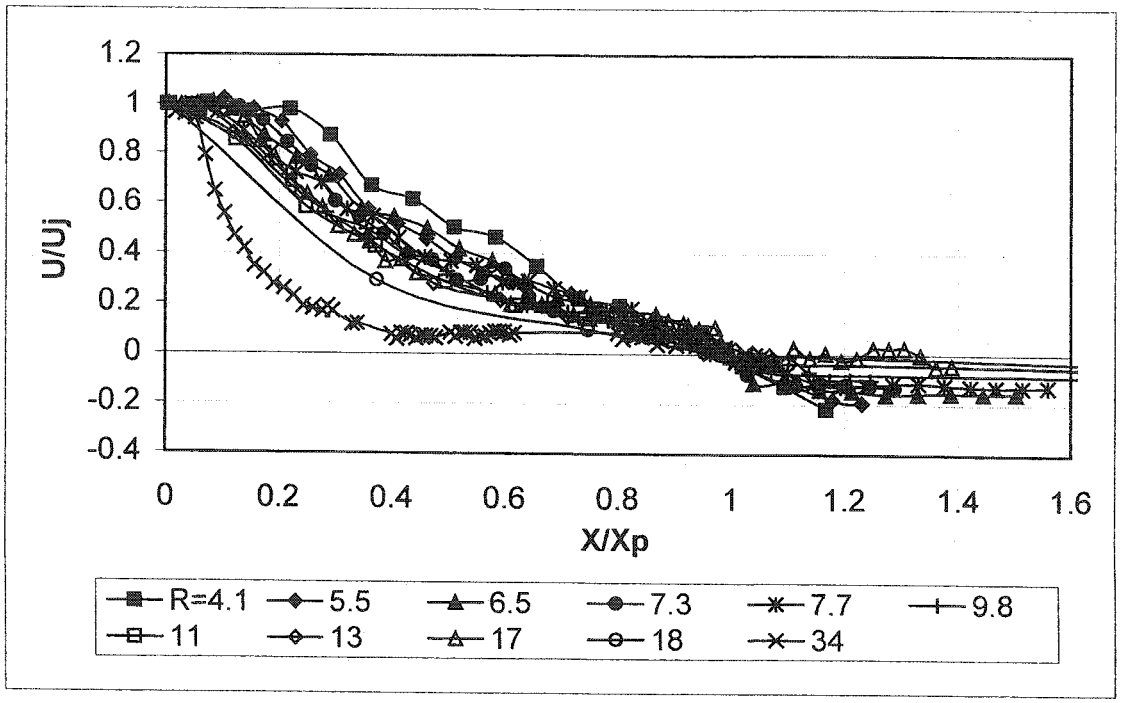

Figure 4-1.d The velocity decay rate along the centerline (D=9.575 mm)

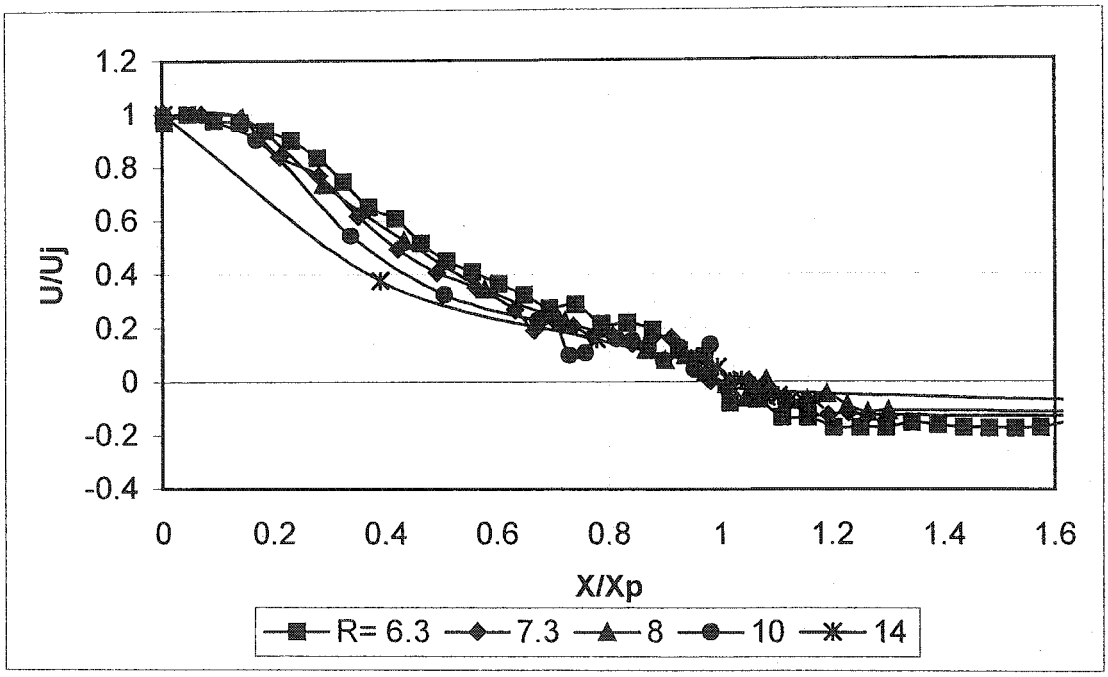

Figure 4-1.e The velocity decay rate along the centerline (D=12.7 mm)

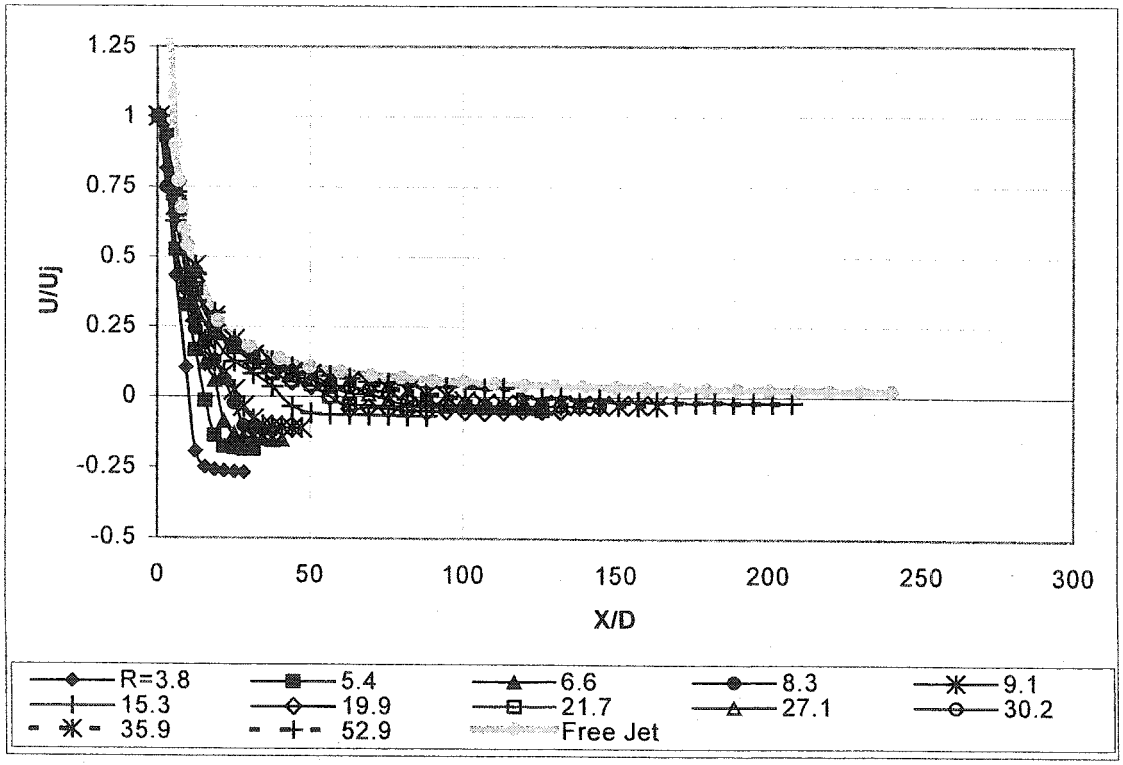

Figure 4-1.f The velocity decay rate along the centerline (D=1.5875 mm)

4.3 Turbulence intensity

Dryden and Kuethe (1930) defined the turbulence intensity initially as the root mean square of turbulence fluctuations:

$$\mathrm{Urms} = \sqrt{\overline{u^2}} \qquad [4\text{-}2]$$

and the relative turbulence intensity was defined as the ratio of turbulence intensity to the mean velocity:

$$\mathrm{TurbulenceIntensity} = \frac{U_{rms}}{U} \qquad [4\text{-}3]$$

Later on, many investigators including those two mentioned above, preferred to use the term Turbulence Intensity" instead of "Relative Turbulence Intensity" (Hinze 1975).

In some cases, it is also preferred to have two references for turbulence: local turbulence intensity with the same definition as equation 4-3 and turbulence intensity in which a constant velocity is used instead of the mean velocity at the point. This term is very useful for the cases where the mean velocity approaches to zero and consequently the turbulence intensity becomes infinity. Capp (1983) and Lam (1991 and 1997) are among those who used this term to display their data. In the case of radial turbulence intensity along the centerline, where the mean radial velocity, V, is zero, the axial velocity is used instead to avoid dividing by zero.

4.3.1 Axial turbulence intensity

4.3.1.1 Local axial turbulence intensity

In figures 4-2.a through 4-2.f the local turbulence intensities are shown. These sketches clearly show the local turbulence intensity along the centerline changes linearly in the range $0 \le \frac{X}{X_p} \le 0.8$. The slope line varies from (H: V) 1:1.25 to 1:1 as the diameter of the jet becomes bigger. For larger nozzle diameter more instability in the local turbulence intensity is predicted. It is also important to view these results keeping in mind the concept of jet confinement, which was previously discussed in Chapter 3.

In figures 4-1 curves show an agreement in the region 0< X/Xp<0.5 where all the curves closely approach the point (0.5,0.5) or attain the slope of 1:1. In the region X/Xp>0.5, curves become steeper and meet at the point (0.8, 1) and have a slope of 1:1.25.

Figures 4-1.d and 4-1.e are two example of the effect of confinement of jet on its behavior. Still in most cases, the points stay on a 1:1 slope line. These two figures also show a high fluctuations in the turbulence intensity, when R is small but when the jet is completely confined, the curves again show the same behavior of the jets in unconfined conditions.

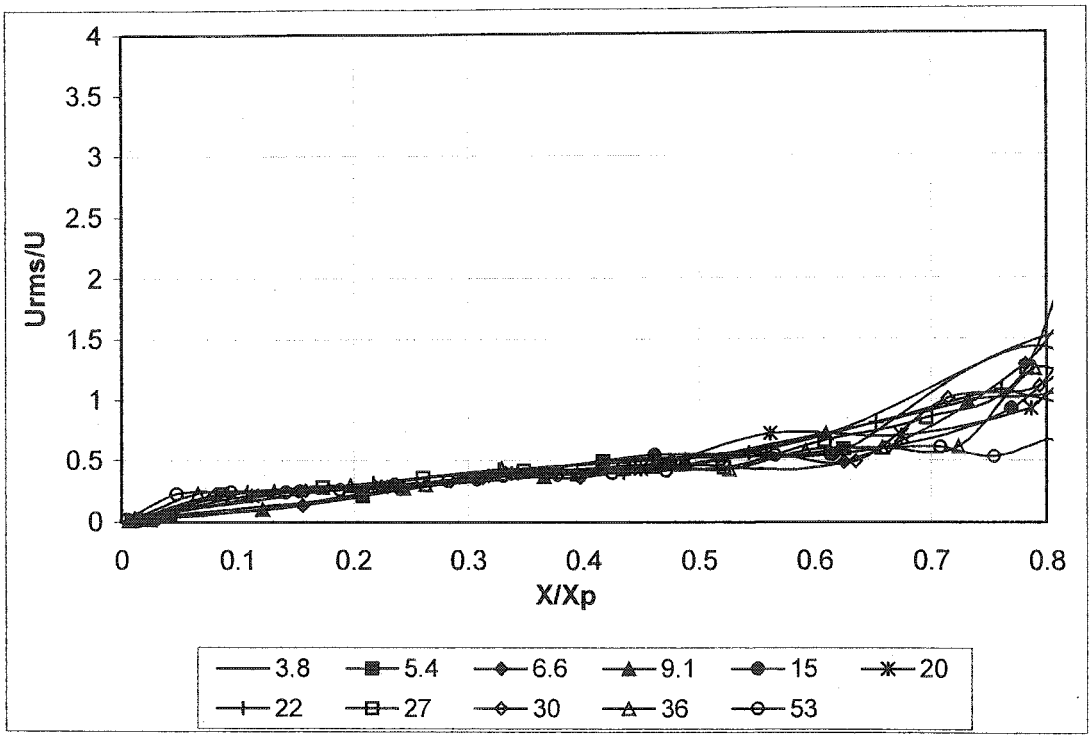

Figure 4-2.a Local axial turbulence intensity along the centerline (D=1.587 mm)

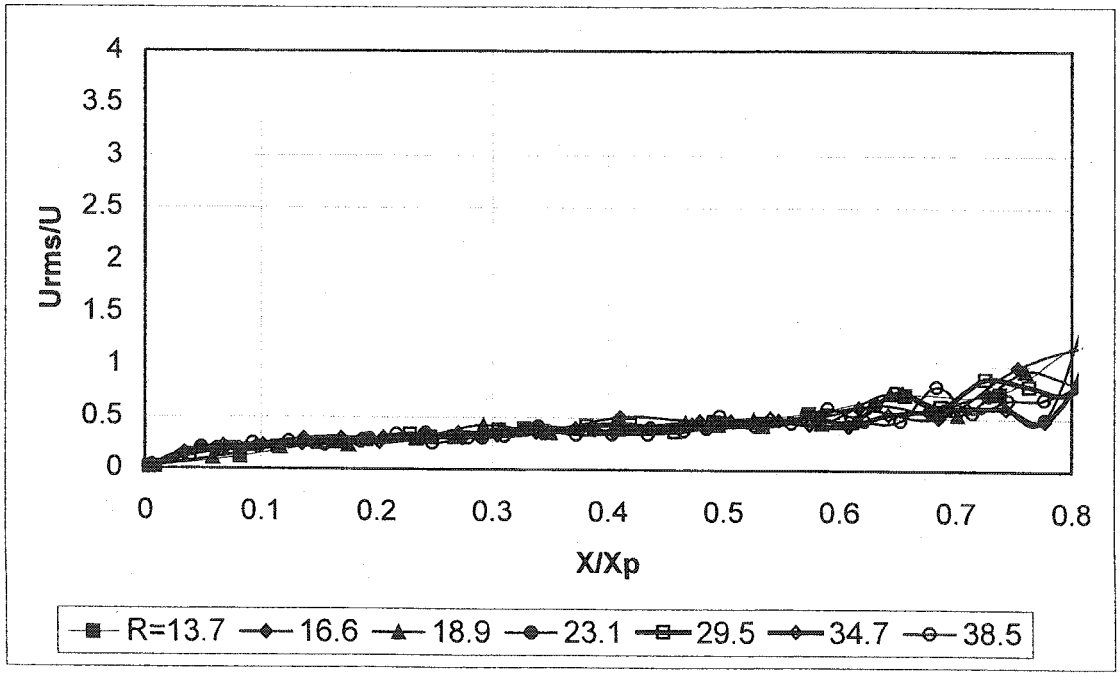

Figure 4-2.b Local axial turbulence intensity along the centerline (D=3.175 mm)

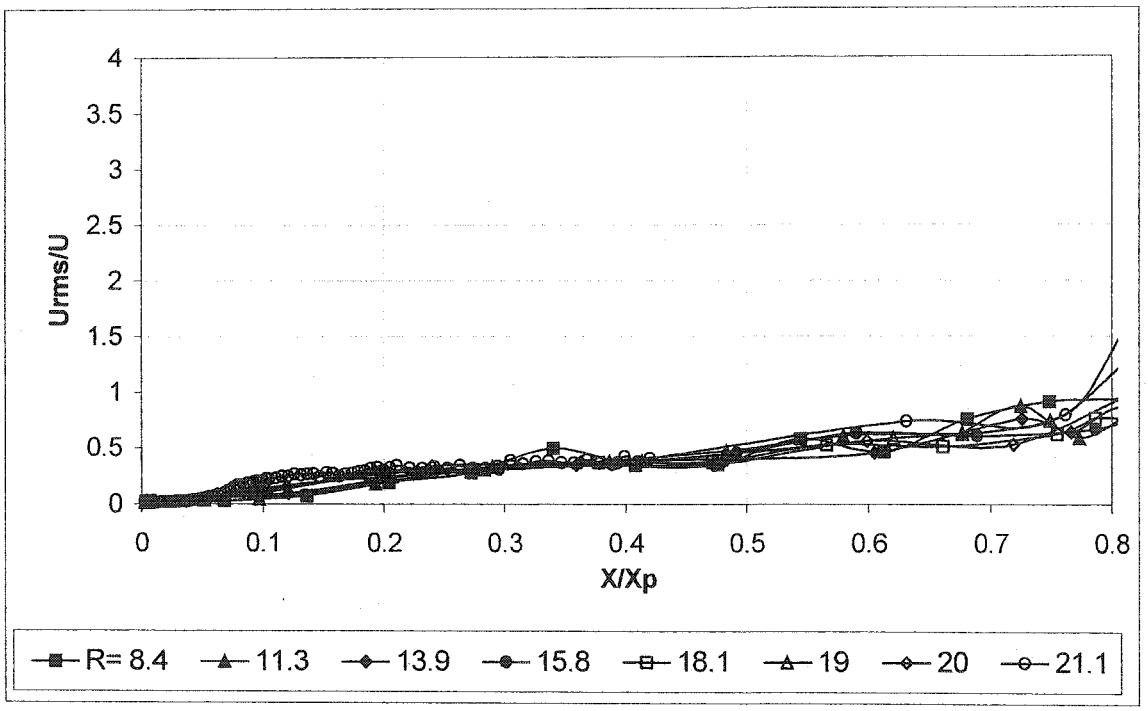

Figure 4-2.c Local axial turbulence intensity along the centerline (D=6.35 mm)

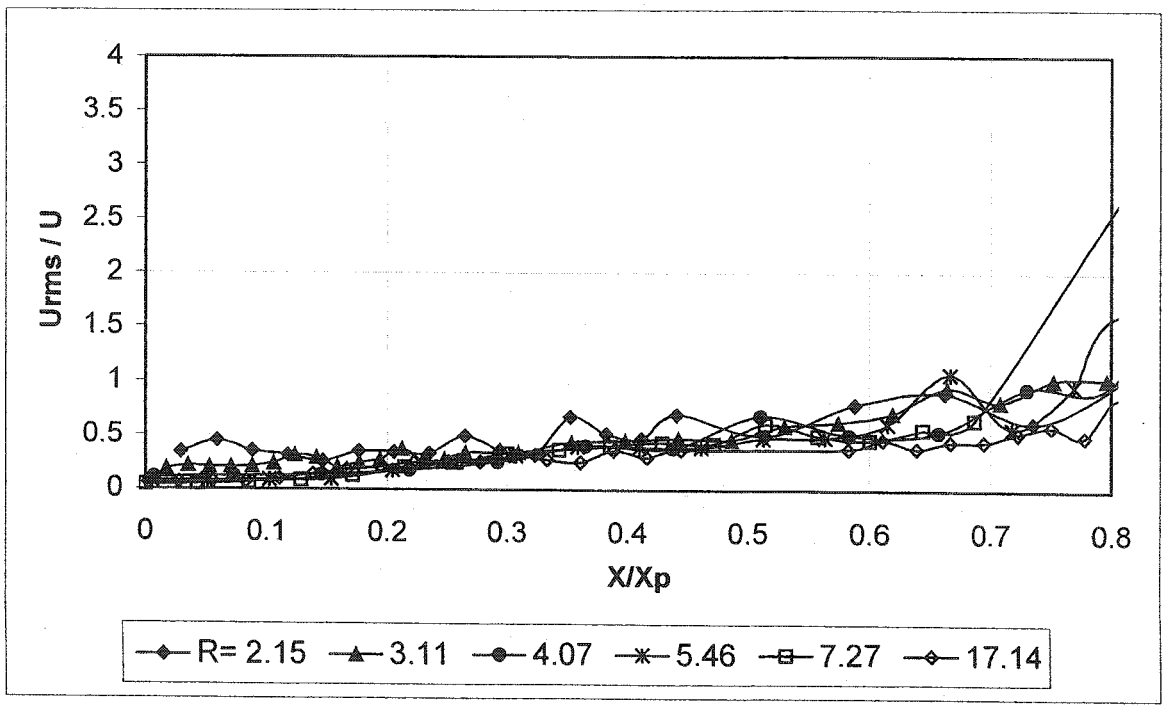

Figure 4-2.d Local axial turbulence intensity along the centerline (D=9.575 mm)

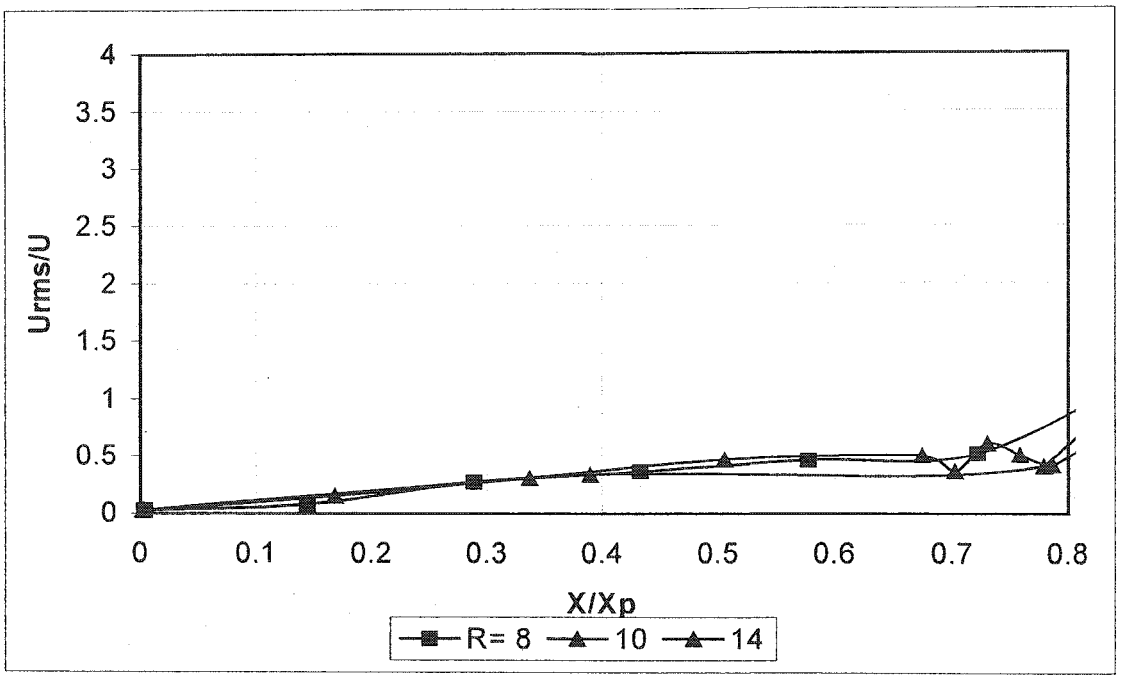

Figure 4-2.e Local axial turbulence intensity along the centerline (D=12.7 mm)

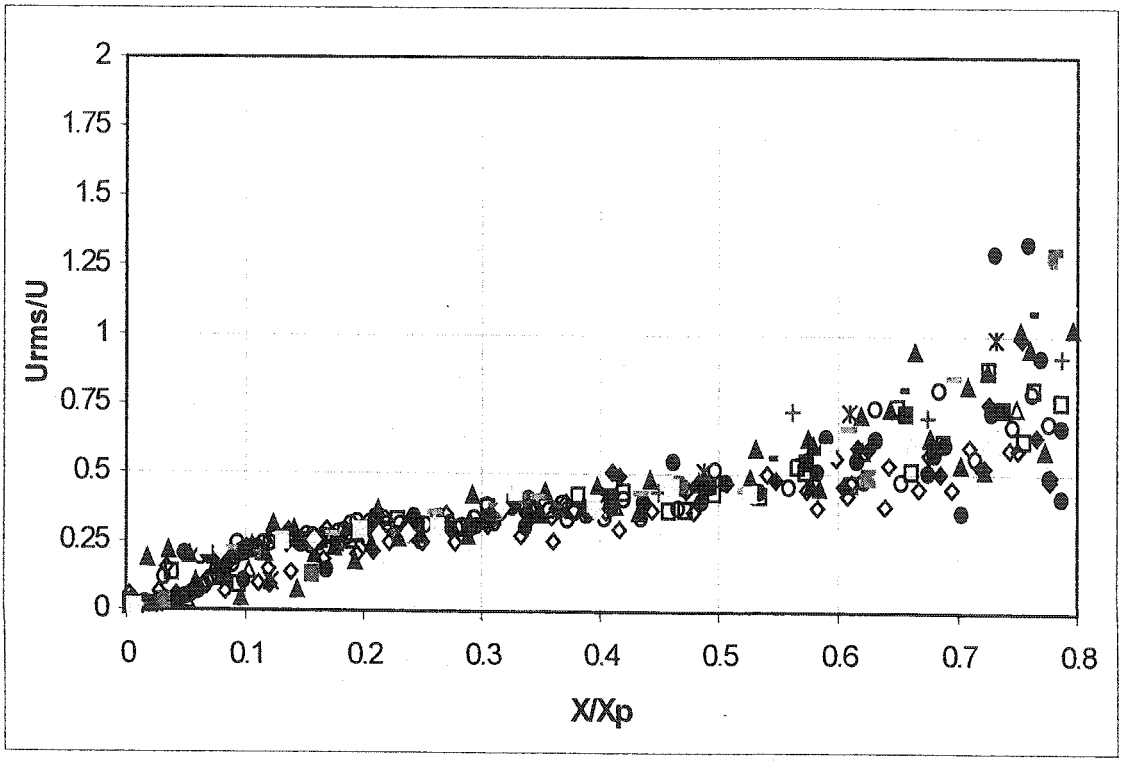

Figure 4-2.f Local axial turbulence intensity along the centerline (all jets)

4.3.2.1 Axial turbulence intensity

Turbulence intensity can be used to identify the domains at which the maximum fluctuation of the velocities occurs. Figures 4-3.a through 4-3.e show such a presentation of turbulence intensity. The first three sets of data show a maximum in the first half of penetration length. As the R for each jet diameter increases, this maximum is getting closer to the jet exit and finally in most cases stay at 0.07 to 0.12 Xp. Also, as the maximum value of the turbulence intensity gets closer to the jet exit, its magnitude decreases.

In the case of confined jet, figures 4-3.d and 4-3.e, the root mean square of velocity fluctuation remains constant along the centerline and increasing the R can reduce the fluctuation in the value of Urms/Uj.

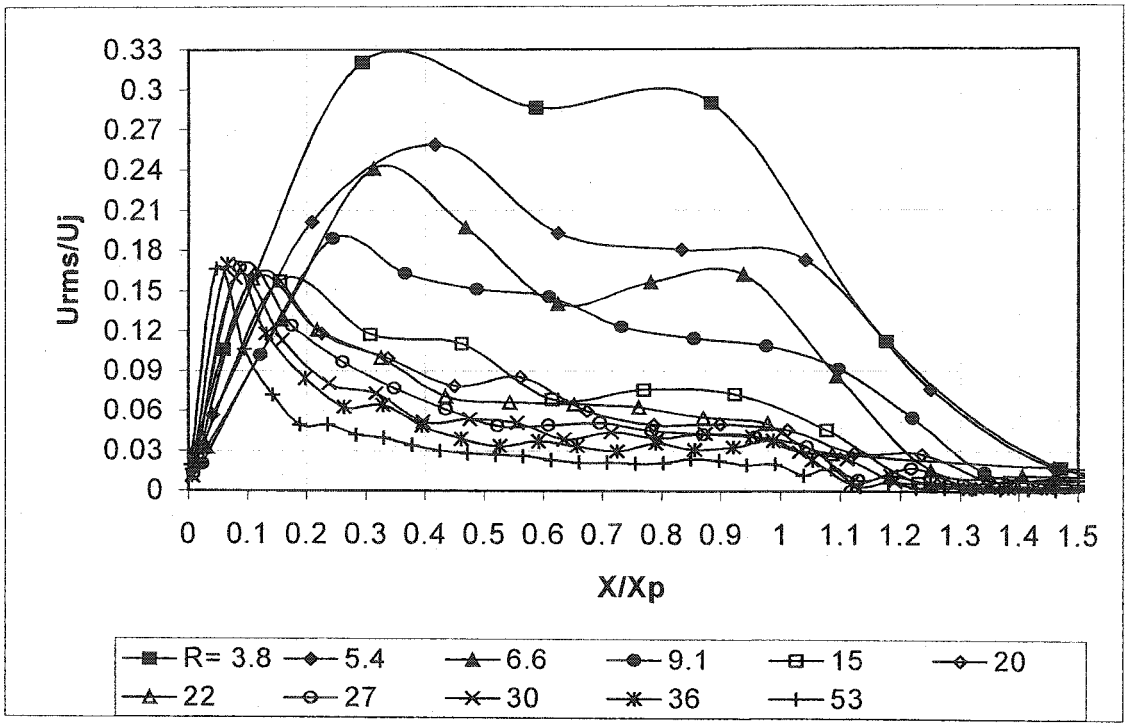

Figure 4-3.a Axial turbulence intensity along the centerline (D=1.587 mm)

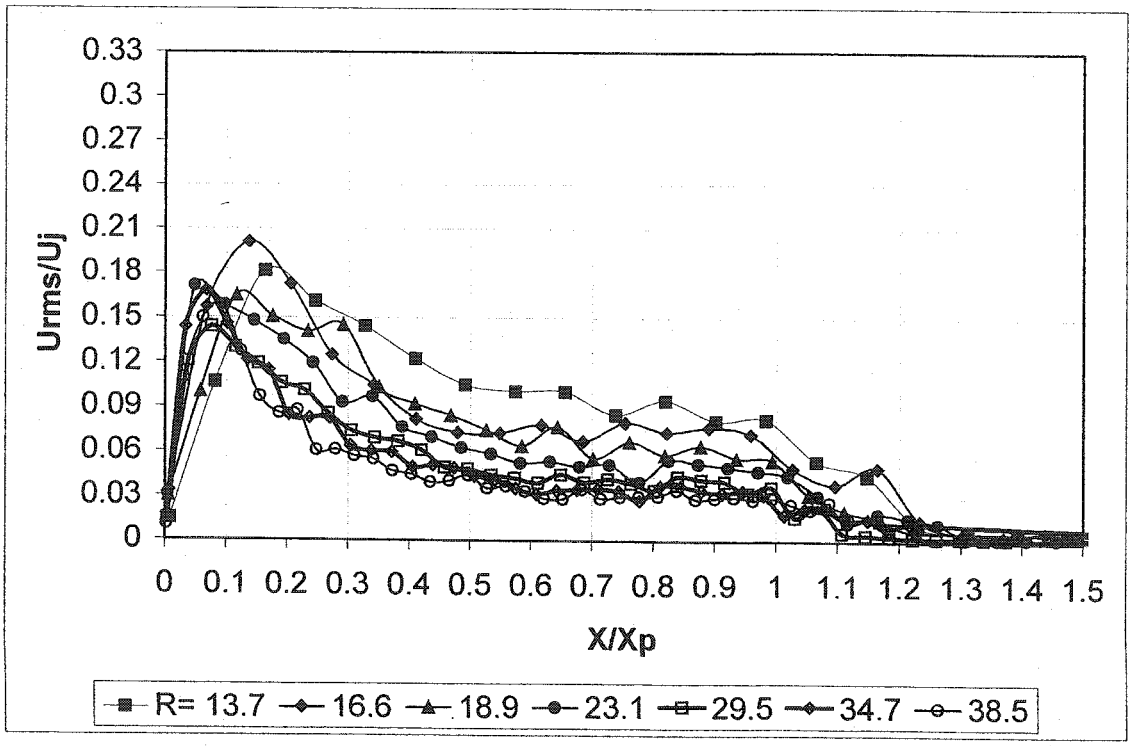

Figure 4-3.b Axial turbulence intensity along the centerline (D=3.175 mm)

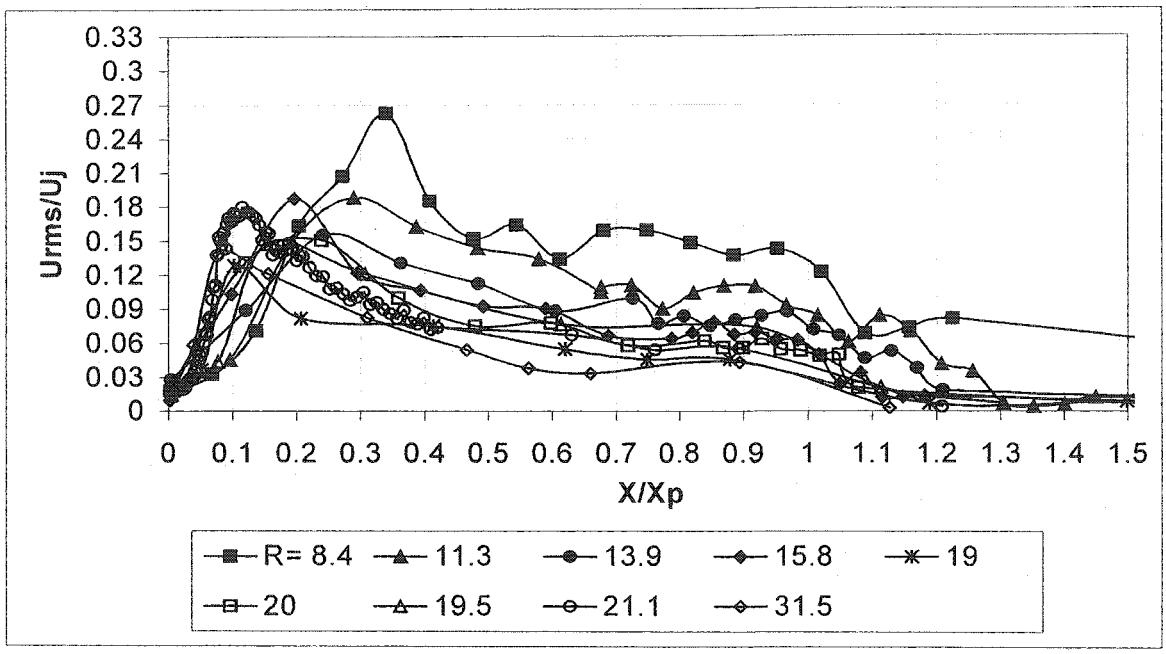

Figure 4-3.c Axial turbulence intensity along the centerline (D=6.35 mm)

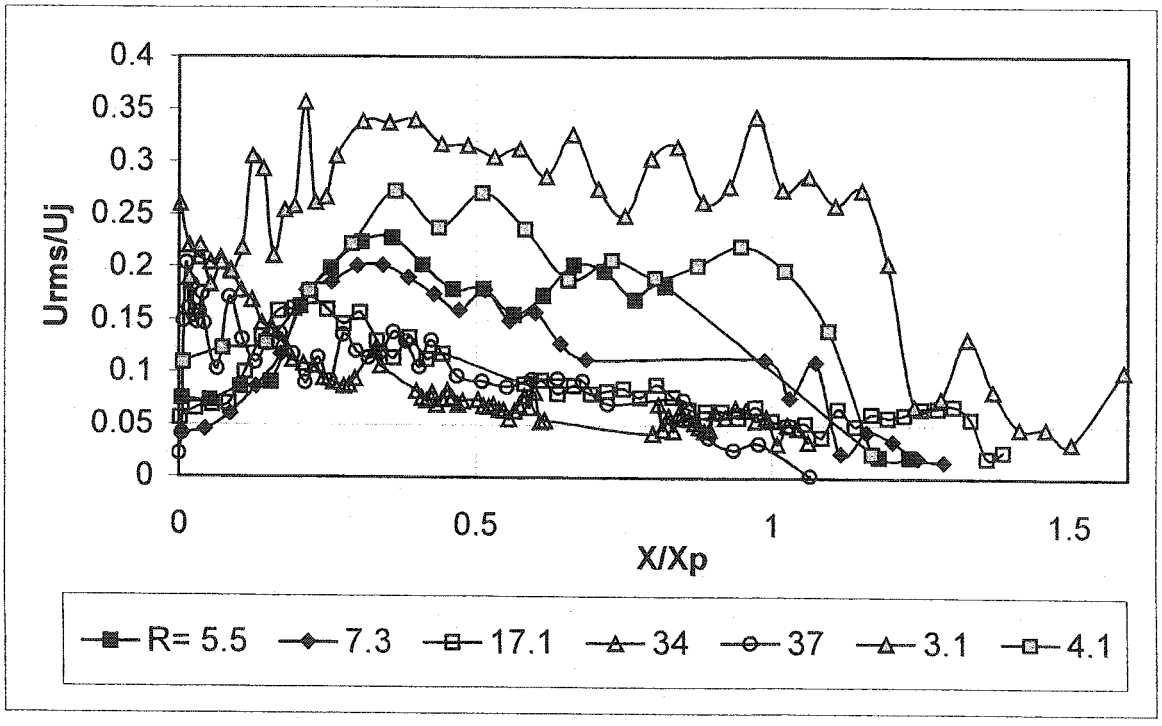

Figure 4-3.d Axial turbulence intensity along the centerline (D=9.575 mm)

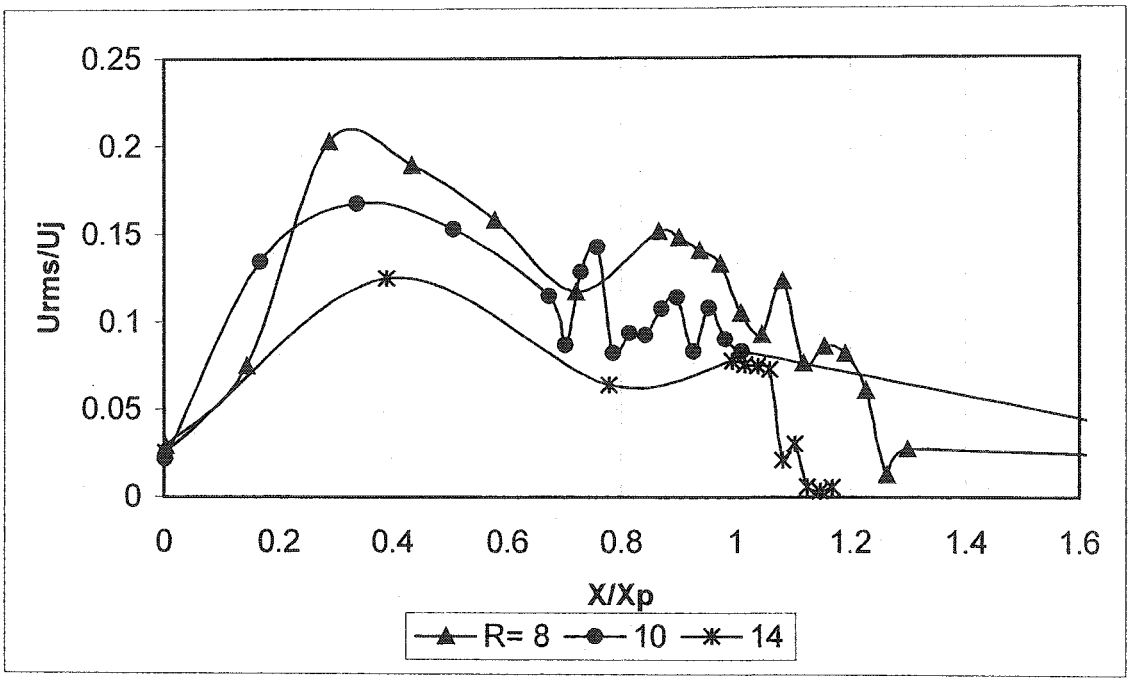

Figure 4-3.e Axial turbulence intensity along the centerline (D=12.7 mm)

4.3.2 Radial turbulence intensity

As it was stated earlier, the Radial velocity fluctuation's intensity, *v*, along the centerline can be defined as the ratio of root mean square of radial velocity fluctuations to a mean velocity. Unlike the axial velocity fluctuation where either jet exit velocity or the axial velocity at the same point can be chosen to calculate the turbulence intensity, the radial velocity along the centerline is zero. Lam (1991) also faced the same problem and chose the jet axial velocity for the reference. Here, following the procedure for axial turbulence intensity, axial velocities of the jet at the centerline and the local point were used to form the radial turbulence intensity and the local radial turbulence intensity respectively.

4.3.2.1 Local radial turbulence intensity

Figures 4-4.a to 4-4.f show the variation of local radial turbulence intensity along the centerline. The graphs show that similar to the axial turbulent intensity, radial turbulent intensity also linearly changes with the distance from the jet exit. Comparing figures 4-2.a to 4-2.f with 4-4.a to 4-4.f, one can notice that there is a very good agreement between these two sets. It is not unexpected since the velocity fluctuation in different directions are not totally independent (Bradshaw 1967,1971,1981, and Hinze 1975). Such an agreement confirms the accuracy of the test procedure.

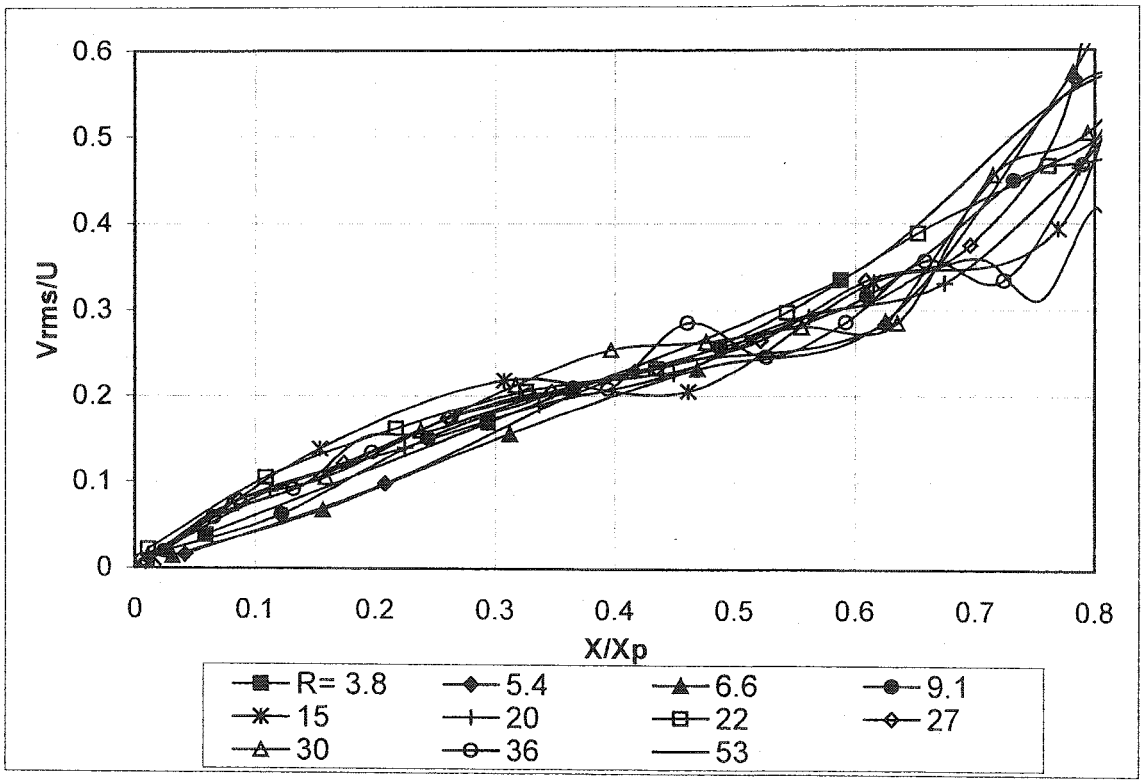

Figure 4-4.a Local Radial turbulence intensity along the centerline (D=1.587 mm)

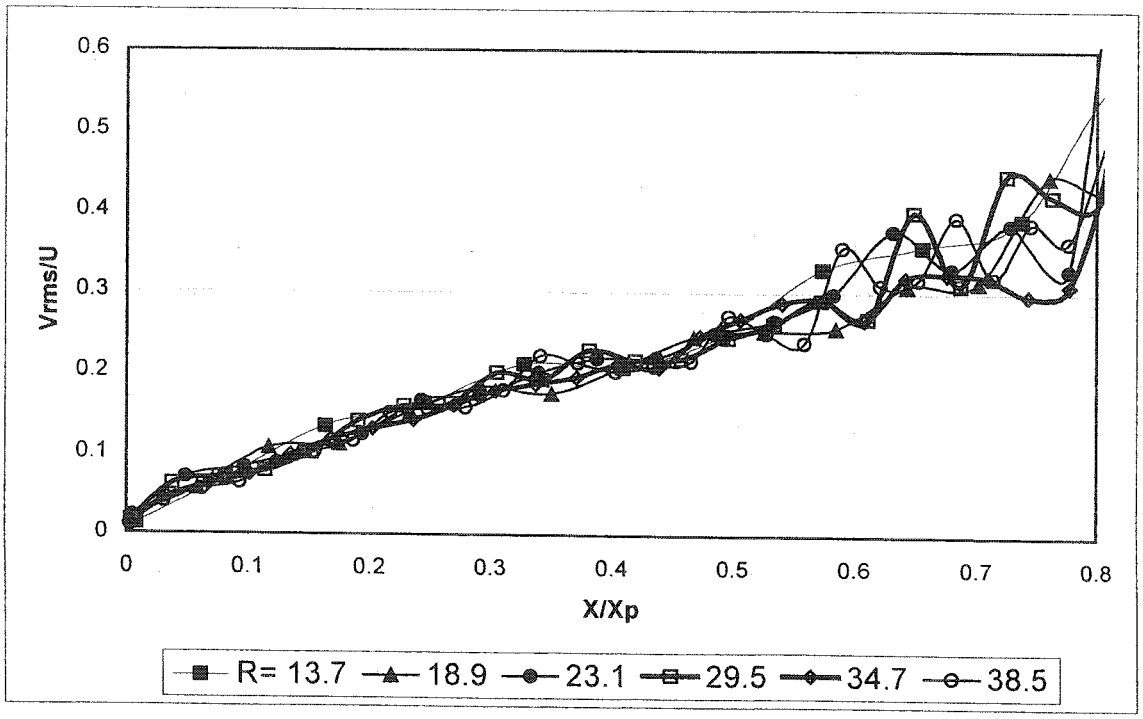

Figure 4-4.b Local Radial turbulence intensity along the centerline (D=3.175 mm)

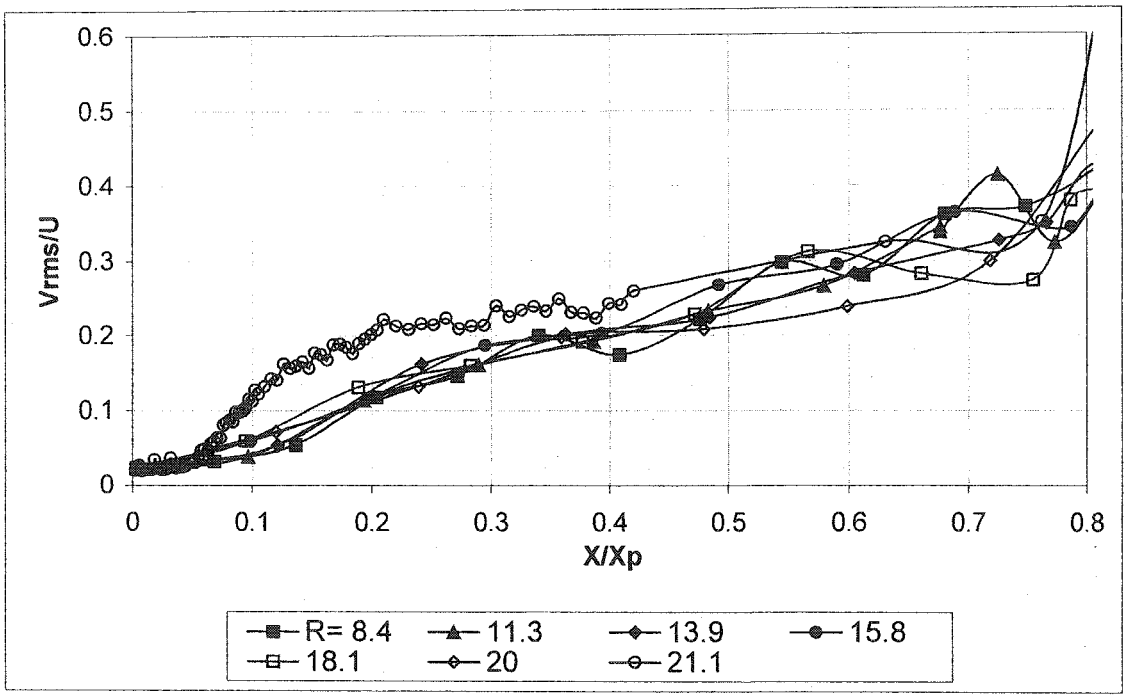

Figure 4-4.c Local Radial turbulence intensity along the centerline (D=6.35 mm)

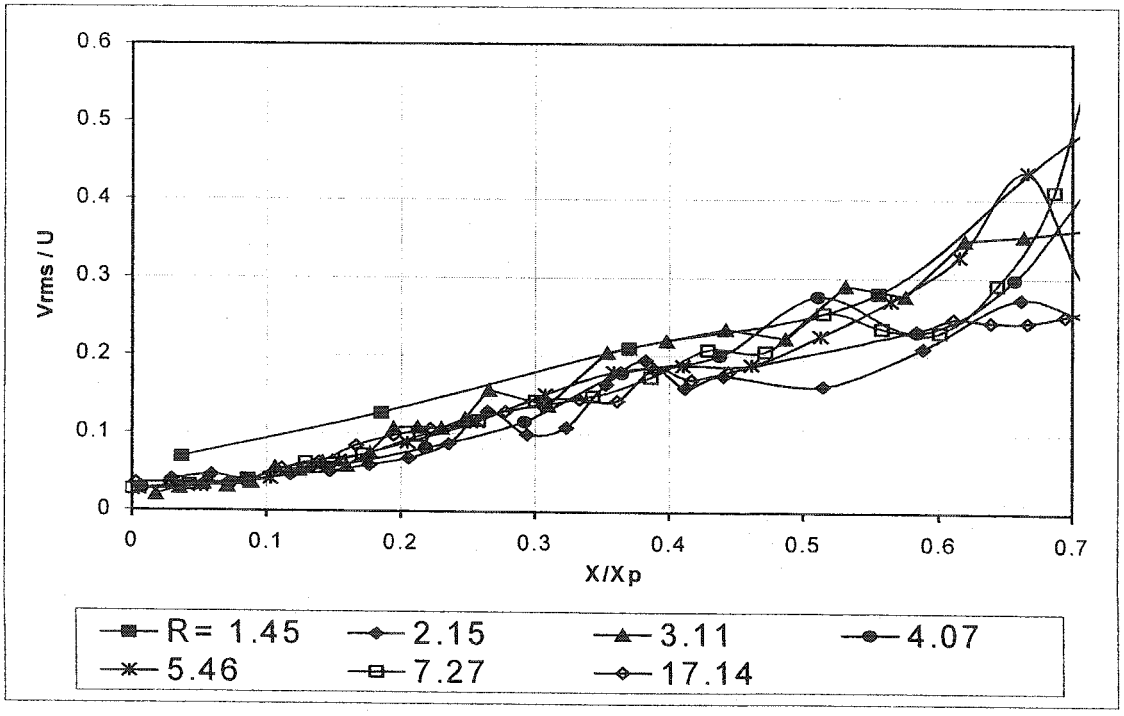

Figure 4-4.d Local Radial turbulence intensity along the centerline (D=9.575 mm)

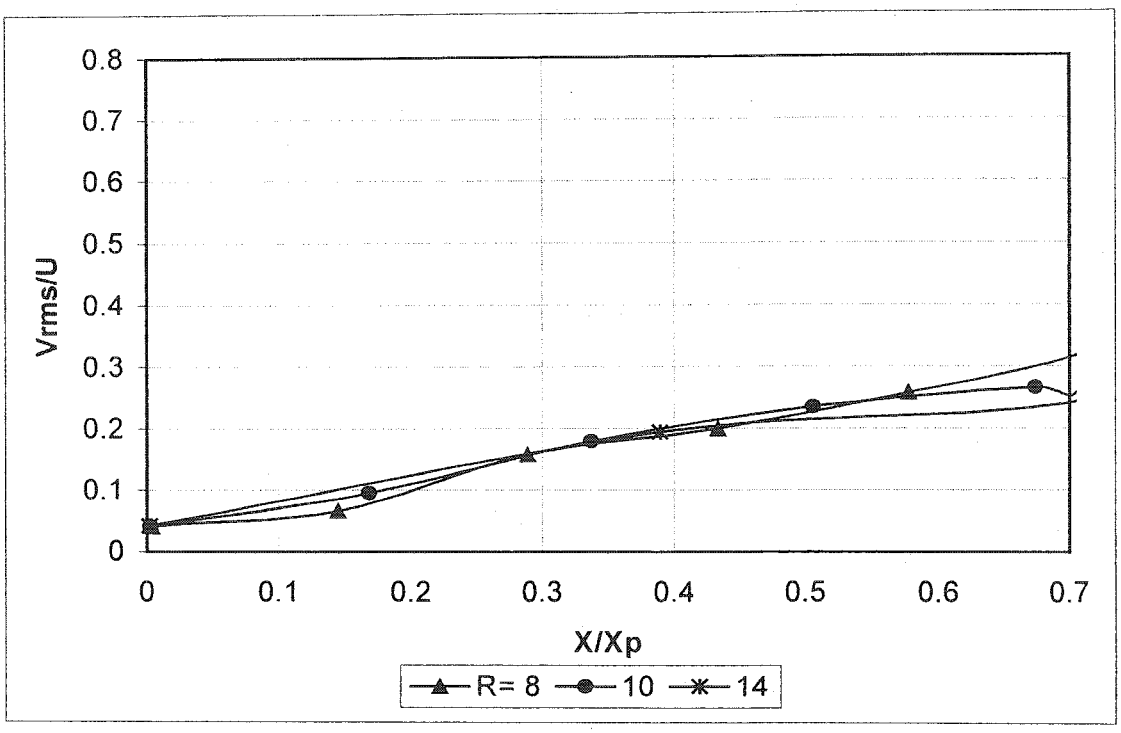

Figure 4-4.e Local Radial turbulence intensity along the centerline (D=12.7 mm)

4.3.2.2 Radial turbulence intensity

Figures 4-5.a through 4-5.f present radial turbulence intensity along the centerline of the jet. These figures show a similarity with the axial turbulence intensity (figures 4-3.a to 4-3.f) in sense of general pattern. In both sets a maximum occurs in the first half of the penetration length and then the fluctuations decline along a smooth curve to a value very close to zero.

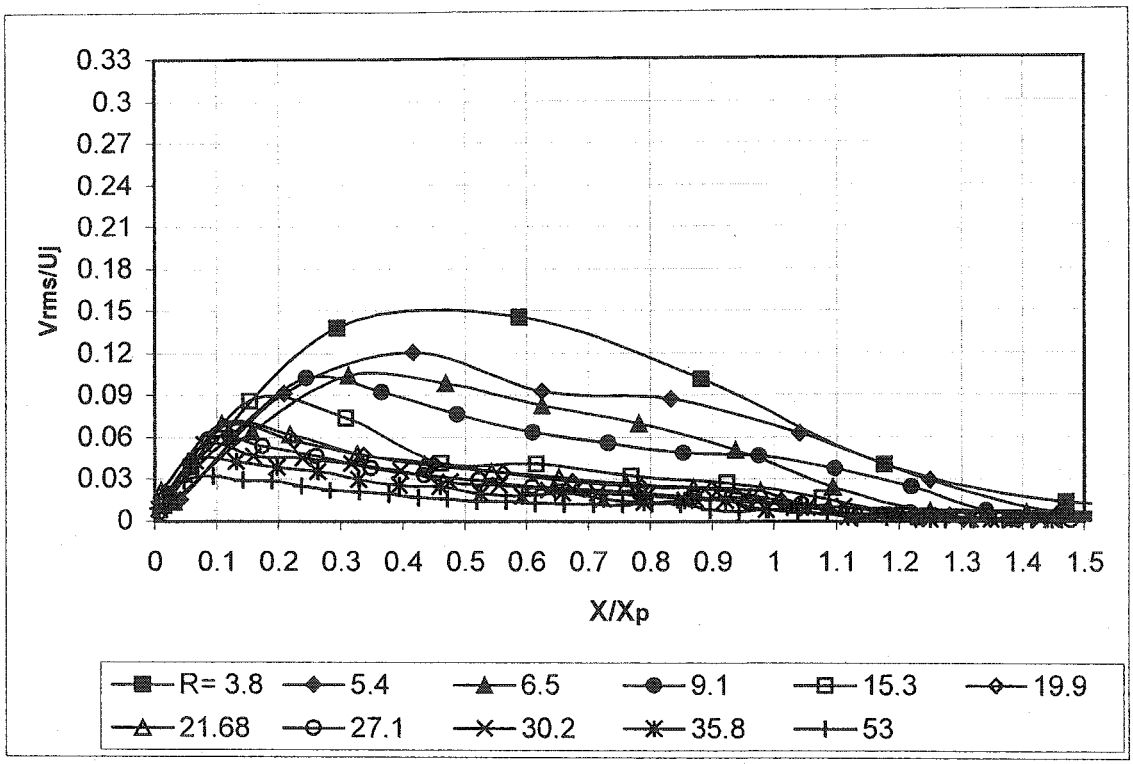

Figure 4-5.a Radial turbulence intensity along the centerline (D=1.587 mm)

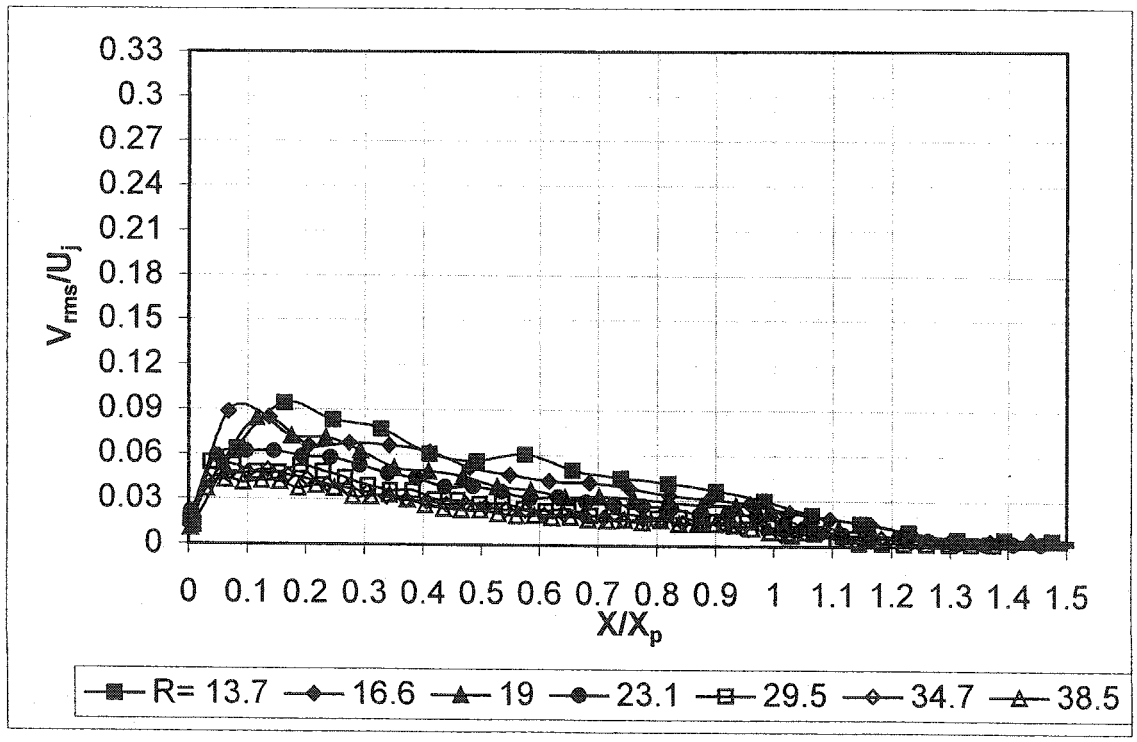

Figure 4-5.b Radial turbulence intensity along the centerline (D=3.175 mm)

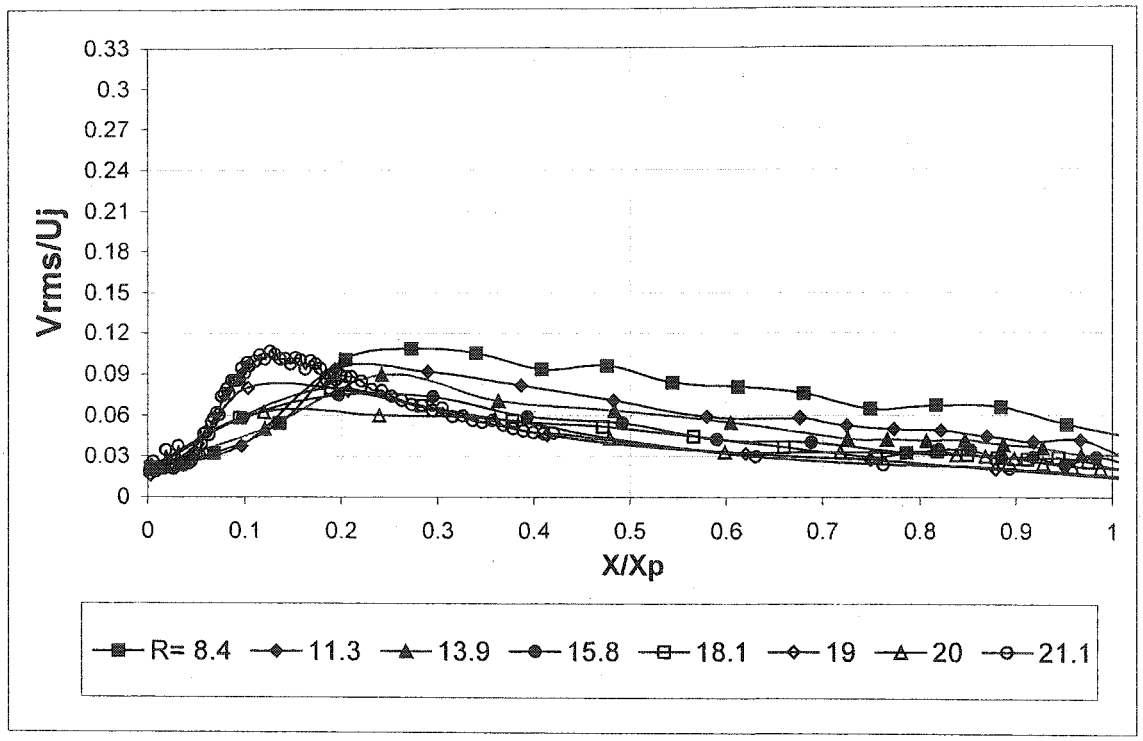

Figure 4-5.c Radial turbulence intensity along the centerline (D=6.35 mm)

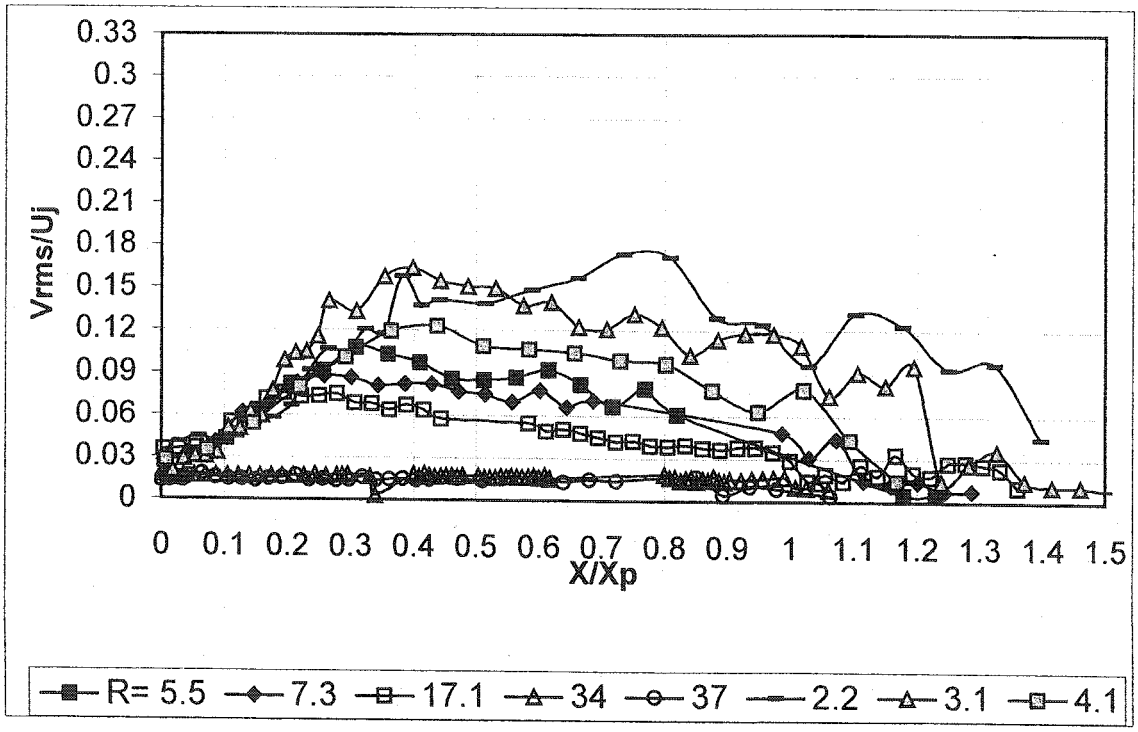

Figure 4-5.d Radial turbulence intensity along the centerline (D=9.575 mm)

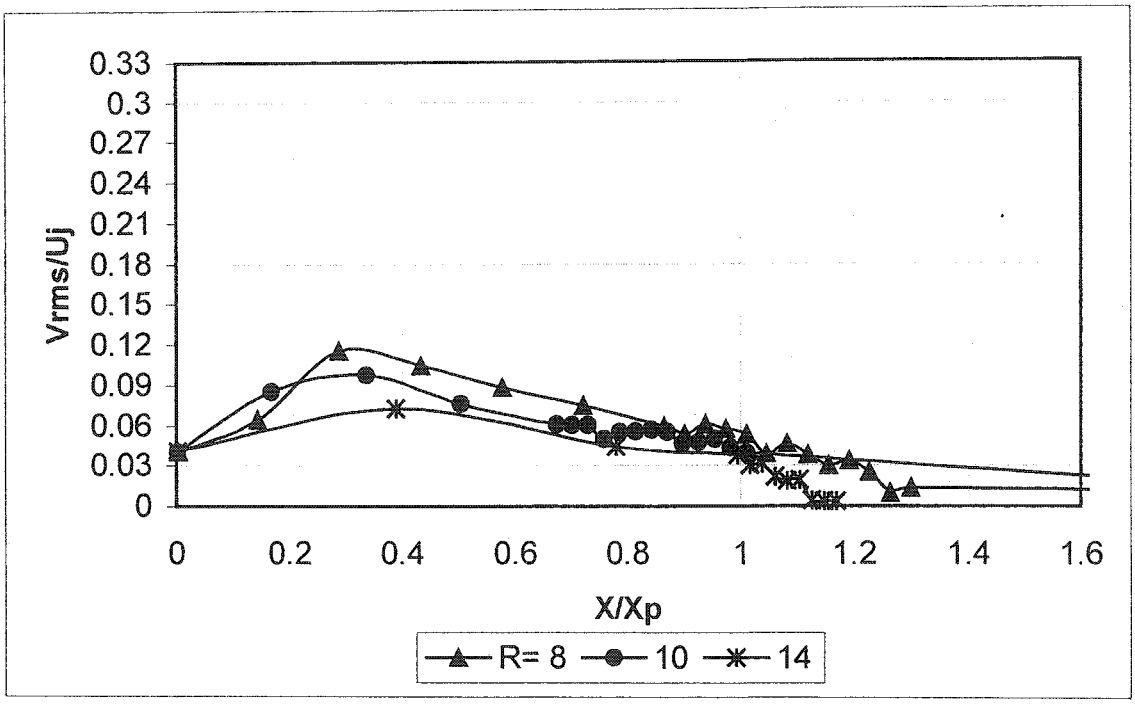

Figure 4-5.e Radial turbulence intensity along the centerline (D=12.7 mm)

4.3.3 Relation between axial and radial turbulence intensity

Since in most cases the axial and radial turbulence intensities linearly change, finding a relation between axial and radial velocities fluctuations can be useful. Figures 4-6 show this ratio for all cases.

As it is seen in the figures 4-6.a through 4-6.f, Vrms/Urms along the centerline gives an almost horizontal line in most cases. For a free unconfined jet this line stays at 0.5 and for the confined jets this value is less than 0.5.

The importance of this relation appears in the measurement of the kinetic energy of turbulence. The kinetic energy of turbulent is defined as (Bradshaw 1971 and Schlichting 2000):

$$k = \frac{1}{2}\rho(U_{rms}^2 + V_{rms}^2 + W_{rms}^2) \qquad [4\text{-}15]$$

Now, using the relation found through the graphs, one can calculate the kinetic energy of turbulent for a counter flowing free jet along the centerline and assuming Vrms and Wrms are equal:

$$k = \frac{1}{2}\rho(U_{rms}^2 + \frac{1}{2}\times 2V_{rms}^2) = \rho U_{rms}^2 \qquad [4\text{-}16]$$

In the radial distance of y, V_{rms}^2 and W_{rms}^2 are not equal and according to Bradshaw (1967) W_{rms}^2 can be evaluated as the average of U_{rms}^2 and V_{rms}^2 or:

$$W_{rms}^2 = \frac{1}{2}(U_{rms}^2 + V_{rms}^2) \qquad [4\text{-}17]$$

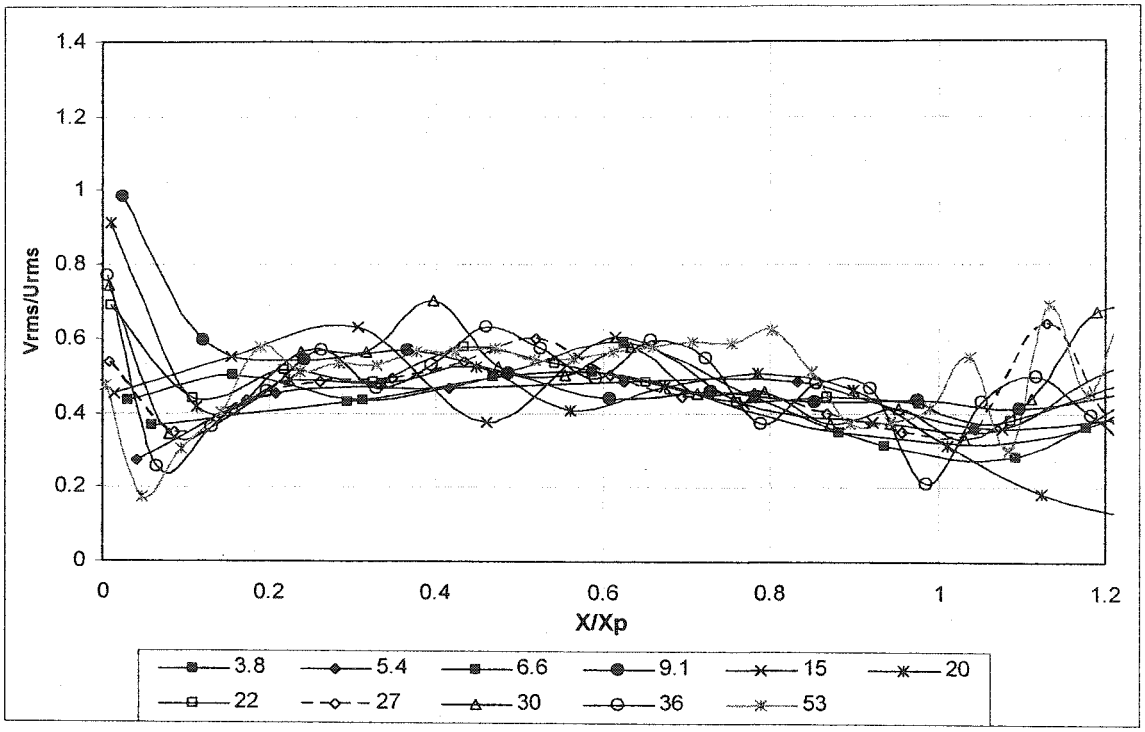

Figure 4-6.a Turbulence intensity ratio along the centerline (D=1.587 mm)

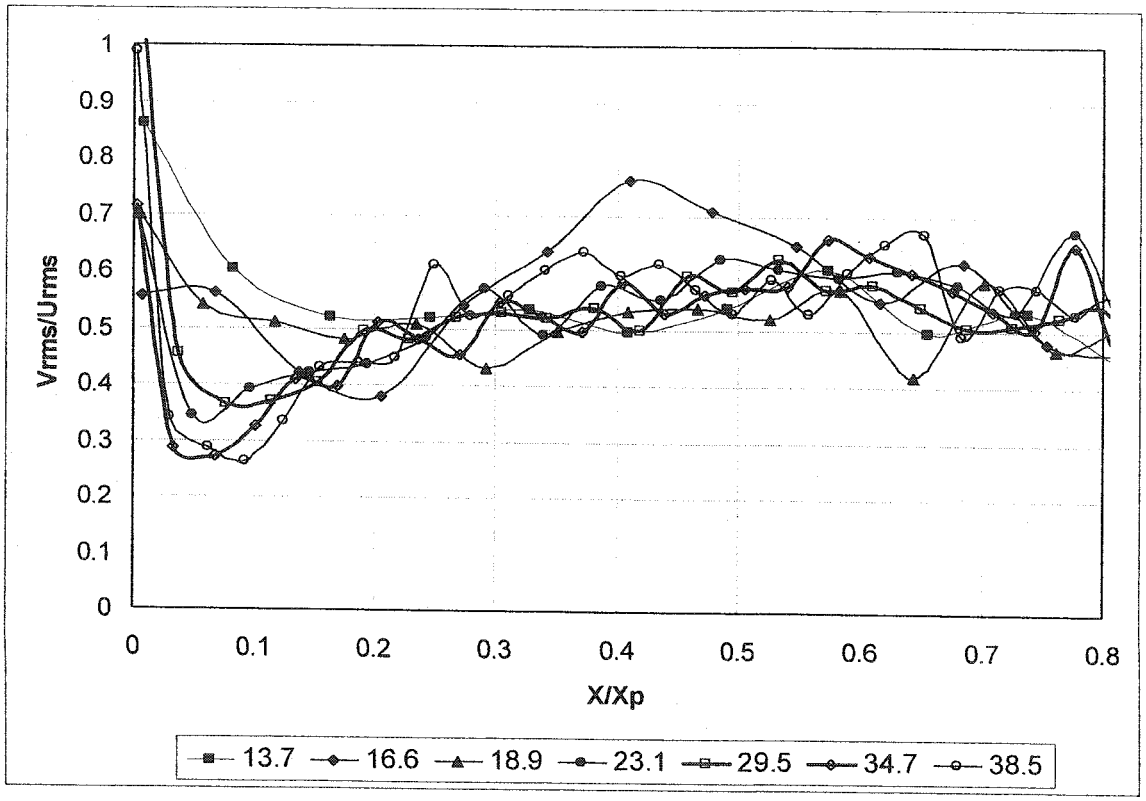

Figure 4-6.b Turbulence intensity ratio along the centerline (D=3.175 mm)

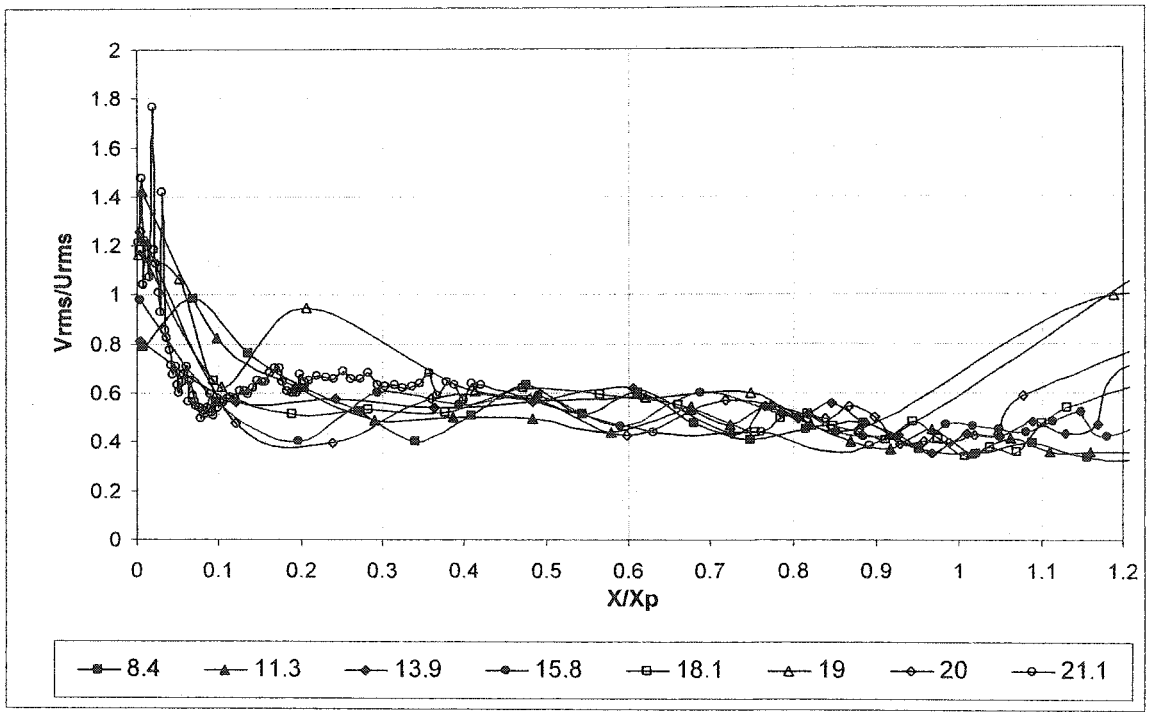

Figure 4-6.c Turbulence intensity ratio along the centerline (D=6.35 mm)

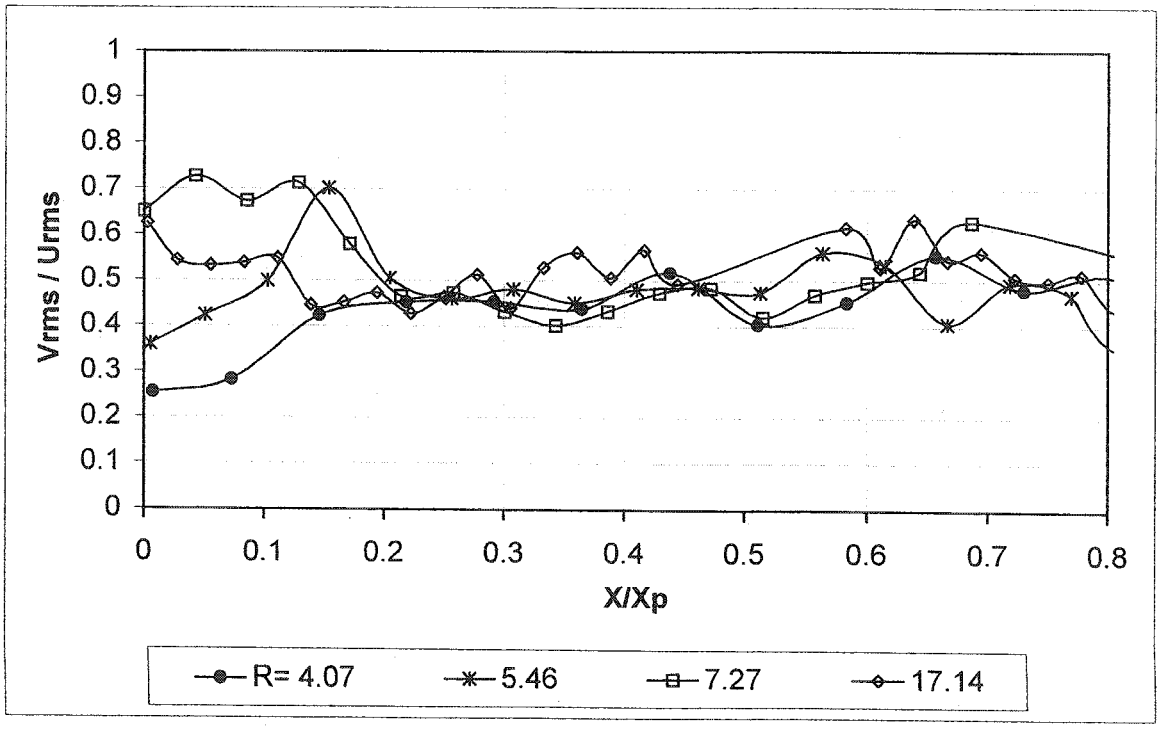

Figure 4-6.d Turbulence intensity ratio along the centerline (D=9.575 mm)

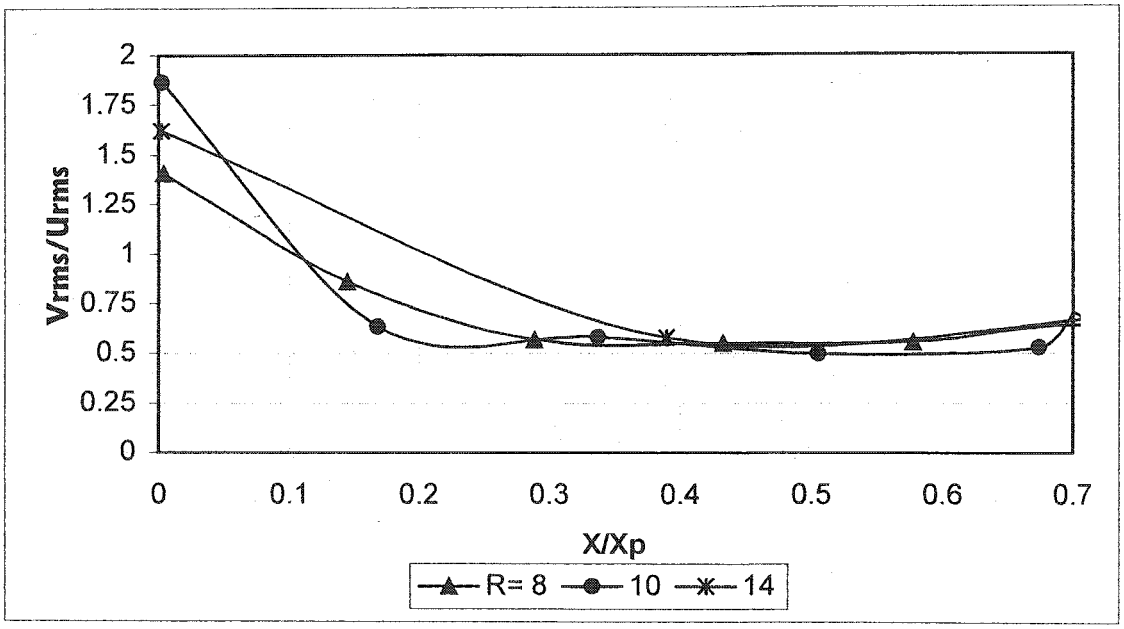

Figure 4-6.e Turbulence intensity ratio along the centerline (D=12.7 mm)

4.4 Other flow characteristics

Beltaos (1973, 1999) presented the centerline velocity decay rate of a counter flowing free jet by the combined term of $\frac{U+U_m}{U_j}\cdot\frac{X_p}{D}$ versus X/Xp. The term $U+U_m$ represents the relative velocity of centerline for an observer moving with main flow. The whole term includes the ratio of the penetration length to the jet diameter. Since Um in the above term prevents it to have negative value and also gives an intersection with the X/Xp axis far from the origin while the term Xp/D multiplies it with a big number. The same graph is prepared with the data from the present study and is shown in Figure 4-7.

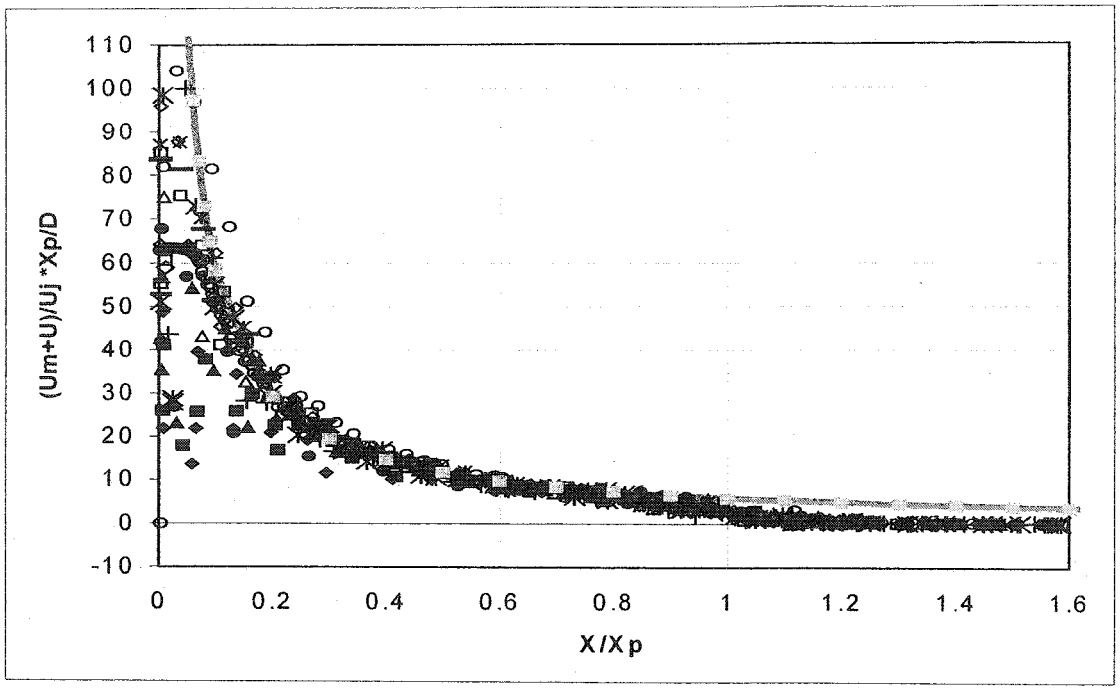

Figure 4-7 Variation of centerline velocity (all jets). The thick gray line denotes the curve (5.83Xp/X)

At this point we can use the same analogy but instead of Um, Urms will be used. The term U+Urms indicates the maximum velocity in the section plus its fluctuation. The resulting graphs are shown in the figures 4-8.a to 4-8.f. As it is seen, all graphs follow the same pattern. In a log-log graph, they typically have a horizontal part followed by a second linear segment to that are asymptotic. They are also tangents to curve in the form of $\frac{\text{const.}}{(X/X_p)}$. A line with the slope of -1.07 shows the latter in the figures. One fact should be noticed that Um is constant and Urms varies and also that the magnitude of Um is much bigger than Urms but these differences do not affect on the value of the constant.

Figures 4-9.a to 4-9.e present the variation of relative momentum factor with the dimensionless distance from the jet exit, X/X_p. The curves in these figures also have a tangent in the form of $\frac{\text{const.}}{(X/X_p)}$. The value of the constant for the present case is 0.052 while for the previous case it was 5.83, almost 100 times higher. In these graphs, for higher velocity ratios, R, curves start from a higher value but very fast they reach the tangential curve while the curves related to smaller R, starts from smaller value and join to the tangential curve in a bigger X/X_p.

From a spectral point of view, all the curves are asymptotic to a line somewhere in the upstream of the jet. This place varies by the velocity ratio. As the velocity ratio increases the convergence of the curve to this asymptotic line is closer to the jet exit.

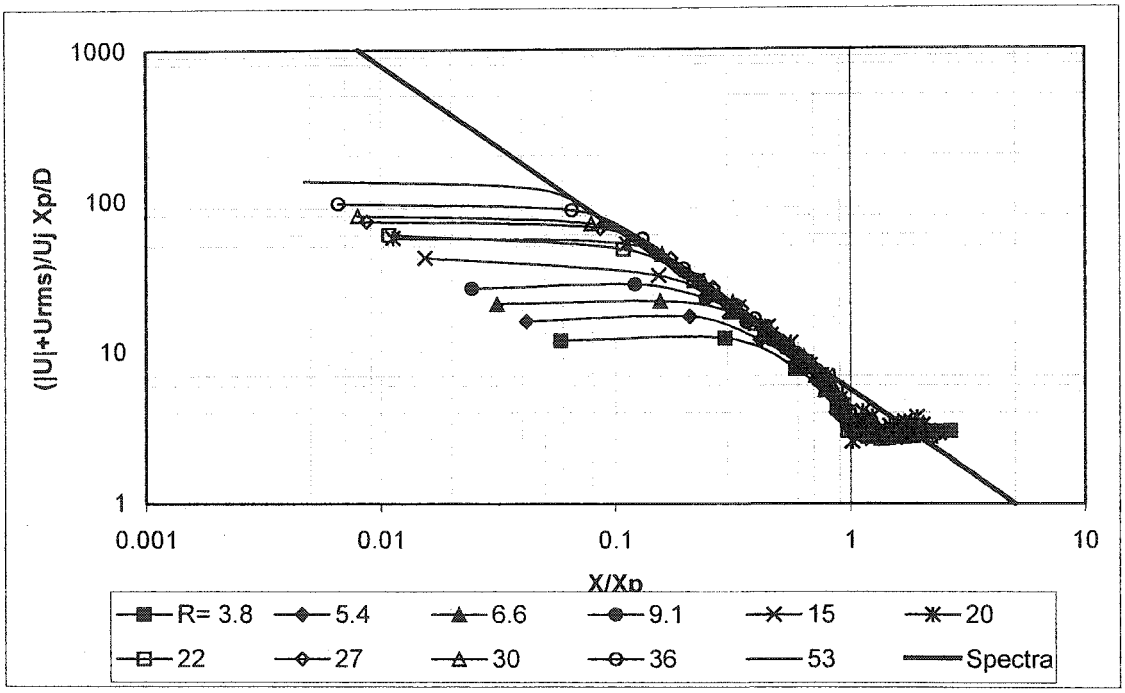

Figure 4-8.a Turbulence and penetration length distribution (D=1.587)

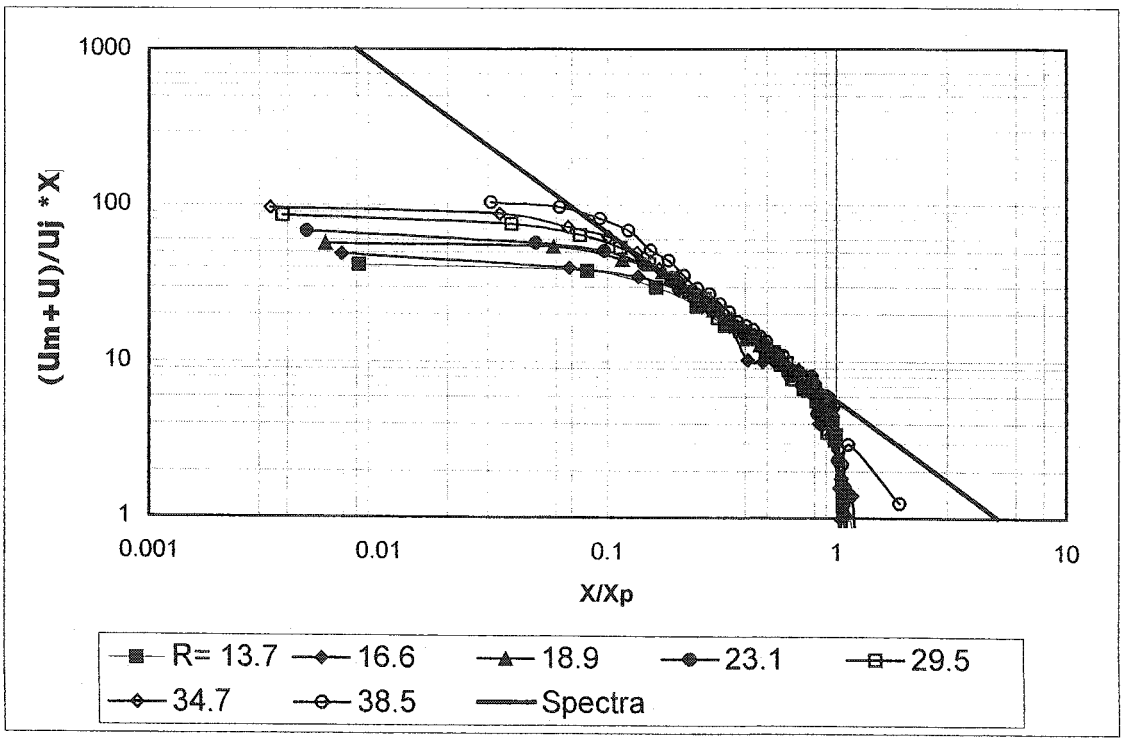

Figure 4-8.b Turbulence and penetration length distribution (D=3.175 mm)

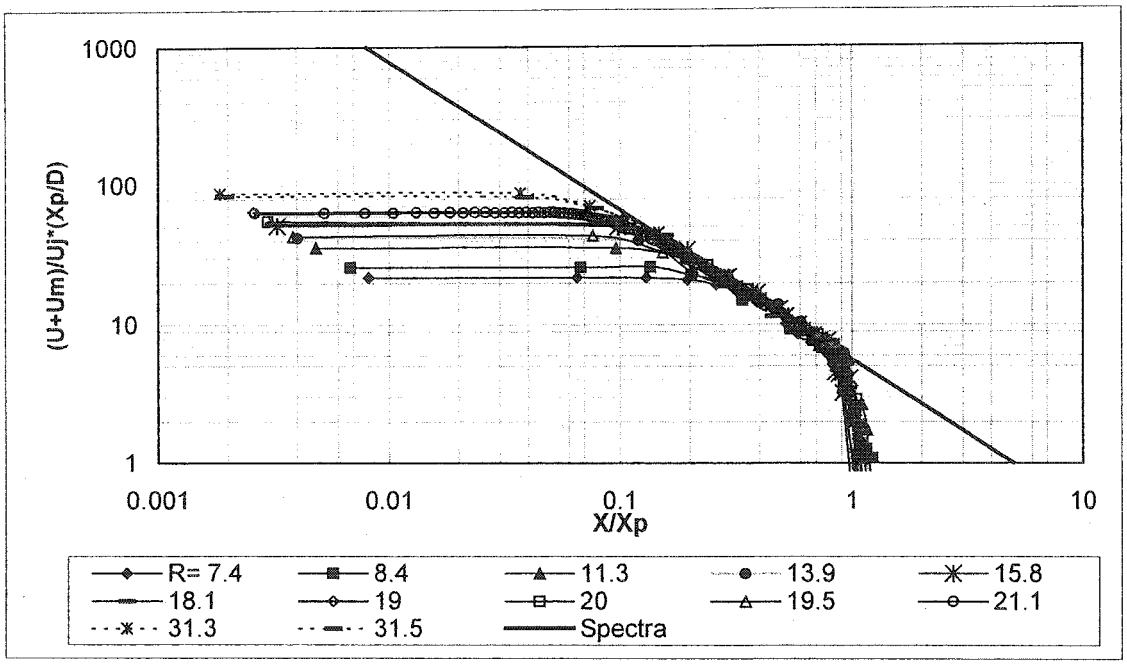

Figure 4-8.c Turbulence and penetration length distribution (D=6.35 mm)

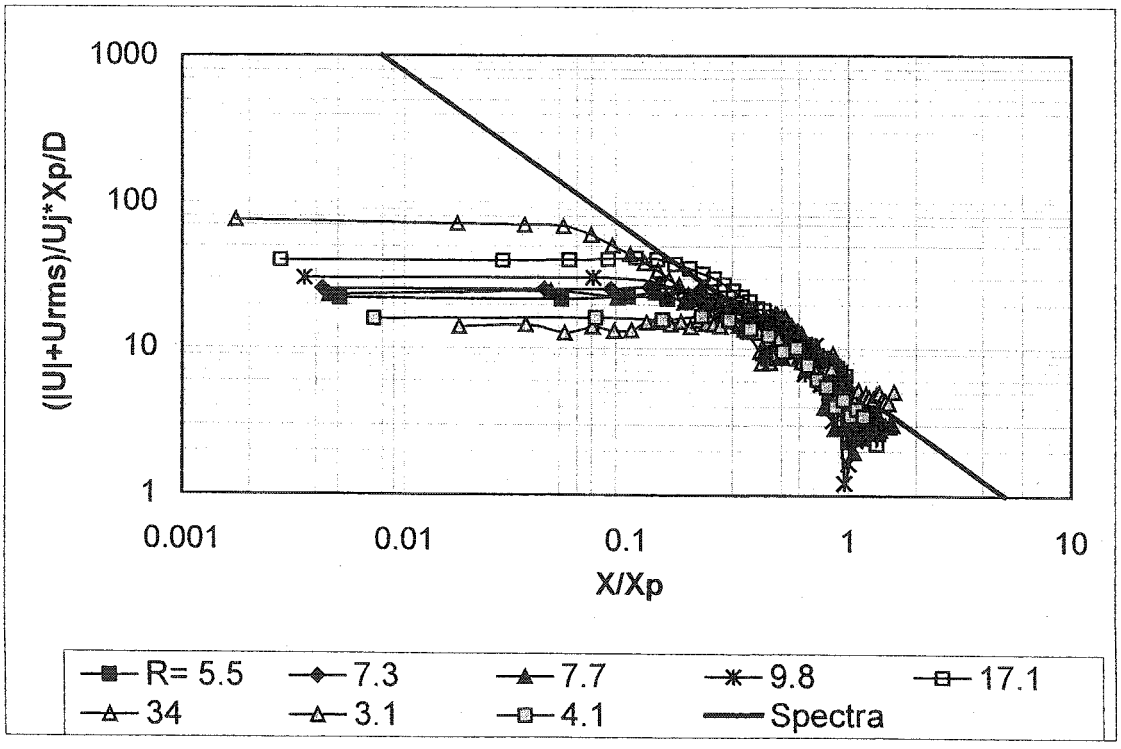

Figure 4-8.d Turbulence and penetration length distribution (D=9.575 mm)

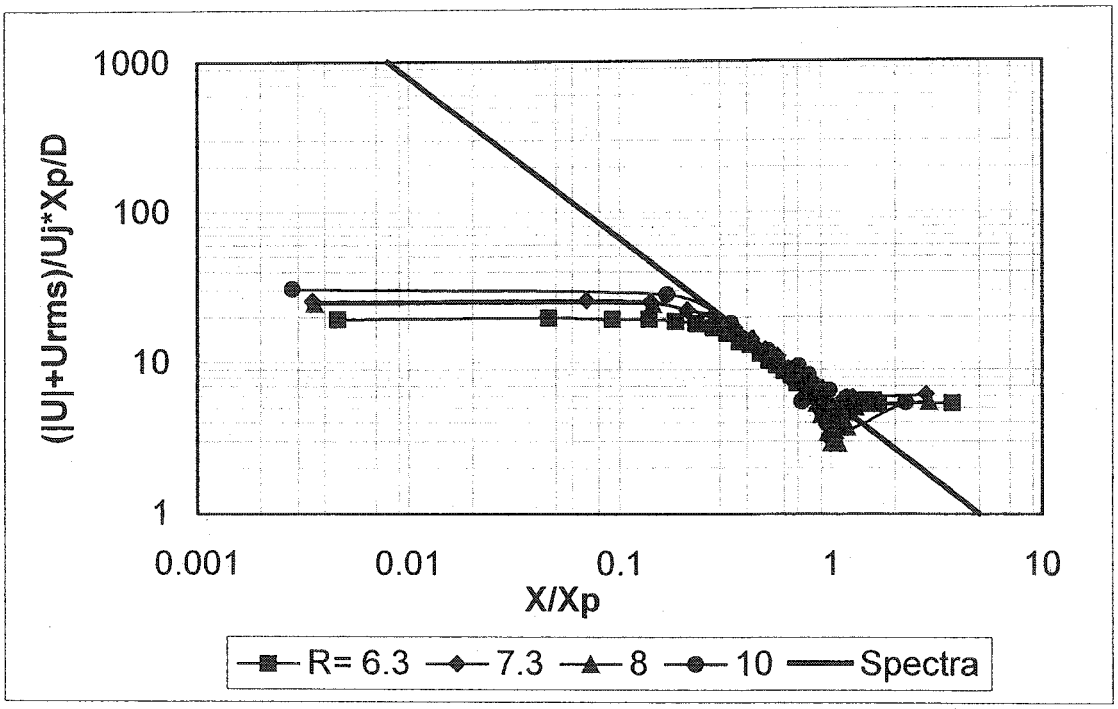

Figure 4-8.e Turbulence and penetration length distribution (D=12.7 mm)

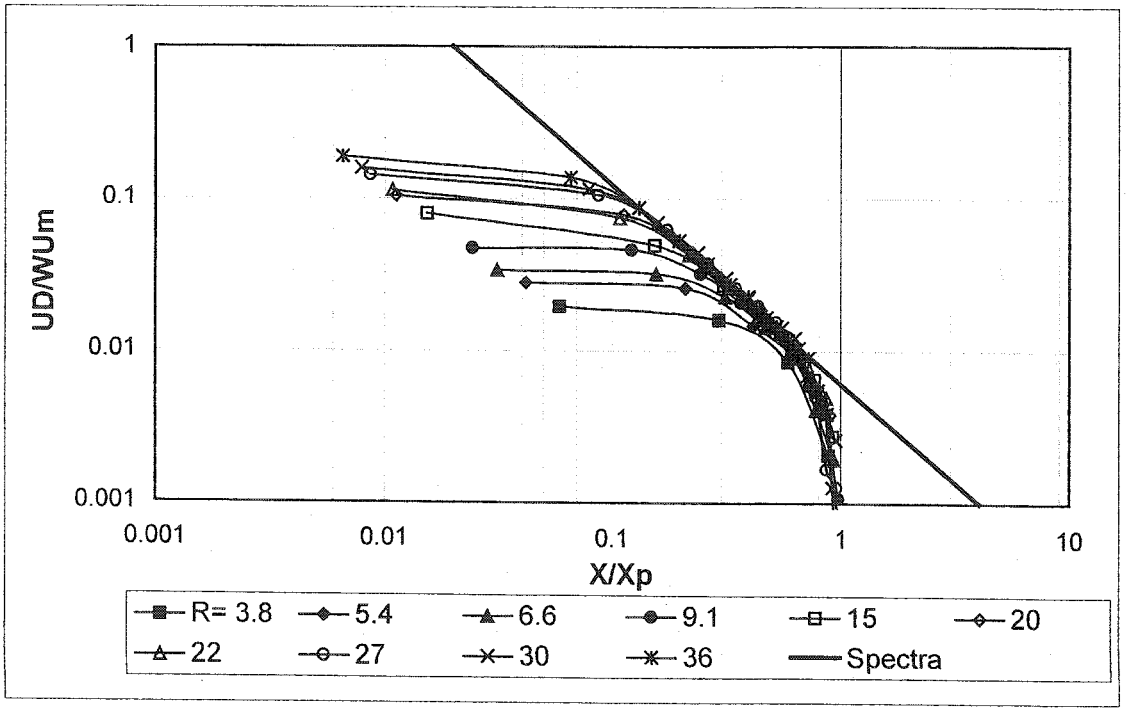

Figure 4-9.a The momentum factor along the centerline (D=1.587 mm)

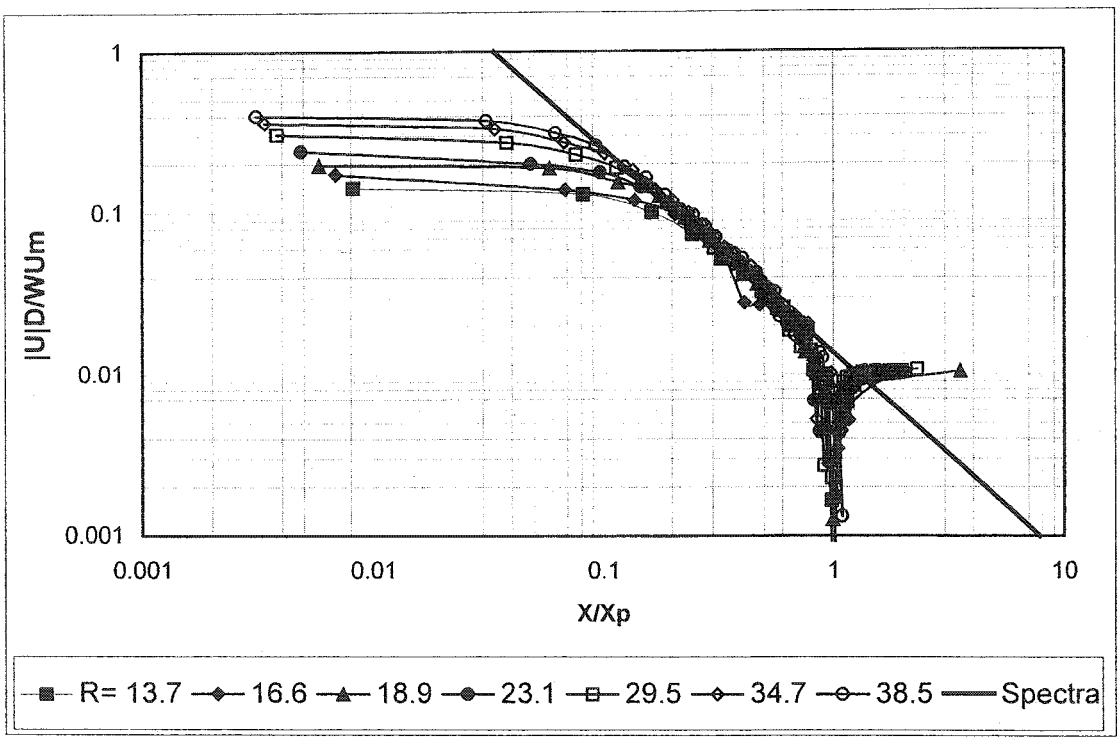

Figure 4-9.b The momentum factor along the centerline (D=3.175 mm)

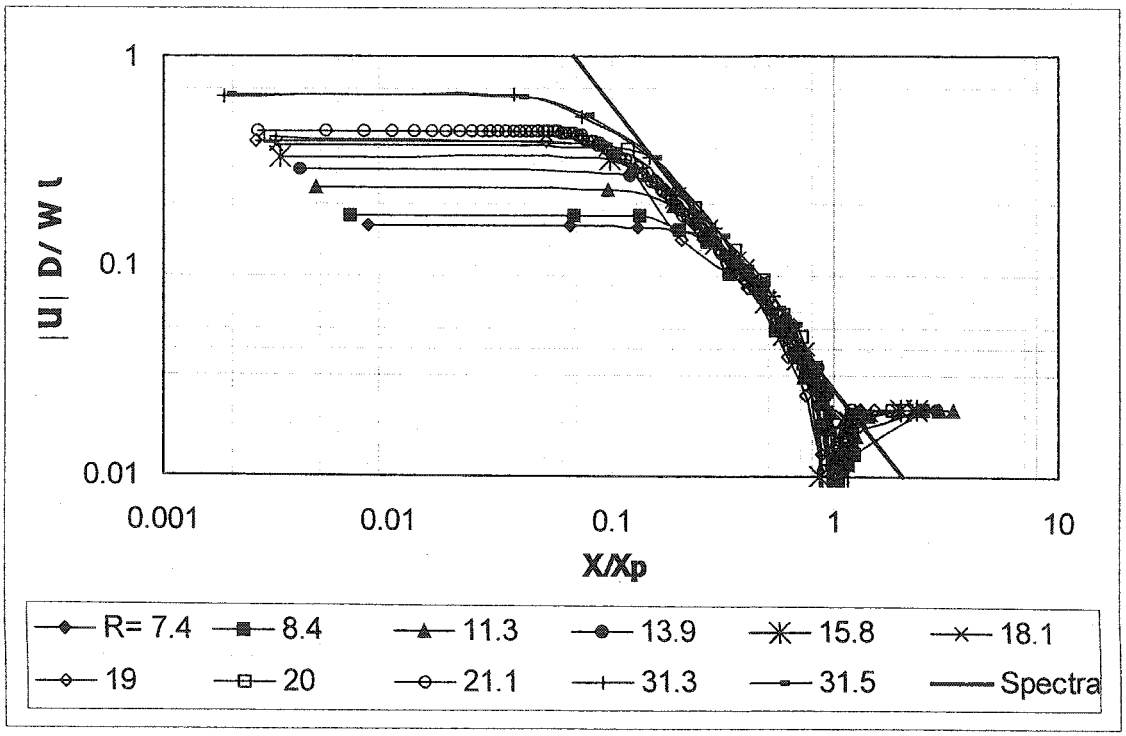

Figure 4-9.c The momentum factor along the centerline (D=6.35 mm)

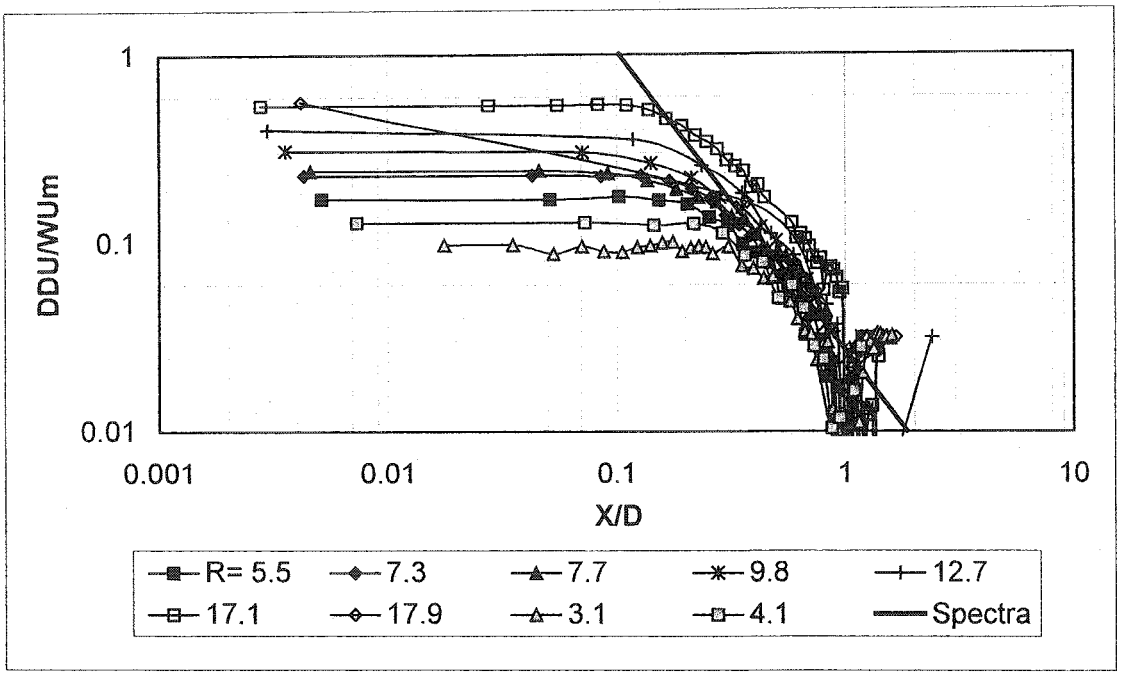

Figure 4-9.d The momentum factor along the centerline (D=9.575 mm)

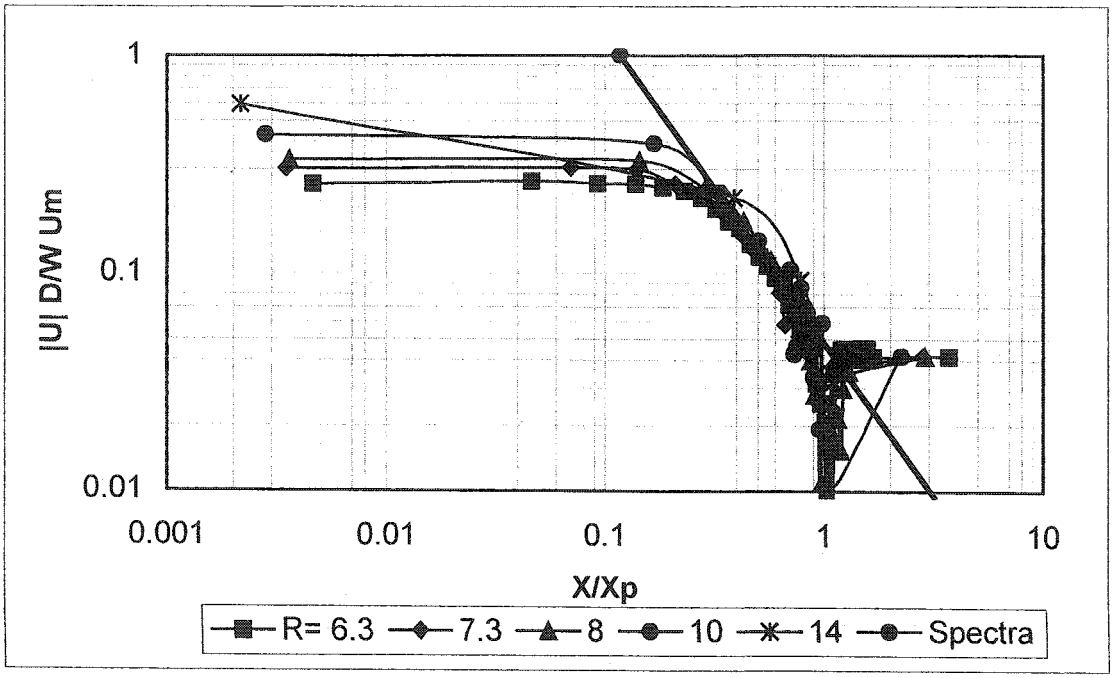

Figure 4-9.e The momentum factor along the centerline (D=12.7 mm)

4.5 Cross sectional flow pattern

Flow pattern along the centerline was previously investigated in several studies (Beltaos 1973, Lam 1995 and 1997, Konig 1991, and Yoda 1995). Since the results of those studies are in an agreement, a new set of experiments is not necessary. Instead, the pattern of flow across the test section was not studied earlier. Chu (1999) performed the only experiment on this issue for a co-flowing jet.

Flow pattern in across the test section was studied using a 9.575 mm nozzle. Assuming reflection factor of 1.333 for water, a mesh of 14 mm in y direction by 10.5 mm in z direction was defined. At each point of this 121 (11X11) points mess, the axial velocity was measured and the results were post processed to fit to the graphical software (Stanford Graphics) format. Figures 4-10.a to 4-10.c show the flow pattern at x=50, x=150, and x=250 mm respectively. The jet mean penetration length was occurred at 375 mm.

Some irregularities in the figures are interpreted as the random nature of the phenomena and difference between real reflection factor and 1.3333 that was used in the probe positioning.

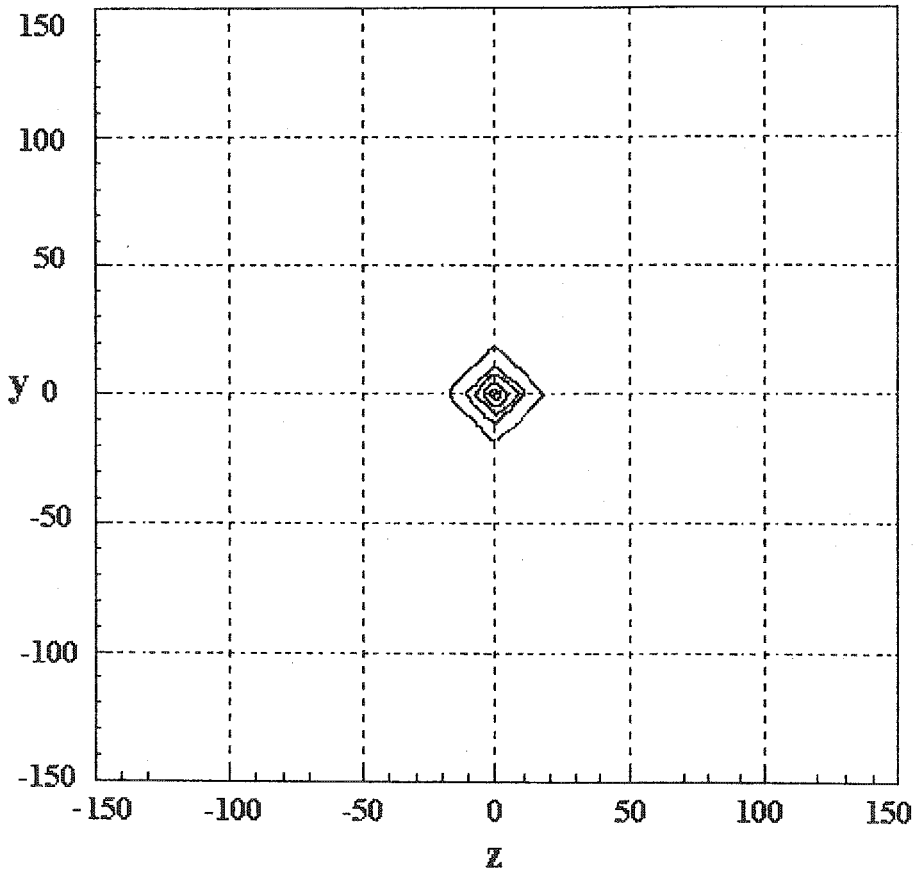

Figure 4-10.a A qualitative representation of velocity distribution across the cross section, X=50 mm. The inner circles were calculated by Stanford Graphics™.

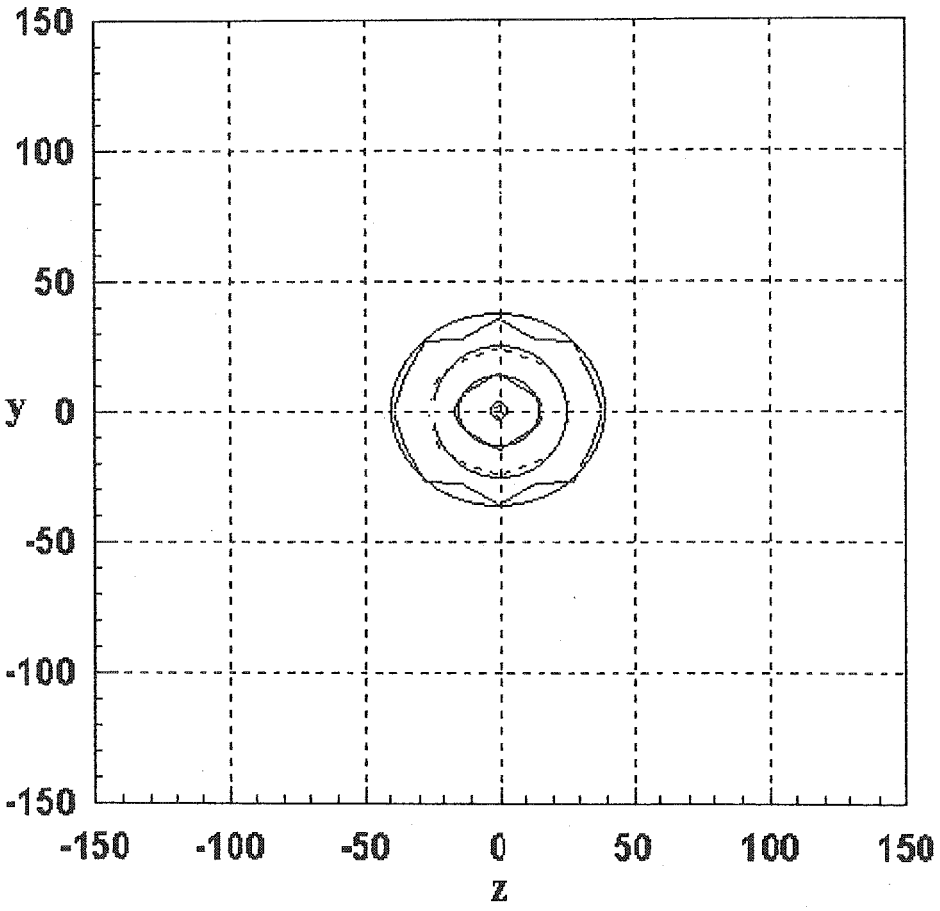

Figure 4-10.b Velocity distribution across the cross section, X=150 mm. The circles are fitted to the figure and the rest was produced by Stanford Graphics™.

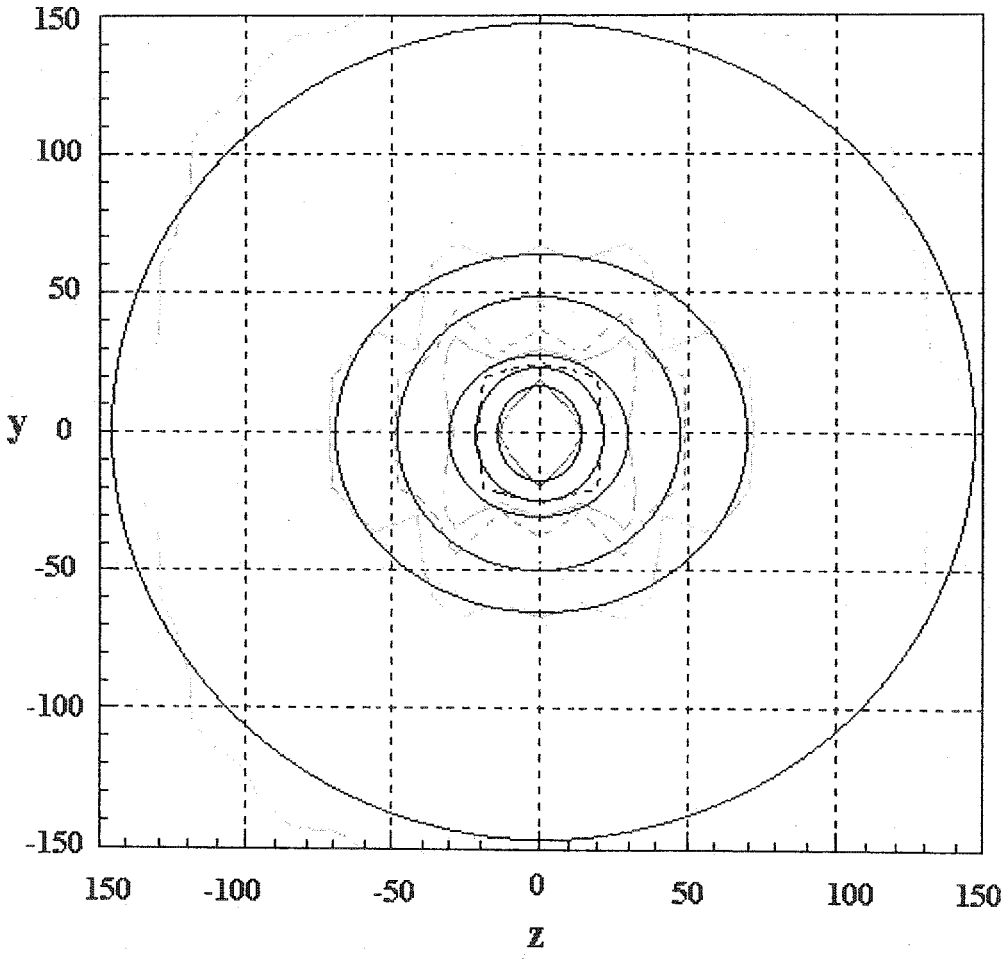

Figure 4-10.c Velocity distribution across the cross section, X=250 mm. The circles are fitted to the figure and the rest was produced by Stanford Graphics™.

Chapter 5

Structure of Turbulence and Energy Balance

5.1 General remarks

The concept of turbulent kinetic energy and its balance has a shorter history than the turbulent modeling since it needs powerful and very accurate devices to record the time and velocity and also some how provide the data to be able to do some calculation on that.

The first measurement technique that was used to measure the properties of turbulence is the hot-wire technique and there is no reliable literature on this subject prior to hot-wire technique. The second technique is based on laser reflection and/or laser refraction or LDA. Measurement from outside of flow region that does not disturb the flow is a big advantage of this technique. Independence from the media and temperature and also direct answer is another

advantage of LDA systems while hot-wires needs frequent calibration (Bradshaw 1971).

In this chapter, after a quick review of hot-wire measurement technique, an analytical approach to the problem of turbulence measurement is presented. Literature review, results of this study, and discussion of the results will follow.

5.2 Hot-wire technique

Hot-wire anemometer is based on the variation of electrical current by changing electrical conductivity due to the change in its temperature. The device has been designed and developed during the past five decades. In this technique, a very fine wire (between 1 to 5 micrometers) of metal (platinum, platinum-iridium, or tungsten) that is heated by an electrical current is used to measure the velocity (Hinze 1975). In the still environment, the heated wire reaches to an ultimate resistance and therefore the current becomes stable. Any flow around it cools down the wire and the current increases. The higher velocity makes the wire cooler and since the metal is very short and fine, a very small fluctuation in velocity can be recorded by a multi meter.

Many devices can be used to measure turbulence occasionally but they are not usually considered as the turbulence measurement devices (Bradshaw 1971). The other devices to record velocity fluctuations are based on laser techniques that are fully explained in Chapter 2.

5.3 Literature review

Since turbulent flow of real fluid is dissipative in nature and converts the kinetic energy into heat, a continuous source of energy is needed to supply the necessary energy for turbulence. The concept of kinetic turbulent energy balance is to find the energy relations between the gain and loss of energy that occur in turbulent flow (Hinze 1975).

Measurement of turbulence started in early 1940 but most standard cases have been investigated later when the hot-wire techniques became more popular. In this part focus is laid on those studies whose results or methods directly were used in this study.

Laufer (1950) reported his investigation on turbulent flow in a two dimensional channel. Using a single hot-wire, he provided a comprehensive measurement data for a 2-D channel. Equity of two lateral fluctuations $\overline{w^2}$ and $\overline{v^2}$ at the centerline of the channel is one of the most interesting results of that study. It shows the symmetry of the flow dictates this property even to a completely three dimensional phenomena like turbulence. He also reported a linear relation between the shear stress and turbulence intensities: $\frac{\overline{uv}}{U^2} = k \frac{\overline{\sqrt{u^2}}}{U} \times \frac{\overline{\sqrt{v^2}}}{U}$ where, k is $-0.5 \sim -0.6$.

Wygnanski and Fiedler (1969) investigated the case of an axisymmetric free jet. They used a 26.416 mm diameter jet issuing into a 2.286 x 2.438 x 5.18 m room from the center of its smaller wall. Velocity of the jet was set to 51 and 72 m/s. this very high velocity was needed to attain the self-preserving condition for jet. Some analytical considerations of their study will be discussed later in this chapter. However, one can point out on their analogy to find dissipation terms and also of the triple velocity correlation that shows the similar behavior at different point across the jet axis. They also calculated the pressure diffusion as the summation of the other terms with a negative sign since there is no reliable way to measure fluctuations in pressure and velocities simultaneously.

Rodi and Spalding (1970) presented a 2-parameter model of turbulence. They assumed the pressure diffusion to be zero. The rest of unknowns could be calculated by solving a system of two equations. They reported that their answers are realistic especially for jets and the model can validate Wygnanski's data (1969).

Townsend (1976) has published the second edition of his text on turbulence, i.e. "The structure of turbulent shear flow". In this text, he has covered a wide variety of turbulent flows based on both analytical and experimental approaches.

Chandrsuda and Bradshaw (1981) studied the turbulent structure of a reattaching mixing layer in a wind tunnel on the backward facing step. They used a cross

hot-wire probe and assumed the unmeasured turbulence fluctuation, $\overline{w^2}$, to be the average of the measured fluctuations, $\overline{u^2}$ and $\overline{v^2}$.

5.4 Kinetic energy of turbulence for counter flowing free round jet

5.4.1 Analytical approach

To derive an equation for turbulent kinetic energy for turbulent round jets, here, the procedure presented by Wygnanski and Fiedler (1969) will be followed for sake of its simplicity. Starting with Navier-Stokes momentum equations,

$$\frac{\partial U^2}{\partial x}+\frac{\partial UV}{\partial r}+\frac{1}{r}\frac{\partial UW}{\partial \phi}+\frac{UV}{r}=\frac{1}{\rho}\frac{\partial \pi}{\partial x}+\nu\nabla^2 U \qquad [5\text{-}1]$$

$$\frac{\partial UV}{\partial x}+\frac{\partial V^2}{\partial r}+\frac{1}{r}\frac{\partial VW}{\partial \phi}+\frac{V^2-W^2}{r}=\frac{1}{\rho}\frac{\partial \pi}{\partial y}+\nu\left(\nabla^2 V-\frac{V}{r^2}-\frac{2}{r^2}\frac{\partial W}{\partial \phi}\right) \qquad [5\text{-}2]$$

$$\frac{\partial UW}{\partial x}+\frac{\partial VW}{\partial r}+\frac{1}{r}\frac{\partial W^2}{\partial \phi}+\frac{2VW}{r}=\frac{1}{\rho}\frac{\partial \pi}{\partial y}+\nu\left(\nabla^2 w-\frac{w}{r^2}+\frac{2}{r^2}\frac{\partial W}{\partial \phi}\right) \qquad [5\text{-}3]$$

and continuity equation:

$$\frac{\partial U}{\partial x}+\frac{1}{r}\frac{\partial (rV)}{\partial r}+\frac{1}{r}\frac{\partial W}{\partial \phi}=0 \qquad [5\text{-}4]$$

where x is the jet axis as defined previously, r is radial direction (r = y) and ϕ is the angular direction. To get rid of ϕ, another axis is defined as $z = r\,\phi = y\,\phi$.

Using the definition of turbulent flow:

$U = \overline{U} + u$, $V = \overline{V} + v$, $W = \overline{W} + w$, and $\pi = P + p$

and multiplying equations 5-1 through 5-3 by U^2, V^2, and W^2 respectively another equation will be found:

$$\frac{\partial}{\partial x}\left(\overline{U^3} + \overline{V^2}\,\overline{U} + 2\overline{Vuv}\right) + \frac{\partial}{\partial x}\left(3\overline{U}\,\overline{u^2} + \overline{u^3} + \overline{v^2 u} + \overline{U}\,\overline{v^2} + \overline{w^2 u} + \overline{U}\,\overline{w^2}\right) +$$
$$\frac{1}{y}\frac{\partial}{\partial y} y\left(\overline{v^3} + \overline{vu^2} + \overline{vw^2}\right) + \frac{1}{y}\frac{\partial}{\partial y} y\left(\overline{V}\,\overline{U^2} + \overline{V^3} + \overline{V}\,\overline{u^2} + \overline{V}\,\overline{w^2} + 3\overline{V}\,\overline{v^2} + 2\overline{U}\overline{uv}\right) +$$
$$\frac{2}{\rho}\left(\overline{U}\frac{\partial P}{\partial x} + \overline{V}\frac{\partial P}{\partial y}\right) + \frac{2}{\rho}\left(\overline{u\frac{\partial P}{\partial x}} + \overline{v\frac{\partial P}{\partial y}} + \overline{w\frac{\partial P}{\partial z}}\right)$$
$$= 2\nu\left[\frac{1}{2}\nabla^2\left(\overline{u^2} + \overline{v^2} + \overline{w^2}\right) + \frac{1}{2}\nabla^2\left(\overline{U^2} + \overline{V^2}\right) - \overline{\left(\frac{\partial u}{\partial x}\right)^2} - \overline{\left(\frac{\partial u}{\partial y}\right)^2} - \overline{\left(\frac{\partial u}{\partial z}\right)^2} - \right.$$
$$\overline{\left(\frac{\partial v}{\partial x}\right)^2} - \overline{\left(\frac{\partial v}{\partial y}\right)^2} - \overline{\left(\frac{\partial v}{\partial z}\right)^2} - \overline{\left(\frac{\partial w}{\partial x}\right)^2} - \overline{\left(\frac{\partial w}{\partial y}\right)^2} - \overline{\left(\frac{\partial w}{\partial z}\right)^2} - \overline{\left(\frac{\partial U}{\partial x}\right)^2} - \overline{\left(\frac{\partial U}{\partial y}\right)^2} -$$
$$\left.\overline{\left(\frac{\partial V}{\partial x}\right)^2} - \overline{\left(\frac{\partial V}{\partial y}\right)^2} - \frac{2}{y^2}\left(v\frac{\partial w}{\partial z} - w\frac{\partial w}{\partial z}\right) - \frac{1}{y^2}\left(\overline{V^2} + \overline{v^2} + \overline{w^2}\right)\right] \qquad [5\text{-}5]$$

Removing the terms of mean flow equation from the above equation, the equation of turbulent kinetic energy will be formed. This form of the turbulent kinetic energy equation was used in this study and it is similar to the one used by Wygnansky (1969) and Hinze (1975) [Equation 5-6].

$$0=\frac{\partial}{\partial x}\left[\overline{U}\left(\overline{u^2}+\overline{v^2}+\overline{w^2}\right)\right]+\frac{1}{y}\frac{\partial}{\partial y}y\left(\overline{V}\left(\overline{u^2}+\overline{v^2}+\overline{w^2}\right)\right)+$$

$$\frac{\partial}{\partial x}\left[\overline{u\left(\overline{u^2}+\overline{v^2}+\overline{w^2}\right)}\right]+\frac{1}{y}\frac{\partial}{\partial y}y\left(\overline{v\left(\overline{u^2}+\overline{v^2}+\overline{w^2}\right)}\right)+$$

$$2\left(\overline{u^2}\frac{\partial\overline{U}}{\partial x}+\overline{v^2}\frac{\partial\overline{V}}{\partial y}+\overline{uv}\frac{\partial\overline{U}}{\partial y}\right)+\frac{2}{\rho}\left(\overline{\frac{\partial uP}{\partial x}}+\frac{1}{y}\frac{\partial}{\partial y}(yvp)\right)+$$

$$2\nu\left[\overline{\left(\frac{\partial u}{\partial x}\right)^2}+\overline{\left(\frac{\partial u}{\partial y}\right)^2}+\overline{\left(\frac{\partial u}{\partial z}\right)^2}+\overline{\left(\frac{\partial v}{\partial x}\right)^2}+\overline{\left(\frac{\partial v}{\partial y}\right)^2}+\overline{\left(\frac{\partial v}{\partial z}\right)^2}+\overline{\left(\frac{\partial w}{\partial x}\right)^2}+\overline{\left(\frac{\partial w}{\partial y}\right)^2}\right]$$

[5-6]

In the above equation some derivatives with respect to x exist. In the jet flow, along the radial direction, these derivatives create some difficulties especially when x between two radial profiles is very big compared to distances between points along the radial axis. To avoid such a problem, another change can be made to equation 5-6. Assuming $\eta=\frac{y}{x}$ and $\overline{q^2}=\overline{u^2}+\overline{v^2}+\overline{w^2}$ the above equation becomes: [5-7]

$$0=-\frac{1}{2}\eta\frac{\partial}{\partial\eta}\left(\frac{\overline{U}}{\overline{U_m}}\frac{\overline{q^2}}{\overline{U_m^2}}\right)+3\frac{\overline{U}}{\overline{U_m}}\frac{\overline{q^2}}{\overline{U_m^2}} \qquad \text{[term A]}$$

$$+\frac{1}{2\eta}\frac{\partial}{\partial\eta}\left(\eta\frac{\overline{V}}{\overline{U_m}}\frac{\overline{q^2}}{\overline{U_m^2}}\right) \qquad \text{[term B]}$$

$$-\frac{1}{2}\left(3\frac{\overline{uq^2}}{\overline{U_m^3}}+\eta\frac{\partial}{\partial\eta}\frac{\overline{uq^2}}{\overline{U_m^3}}\right) \qquad \text{[term C]}$$

$$-\frac{1}{2}\eta\frac{\partial}{\partial\eta}\left(\eta\frac{\overline{vq^2}}{\overline{U_m^3}}\right) \qquad \text{[term D]}$$

$$+\frac{\overline{uv}}{\overline{U_m^2}}\frac{\partial}{\partial\eta}\left(\frac{\overline{U}}{\overline{U_m}}\right) \qquad \text{[term E]}$$

$$+\frac{\overline{v^2}}{\overline{U_m^2}}\frac{\partial}{\partial\eta}\left(\frac{\overline{V}}{\overline{U_m}}\right) \qquad \text{[term F]}$$

$$-\left(\frac{\overline{u^2}}{\overline{U_m^2}}\right)\left(\frac{\overline{U}}{\overline{U_m}}+\eta\frac{\partial}{\partial\eta}\frac{\overline{U}}{\overline{U_m}}\right) \qquad \text{[term G]}$$

$$+\frac{1}{\rho}\left[\frac{1}{\eta}\frac{\partial}{\partial\eta}\left(\eta\frac{\overline{vq^2}}{\overline{U_m^3}}\right)-\eta\frac{\partial}{\partial\eta}\left(\frac{\overline{vp}}{\overline{U_m^3}}\right)-3\frac{\overline{uq^2}}{\overline{U_m^3}}\right]+ \qquad \text{[term H]}$$

$$\frac{\nu x}{U_m^3}\left[\overline{\left(\frac{\partial u}{\partial x}\right)^2}+\overline{\left(\frac{\partial u}{\partial y}\right)^2}+\overline{\left(\frac{\partial u}{\partial z}\right)^2}+\overline{\left(\frac{\partial v}{\partial x}\right)^2}+\overline{\left(\frac{\partial v}{\partial y}\right)^2}+\overline{\left(\frac{\partial v}{\partial z}\right)^2}+\overline{\left(\frac{\partial w}{\partial x}\right)^2}+\overline{\left(\frac{\partial w}{\partial y}\right)^2}\right] \text{[term I]}$$

In other words, the turbulence kinetic energy includes five parts: convection [terms A and B], diffusion [terms C and D], production [terms E, F, and G], pressure diffusion [term H], and dissipation [term I]. Hinze (1975) presented the derived equation in cylindrical coordinates:

(Convection) $$\frac{\partial}{\partial z}(\overline{U}_z\frac{\overline{q^2}}{2})+\frac{1}{r}\frac{\partial}{\partial r}r(\overline{U}_z\frac{q^2}{2})+$$

(Diffusion) $$\frac{\partial}{\partial z}(u_z\frac{\overline{q^2}}{2})+\frac{1}{r}\frac{\partial}{\partial r}r\overline{u_r\frac{q^2}{2}})+$$

(Production) $$\overline{u_r u_z}\frac{\partial\overline{U}_z}{\partial r}+\overline{u_z^2}\frac{\partial\overline{U}_z}{\partial z}+\overline{u_r^2}\frac{\partial\overline{U}_r}{\partial r}+$$

(Pressure diffusion) $$\frac{1}{\rho}\left(\frac{\partial}{\partial z}\overline{u_z p}+\frac{1}{r}\frac{\partial}{\partial r}r\overline{u_r p}\right)+$$

(Dissipation) $$\nu\overline{\frac{\partial u_i}{\partial x_j}\frac{\partial u_i}{\partial x_j}}=0 \qquad \text{[5-8]}$$

The last term is written in Cartesian coordinates since there is no accurate way to provide information about the ϕ component of velocity fluctuation in (r, ϕ, z) system.

All terms in the equation are measurable. With a 2-D probe, we cannot measure all velocity components at the same time. According to Laufer (1954) and Wygnanski and Fiedler (1969), an approximation can be made to reduce the number of dissipation terms assuming isotropic turbulence. By this assumption, the mean square derivatives with respect to a given direction are related to each other. The assumption can be expressed by the following equations:

$$\kappa\overline{\left(\frac{\partial u}{\partial x}\right)^2} = \overline{\left(\frac{\partial v}{\partial x}\right)^2} = \overline{\left(\frac{\partial w}{\partial x}\right)^2} \qquad [5\text{-}9]$$

$$\overline{\left(\frac{\partial u}{\partial y}\right)^2} = \kappa\overline{\left(\frac{\partial v}{\partial y}\right)^2} = \overline{\left(\frac{\partial w}{\partial y}\right)^2} \qquad [5\text{-}10]$$

$$\overline{\left(\frac{\partial u}{\partial z}\right)^2} = \overline{\left(\frac{\partial v}{\partial z}\right)^2} = \kappa\overline{\left(\frac{\partial w}{\partial z}\right)^2} \qquad [5\text{-}11]$$

$$\kappa = 1 + e^{-200y^2} \qquad [5\text{-}12]$$

Assuming $\overline{\left(\frac{\partial u}{\partial y}\right)^2} \approx \overline{\left(\frac{\partial u}{\partial z}\right)^2}$ the dissipation terms reduce to:

$$\frac{\nu x}{U_m^3}\left[\overline{\left(\frac{\partial u}{\partial x}\right)^2} + 2\overline{\left(\frac{\partial v}{\partial x}\right)^2} + 2\overline{\left(\frac{\partial u}{\partial y}\right)^2}\left(2 + \frac{1}{1 + \mathrm{EXP}(-200y^2)}\right)\right] \qquad [5\text{-}13]$$

Since most of the assumptions made here are validated for a free submerged jet, the equation is valid inside the jet region. Some results for the mixing layer will also be presented and compared with the existing data.

5.4.2 Limitations of a counter jet

As previously discussed in Chapter 3, the penetration length is a very important characteristic of a counter jet and there is a lot of fluctuation in all jet properties close to the stagnation point including the length itself. To avoid such affection, all measurement should be done in the area closer to the jet exit. There is not a certain criterion for this length but Lam (1997) presents the minimum penetration length for a 10 mm diameter jet as well as the maximum. According to his data,

$$x_p = 2D\frac{U_j}{U_m} \qquad [5\text{-}14]$$

can be considered for the minimum penetration length. According to Beltaos (1973), beyond $x=0.8x_p$ the jet can be treated as a source. On the other hand, to attain self-preservation, a minimum distance of 20 D should be there from the jet exit. It means:

$$20D \le x \le 0.8x_p = 1.6D\frac{U_j}{U_m} \qquad [5\text{-}15]$$

This provides an acceptable condition for the test $\frac{U_j}{U_m}$ that should be equal to or greater than 12.5. During the test, always the priority was given to the first condition since Bradbury (1967) explained that even a very small movement in

the body of fluid in which jet enters even if it has the same direction as jet, cancels the self preservation condition for the jet.

5.5 Results of test in the jet region

In this part the results of this research on the structure of flow will be discussed. During data post-processing, some assumptions were made to cover for the lack of data on some properties.

Since a 2-D probe used to measure the velocity components, the third velocity component was not measured. To find $\overline{q^2} = \overline{u^2} + \overline{v^2} + \overline{w^2}$, following Bradshaw (1967, 1981), the relation $\overline{w^2} = \frac{1}{2}\left(\overline{u^2} + \overline{v^2}\right)$ was used to approximate $\overline{w^2}$.

Also, since measurement of instantaneous pressure is not possible, the pressure diffusion terms was calculated as a closure to the equation of turbulent kinetic energy [Eq. 5-7]. To calculate the derivatives, central derivation scheme was used for all terms except for the dissipation terms where derivatives respected to x, the axial axis, are calculated through a one step forward scheme or:

Central differentiation: $\frac{\partial f}{\partial \eta} = \frac{\Delta f}{\Delta \eta} = \frac{1}{2\Delta \eta}(f_{i+1} - f_{i-1})$ [5-16]

Forward differentiation: $\frac{\partial f}{\partial f} = \frac{\Delta f}{\Delta x} = \frac{1}{\Delta x}(f_{i+1} - f_i)$ [5-17]

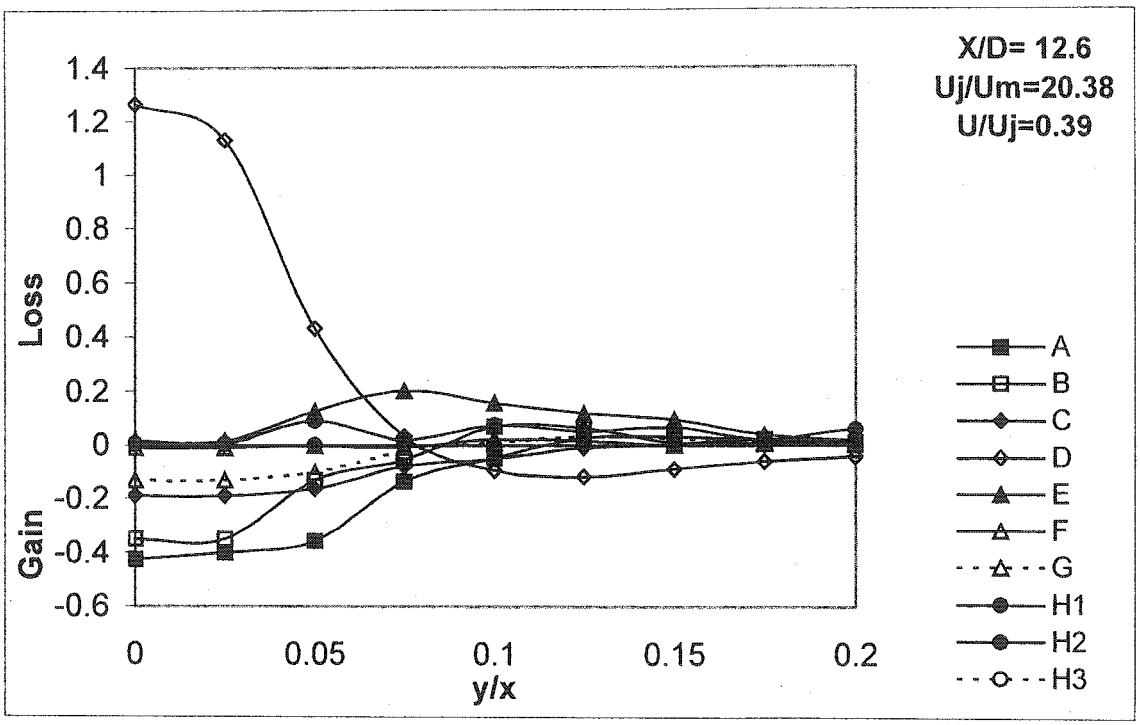

Figure 5-1 Terms of turbulence kinetic energy

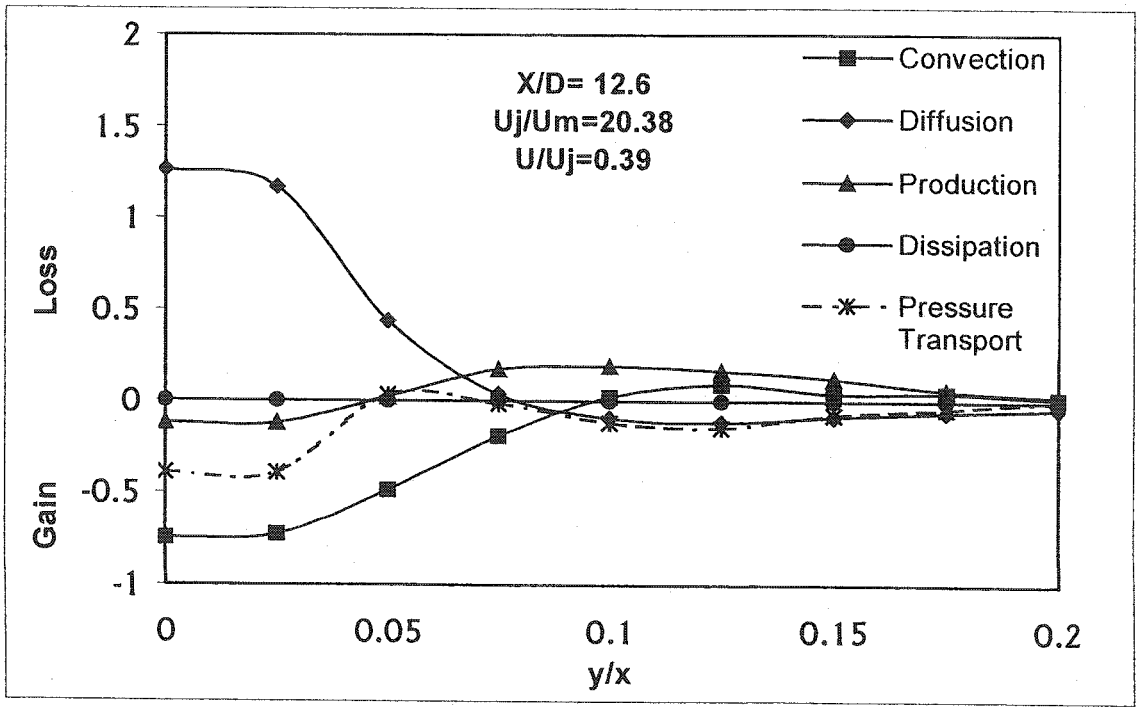

Figure 5-2 Balance of turbulent kinetic energy 80 mm upstream of the jet

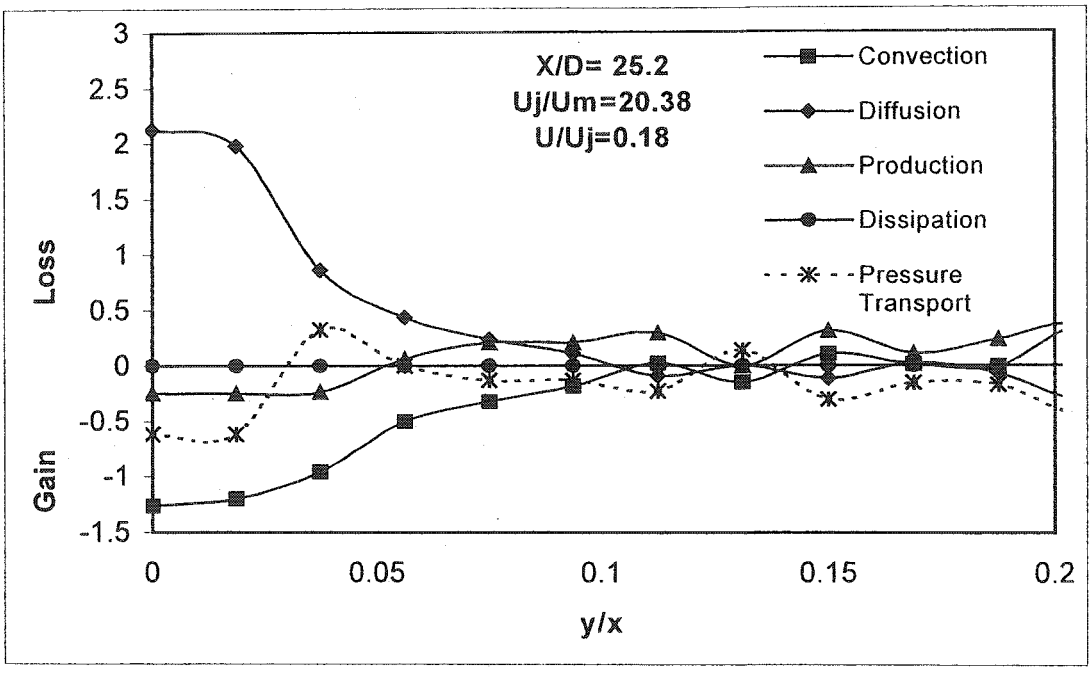

Figure 5-3 Balance of turbulent kinetic energy 160 mm upstream of the jet

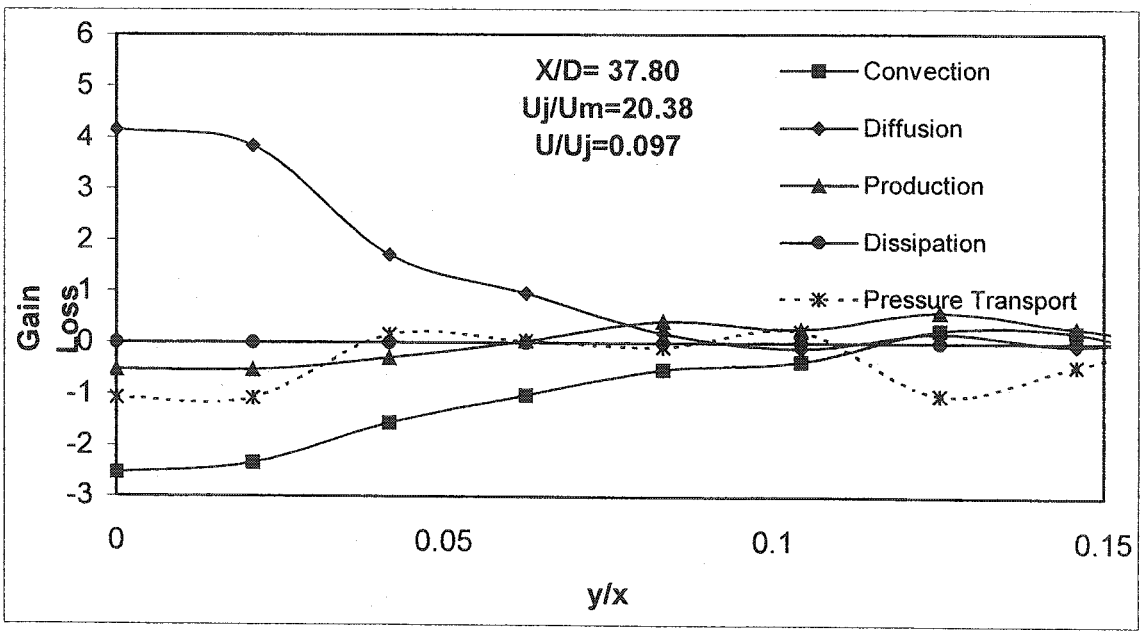

Figure 5-4 Balance of turbulent kinetic energy 240 mm upstream of the jet

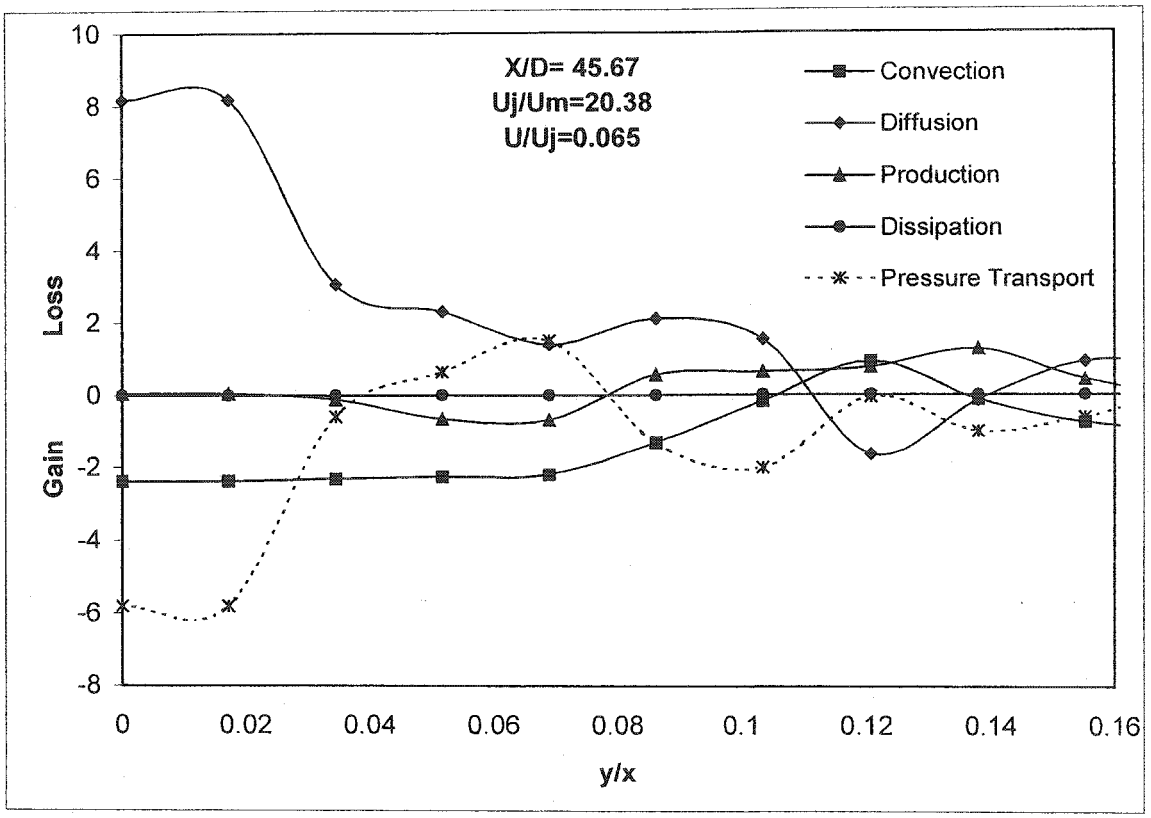

Figure 5-5 Balance of turbulent kinetic energy 290 mm upstream of the jet

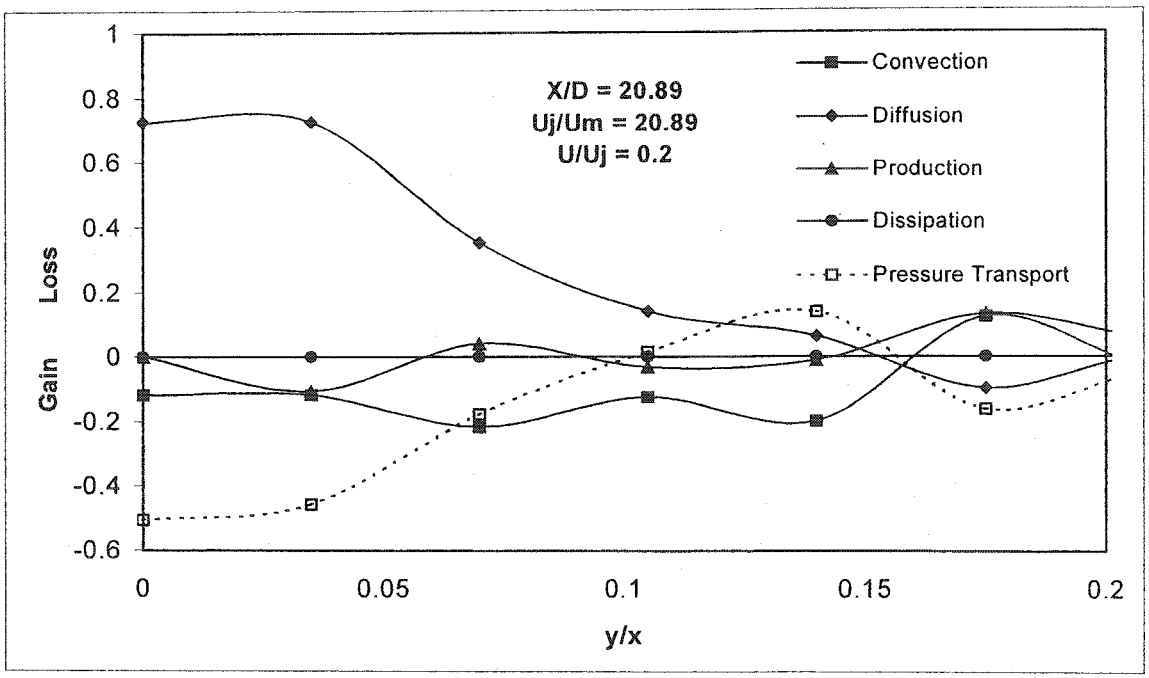

Figure 5-6 Balance of turbulent kinetic energy 200 mm upstream of the jet

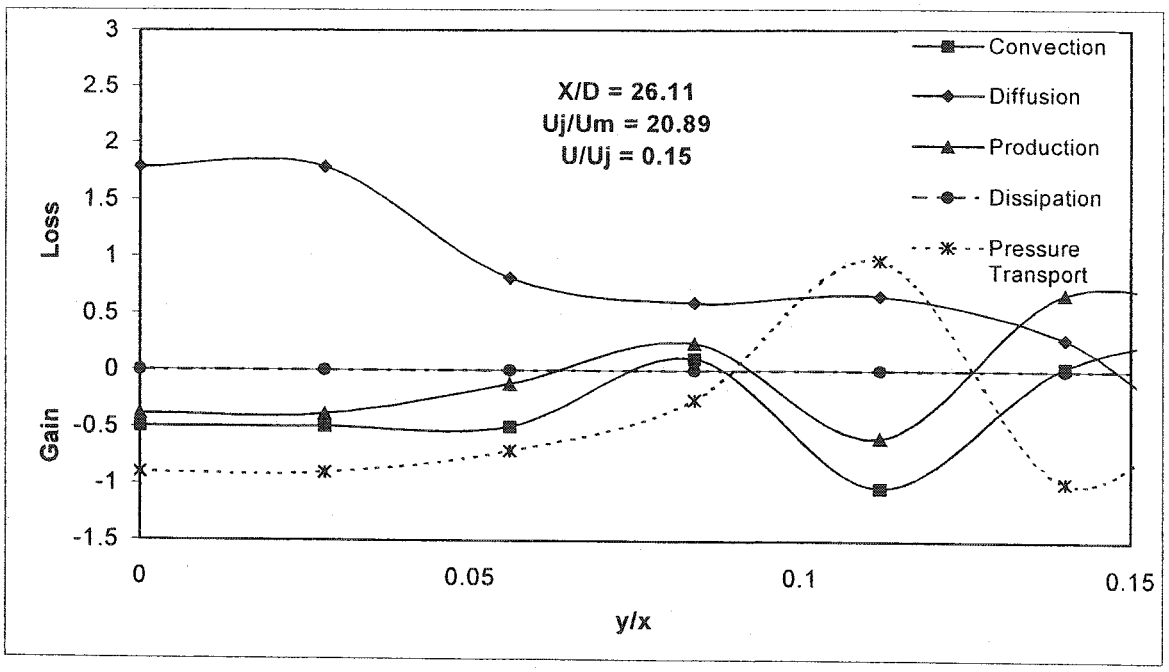

Figure 5-7 Balance of turbulent kinetic energy 250 mm upstream of the jet

A comparison between the above curves show that the balance of energy show an agreement in terms of similarity along the jet axis. Although at points close to the penetration length the velocity fluctuations in all directions are extremely high, still we can see the pattern of the energy balance is the same.

There is another agreement in the above figures in terms of the weight of each term in the energy equation. In all cases, the biggest absolute value of the terms belongs to the diffusion in the region close to jet axis.

Comparing these graphs with those presented by Wygnanski and Fiedler (1969) for a free round jet, one immediately notices the difference in the magnitude of the terms since those are a hundred times less than the present data (Figs. 5-1 to 5-7). This huge difference is because of the dividing of all terms by U_m^3. Since the rate of decay of centerline velocity for counter flowing free jet is higher than for a submerged jet at each point, this U_m^3 for submerged jet is much bigger than of counter jet. For example at the distance close to self-preserving condition, x/D=20, the centerline velocity of a submerged jet is $U_0 = U_j \frac{5.4}{x/D} = U_j \frac{5.4}{20} = 0.27U_j$ while the velocity of a counter jet at the same place will be less than 10% of the jet velocity (Figs. 4-1.a through 4-1.e). Since the jet velocity by itself in the tests by Wygnanski and Fiedler (1969) is at least 5 times more than those of the present study, this difference is understandable.

5.6 Results of tests in the mixing layer

As Chandrsuda and Bradshaw (1981) reported, the structure of flow in the mixing region is completely different than that of the flow in the jet or channel. On the other hand, the mixing layer has higher fluctuations in energy terms in the region far from the jet exit but switching between loss and gain in energy is much less in vicinity of the jet exit. It can be interpreted by the flow pattern reported by Yoda and Fiedler (1996). In the area closer to the jet exit, outside of the jet region, velocity has a very uniform shape and therefore mixing region is very small while in $X/X_p>0.5$ the jet is expanded enough to provide a bigger mixing region.

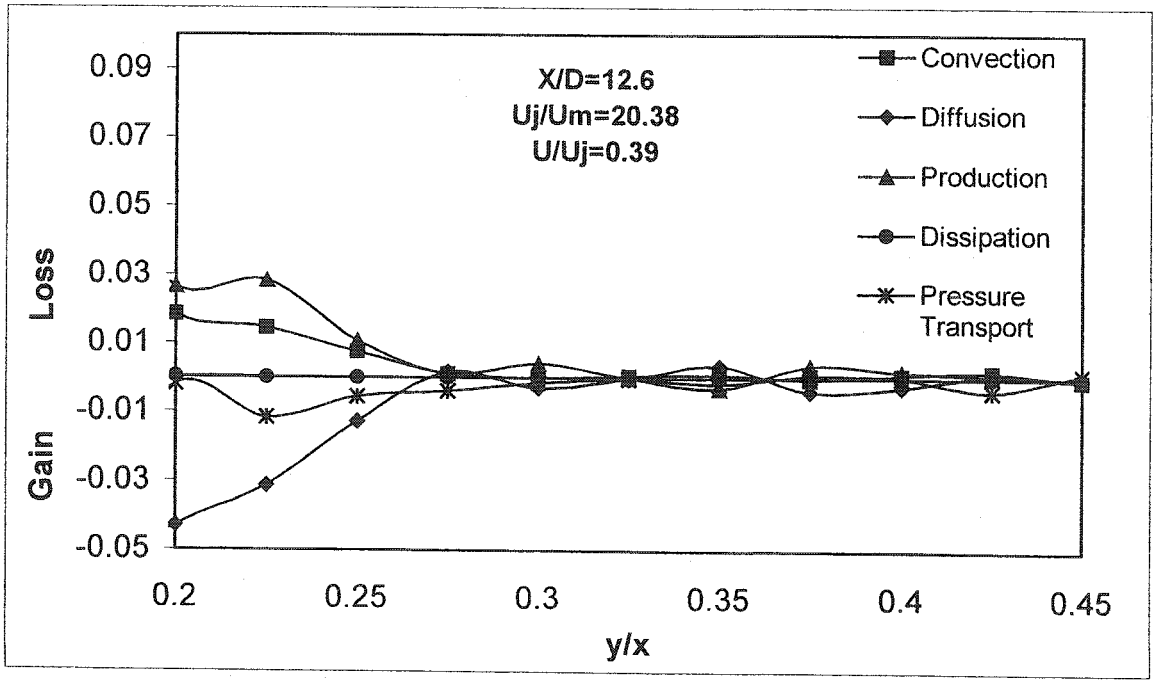

Figure 5-8 Energy balance in mixing layer between jet and return flow X=80 mm

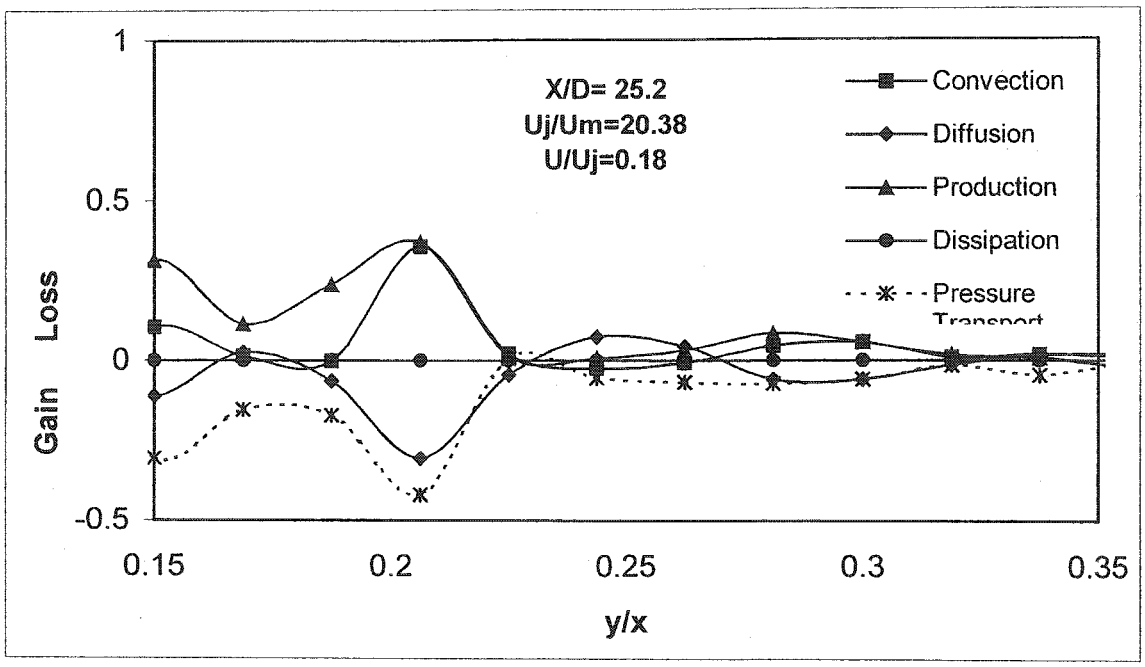

Figure 5-9 **Energy balance in mixing layer between jet and return flow, X=160mm**

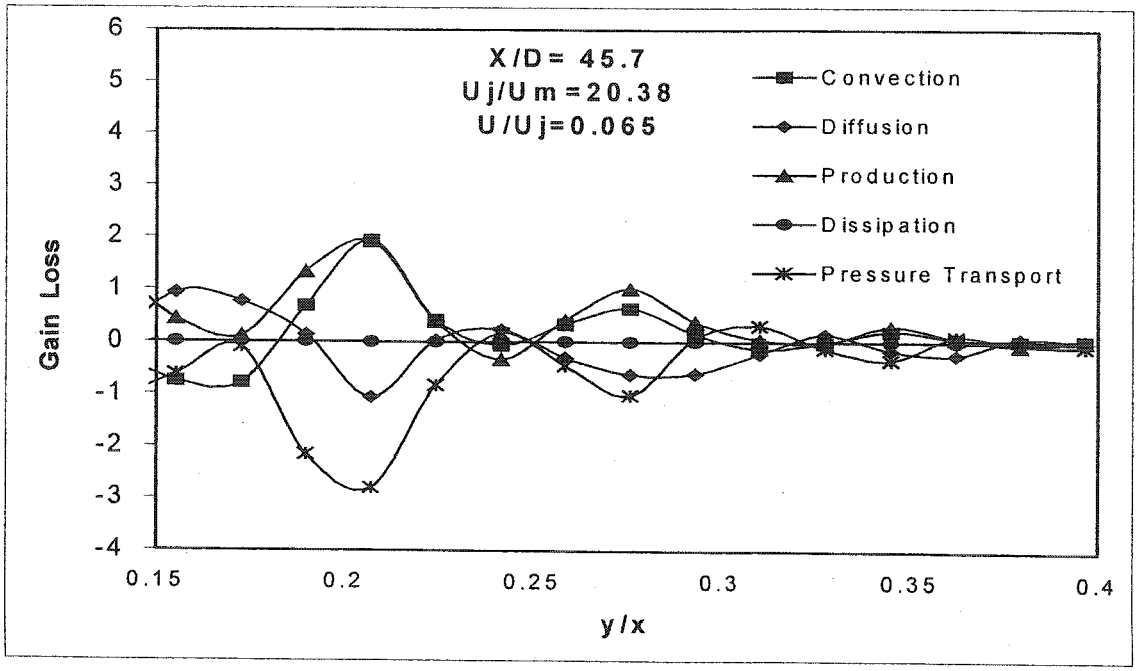

Figure 5-10 **Energy balance in mixing layer between jet and return flow, X=290mm**

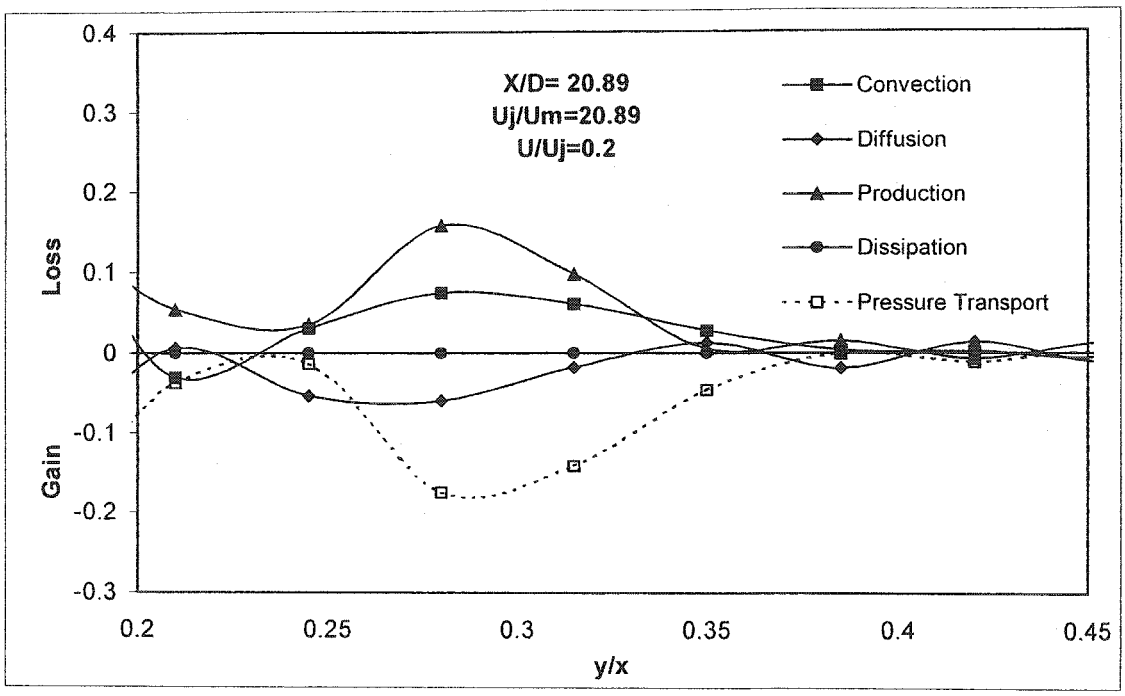

Figure 5-11 Energy balance in mixing layer between jet and return flow, X=200mm

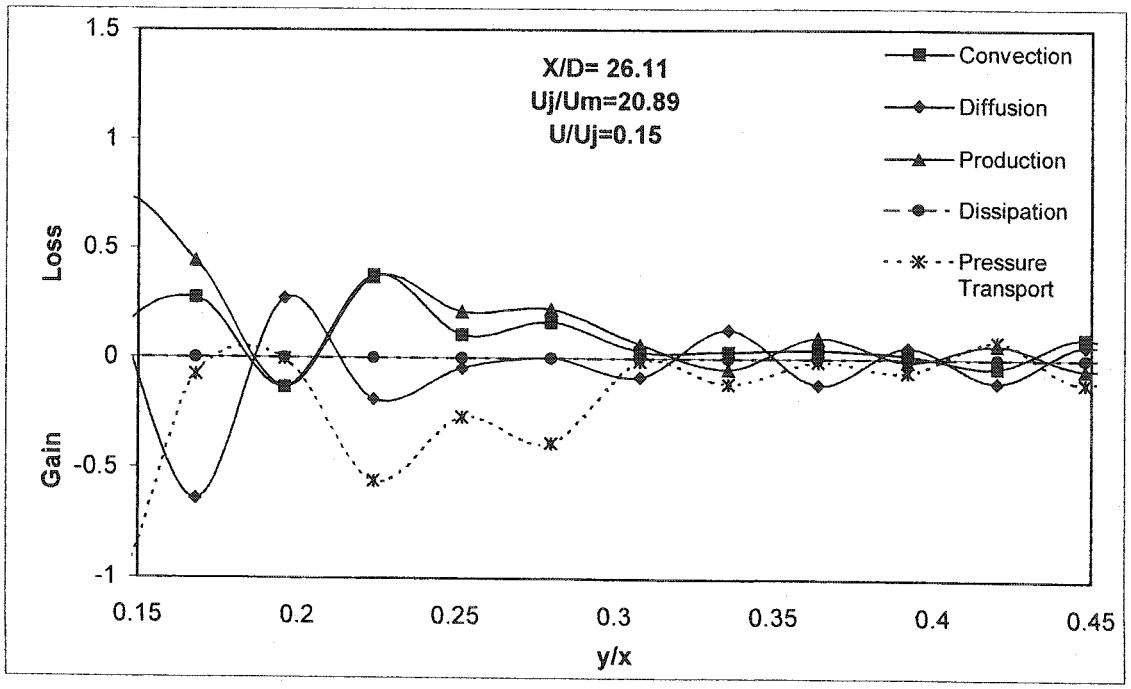

Figure 5-12 Energy balance in mixing layer between jet and return flow, X=250mm

Chapter 6

Numerical tests

6.1 General

Reynolds-averaged Navier-Stokes equations are the starting points to solve turbulence problems numerically. The direct numerical solution (DNS) is very difficult and expensive to solve real life problems (Cebeci 1999). Finding the right model of turbulence for the free submerged jet is not difficult. There is an agreement in literature that the zero equation model works very well for those jets (Wilcox 1993 and Cebeci 1999) while not much has been stated about the counter flowing free jet.

6.2 Choosing a model

To find the right model(s) to solve counter flowing free jet numerically, three models have been chosen: mixing length model, $k-\varepsilon$ model, and $k-\omega$ model. The first model is the one most recommended for submerged jets (Wilcox 1993,

Cebeci 1999), the second model is the most popular (Wilcox 1993), and the last one is mostly recommended by Wilcox (1993) since it gives very good answers in most cases.

All of the three models mentioned above have been tested for two cases: with and without a tracer in jet flow. Among them only the $k-\omega$ model did not answer well and even in most cases failed to converge as the problem of instability occurred. Therefore, the two models, namely the mixing length and the $k-\varepsilon$, have been chosen as the appropriate models.

6.3 Results and discussion

6.3.1 Mixing length model

Figures 6-1 through 6-3 are resulted from mixing length model for counter flowing free jet. The pattern is not very close to what was obtained by measurement and what was reported by Yoda (1996).

As shown in Figure 6-1, the model shows two vortices, which are parts of a vortex whose axis is a circle around the jet centerline. This vortex was not captured in the measurement. The model also predicts a penetration length is 22D when the velocity ratio is 10 that is slightly less than the measurements which suggests a penetration length of $X_p = 26D$.

The following Figures (6-2 and 6-3) show the cross sectional flow pattern which is supported with the measurement in the present study (Chapter 4) and also the available data reported by Chu (1999).

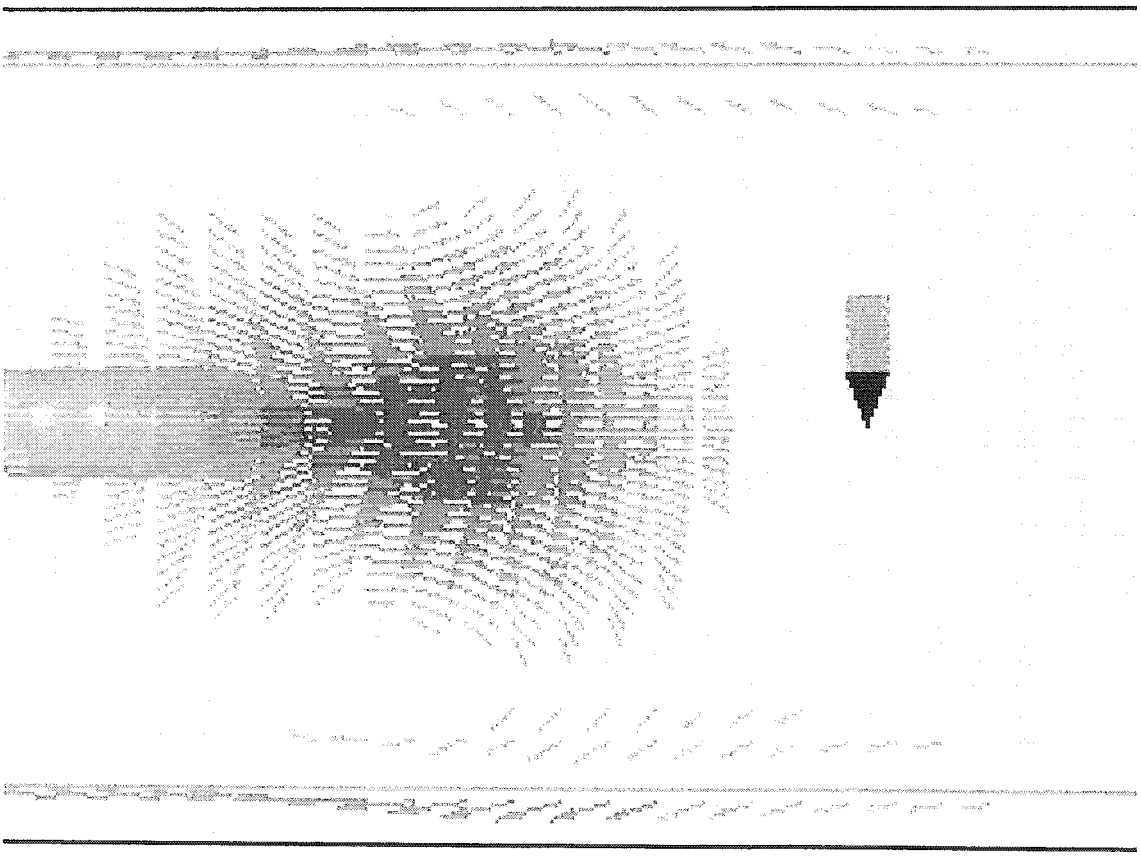

Figure 6-1 Velocity pattern and penetration length calculated by a mixing length model (Uj=3 m/s, Um= 0.3 m/s, D=10 mm, W=300 mm)

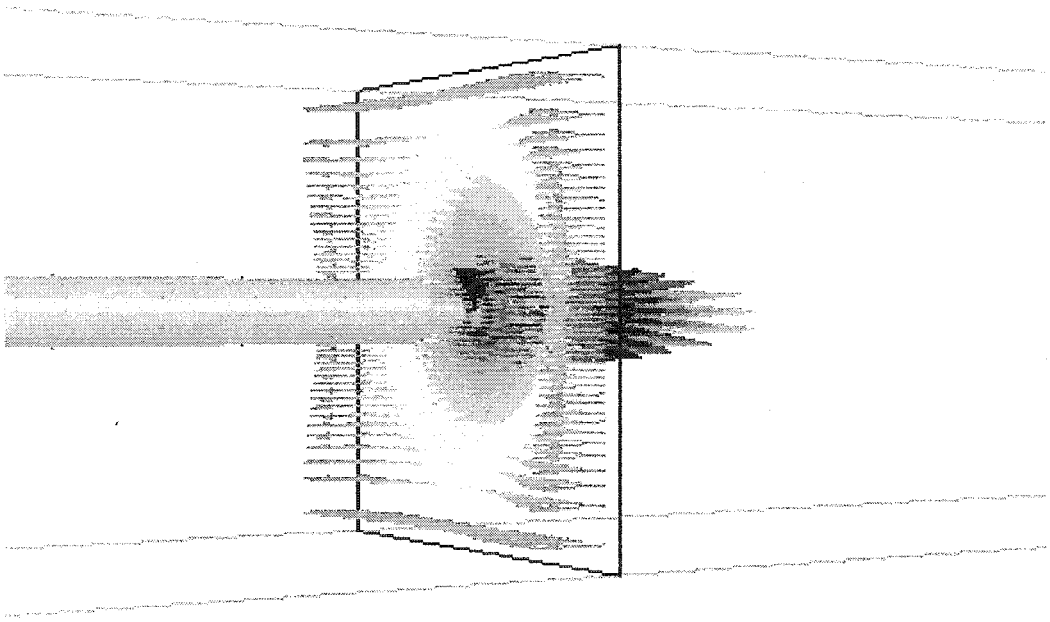

Figure 6-2 **The cross sectional flow pattern. Co-center circles show the model is successful in generating this pattern.**

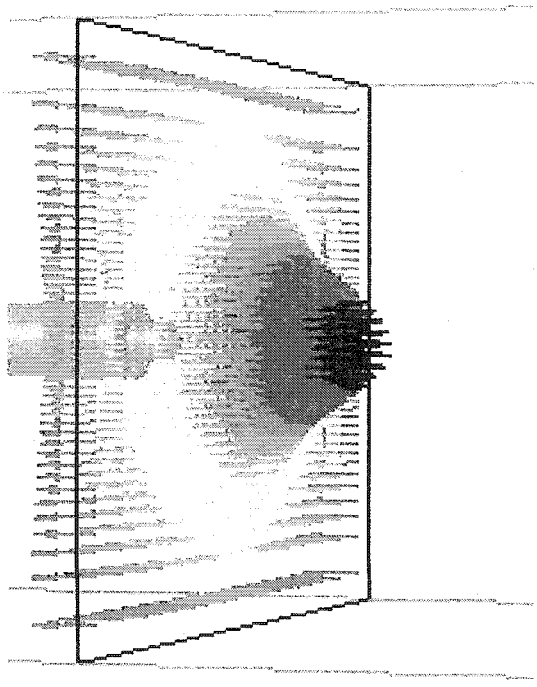

Figure 6-3 **Velocity vectors at the jet exit from another angel.**

Mixing length theory is based on the similarity of the Reynolds's shear stress along the shear layer with the molecular momentum transport process and the idea of eddy viscosity [Eqs. 6-1 and 6-2](Wilcox 1993).

$$\tau_{xy} = -\rho\overline{uv} = 0.5\rho V_{mix} L_{mix} \left|\frac{dU}{dy}\right| \qquad [6\text{-}1]$$

$$\mu_T = \rho L_{mix}^2 \left|\frac{dU}{dy}\right| \qquad [6\text{-}2]$$

A model based on this theory will have a good answer in the case of momentum transport. The boundary conditions are:

$$U(x,y) \to 0 \qquad \text{as} \qquad y \to \infty \qquad [6\text{-}3]$$

and

$$\frac{\partial U}{\partial y} = 0 \qquad \text{at} \qquad y=0 \qquad [6\text{-}4]$$

The later condition exists in both kinds of the jets, submerged free and counter flowing free jets, but there is a big difference in the first condition between two kind of jets.

Another reason is the pressure distribution in counter flowing free jets, unlike the submerged free jets, is not simply related to the velocity of flow outside the jet (Hill 1967).

6.3.2 $k-\omega$ Model

This model initially was presented by Jones and Launder (1972). Launder and Sharma (1974) modified some closure coefficients. This model very soon became the most popular two-equation model of turbulence (Wilcox 1993).

Since the model is based on the turbulent kinetic energy and its dissipation with no other assumption based on similarity, a good answer is expected. Figures 6-4 through 6-7 show the results of the runs with this model.

Figures 6-4 and 6-5 show the result of the numerical tests on penetration length.

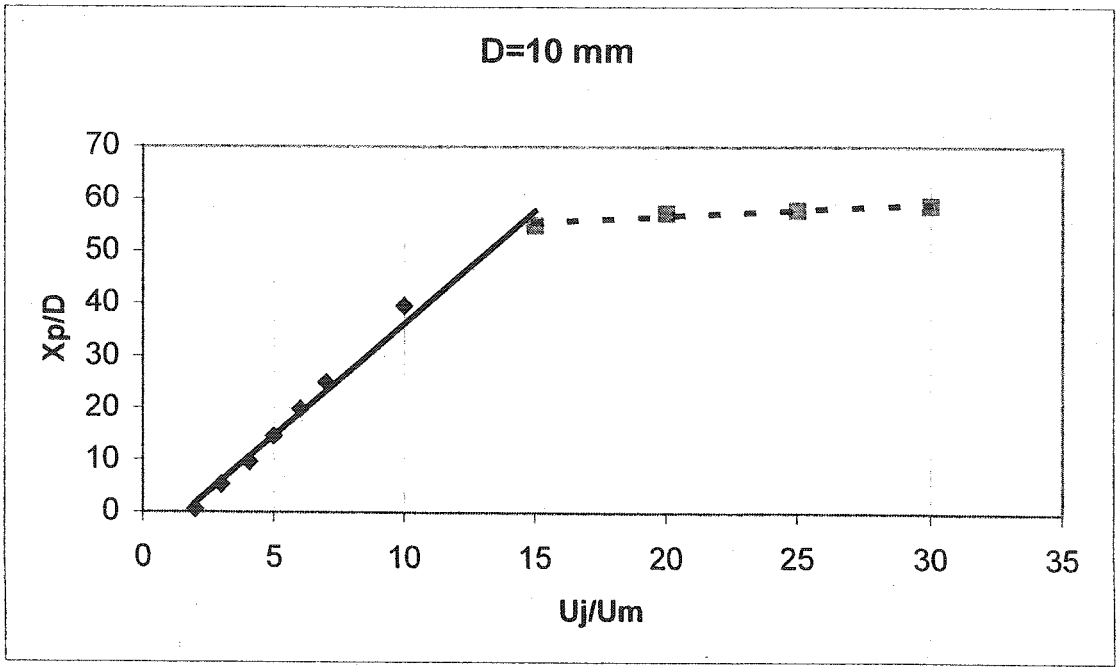

Figure 6-4 Penetration Length calculated by a $k-\varepsilon$ model for a jet (D=10 mm).

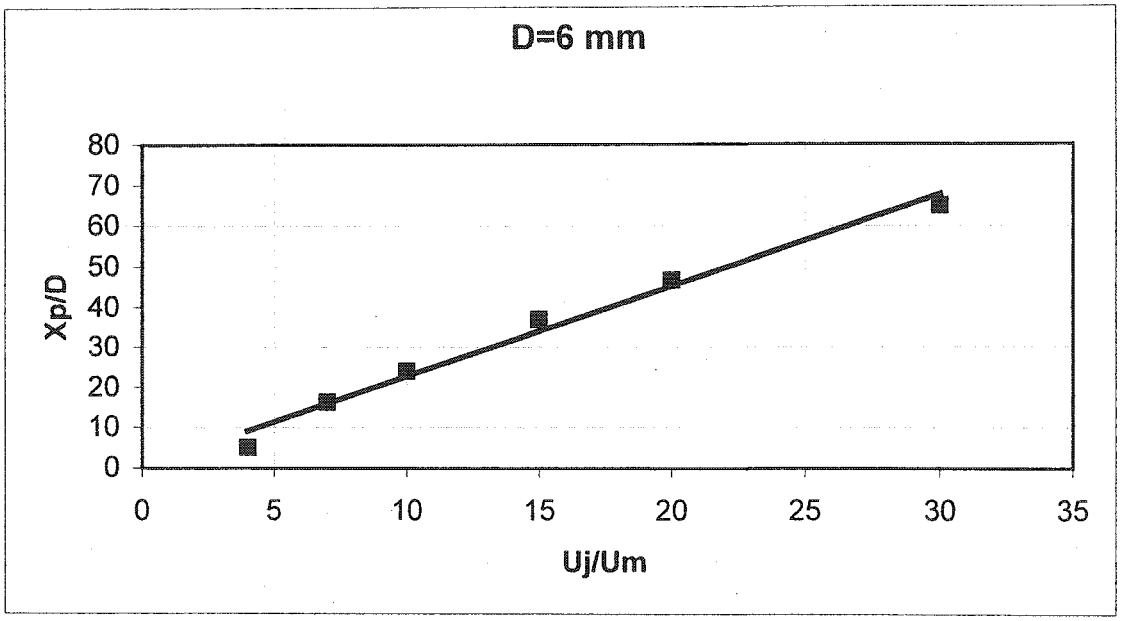

Figure 6-5 Penetration Length calculated by a $k-\varepsilon$ model for a jet (D=6 mm).

As it is seen, the penetration length calculated by this model for D= 10 mm is longer than that found out by the direct measurement by LDA technique while it has a better agreement for D= 6mm. This is also important to point out that this length for D=10 mm is in complete agreement with the result found by Yoda (1996) and Lam (1997) for the maximum penetration length.

Other geometrical characteristics of the jet such as the maximum expanding width of jet has better agreement with our measurement by LDA than the results by Yoda (1996) and Lam (1997). The reason is the method used by those investigators is based on the laser sheet photography that has no discrimination about the direction of flow and they can only measure the concentration of the fluorescence materials injected by the jet through the measurement of brightness

of each point. Now, looking at the result of calculation to find the concentration, one can see that the result of the numerical test has a very good agreement with data presented by the mentioned researchers. Figure 6-6 shows the concentration distribution of the jet flow.

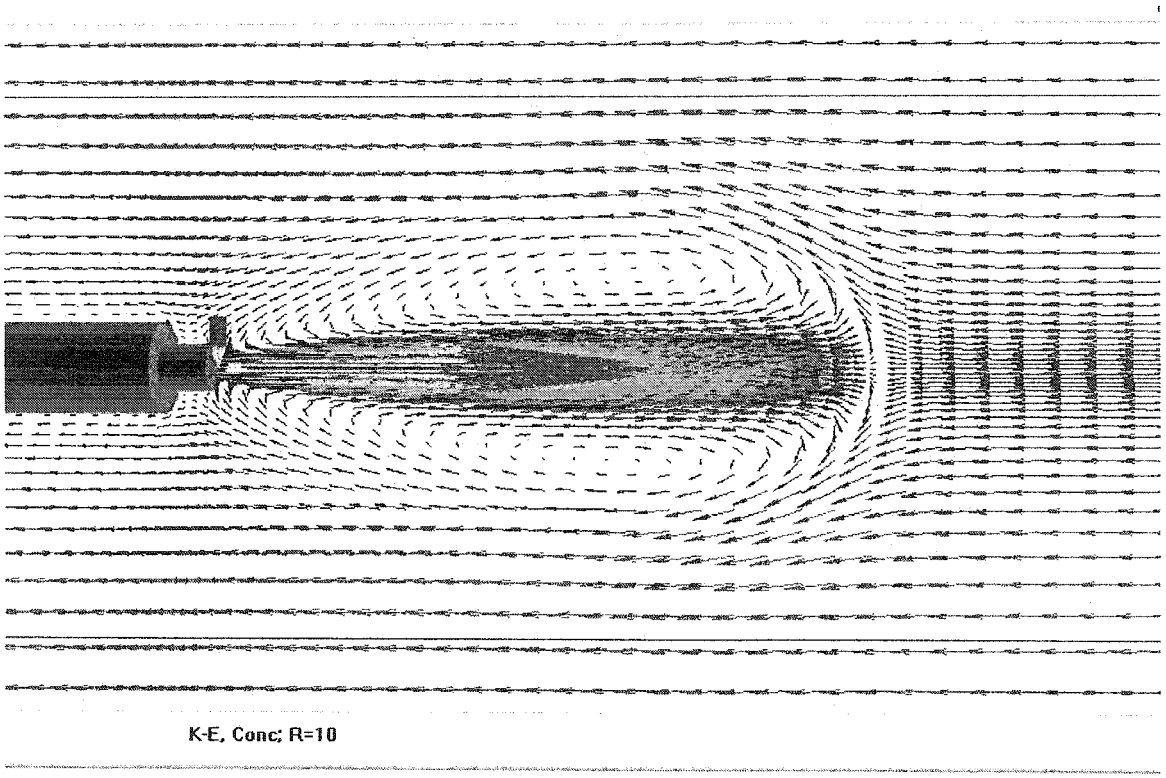

Figure 6-6 Flow pattern calculated by a $k-\varepsilon$ model.

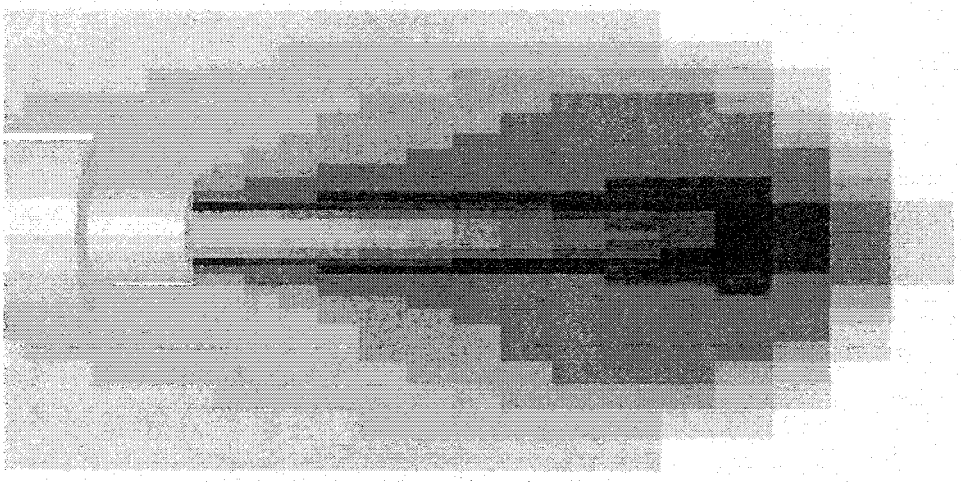

Figure 6-7 Concentration distribution calculated by a $k-\varepsilon$ model (D=10 mm and U_j/U_m =7)

In the above Figure, Fig. 6-7, the maximum lateral expansion of the jet is about 7 times of the jet diameter which is equal to the average value reported by Lam (1998) and agrees with 7.5D for U_j/U_m=7.5 reported by Yoda (1996).

These examples show the result of the limited numerical tests on the counter flowing free round jet by Phoenics in the sense of the geometry and concentration is reliable.

Chapter 7

Mixing properties of counter flowing free jet

7.1 General remarks

One of the applications of the jets is related to their ability to mix two or more fluids. The importance of jets in mixing process was previously discussed in chapter 1. This application for jet, traditionally was the reason to use them in chemical mixing, waste dilution, combustion reactors, and burner motors. It is also important to know that the mixing depends on time as well as space. Spalding (1971, 1983) mentions a phenomenon in reactors using jets called "unmixedness". He explained that in a reactor where a high concentration of fuel and oxidant are available, in some cases the reaction process is very slow since fuel and oxidant arrive at the same point but at *different times*. The present study did not deal with time and only focused on the spatial characteristics of mixing.

Mixing of a tracer injected as a counter flowing free jet into the main flow is characterized by two distinct mixing regions: downstream jet wake and upstream of the jet exit. Mixing in upstream is fast and according to the reports by Lam (1995, 1997) and Yoda (1995) is efficient. However, it is not complete. Since this part of mixing has already been investigated, mixing downstream of the jet was studied in this research. After a short review of literature, the sampling, calculation and calibration processes are presented later in this chapter.

7.2 Review of literature

Bradshaw (1971) recommended several methods to measure the concentration using hot-wire techniques. Several other methods such as Laser Induced Fluorescence or LIF (Lam 1995, 1997, Yoda 1996, and Chu 1999), PIF, colorimeter Ramaprian 1989), and also conductivity meter have been used by investigators to determine the mixing characteristics.

Mixing of a tracer in a pipe flow by natural turbulence needs a very long distance, 100~150 pipe diameter, to achieve complete mixing (Evans 1967). This distance is inconveniently large to be considered a mixing device (Morgan et al. 1976).

Holly et al. (1972) published an article on the concentration study in an open channel to investigate the dilution of highly concentrated salt-water solution in to another body of water. Some of his analogies such as the procedure to evaluate

the concentration diffusion were used in the present study. He used a conductivity meter to measure the concentration distribution.

Ramaprian (1989) used a colorimeter to measure the concentration of dye at different points in a cross jet. This method is based on the comparison between the intensity and frequency of light passing a constant distance and the reading recorded by a detector. Since the study was performed in an open channel, there was no limitation for the access to the measurement point.

7.3 Results and discussion

In this study, it was not possible to use measurement techniques that need access to the test section such as colorimeter. Instead, food color and table salt (NaCl) were used as tracers and the measurement of conductivity was correlated with concentration (Chapter 2). LDA techniques were used to measure both jet and main flow velocities directly.

To find the relation between salt concentration in the tap water and the conductivity of the solution, a calibration test was performed prior to the main experiment. In the first stage, tap water from the laboratory sump was taken to provide sequential concentrated NaCl solution. 20 samples including distilled water, tap water, and salt-water solution with various concentrations were provided. Concentration was in the range of maximum 80000 mg/L to a minimum

of 24 mg/L. Figure 7-1 shows the variation of conductivity with concentration. The conductivity of the tap water was in the range 425~ 475 μmho in the upstream region of the jet and the concentration of samples in downstream (jet wake region) was kept to a maximum of 1000 μmho.

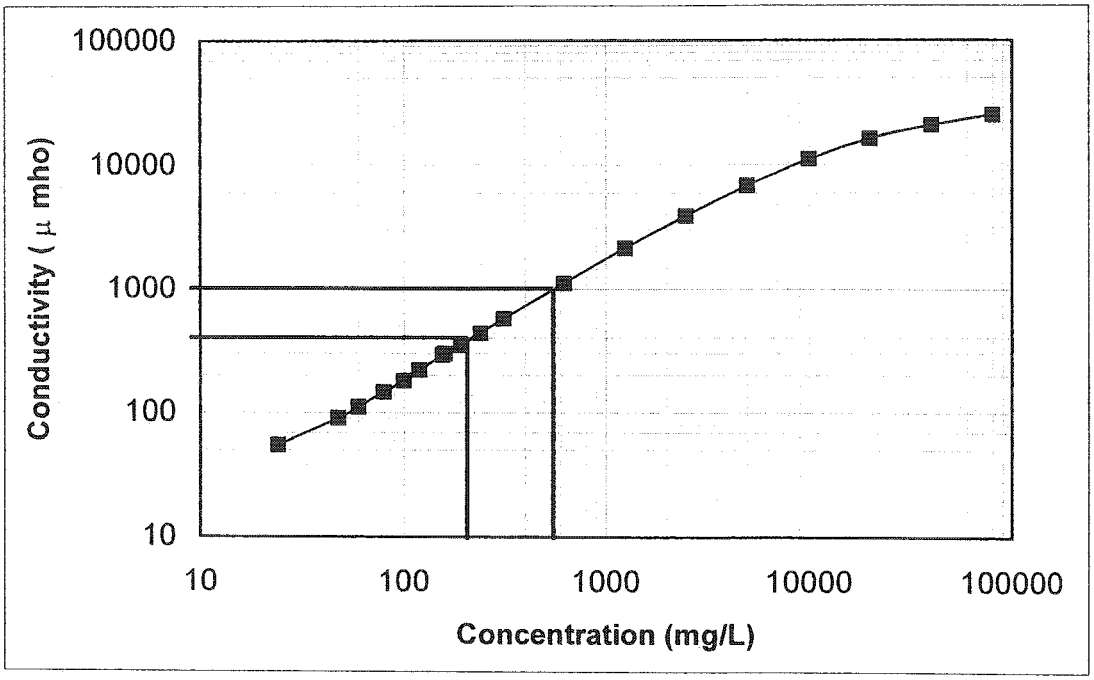

Figure 7-1 Relationship between conductivity and concentration. Bold lines show the range of concentrations of the samples.

As seen in Figure 7-1, conductivity and concentration are linearly proportional to each other up to a certain value of concentration (6000 mg/L). To ensure that the range of conductivity, which was measured in this study, falls in the linear part, another figure is provided [Fig. 7-2].

Since all of the readings for the samples fall in the above linear domain, for the rest of this chapter conductivity is used in place of concentration. Also, for each sample, the conductivity component related to main flow upstream of the jet region was subtracted from the conductivity of mixed flow measured by the sample.

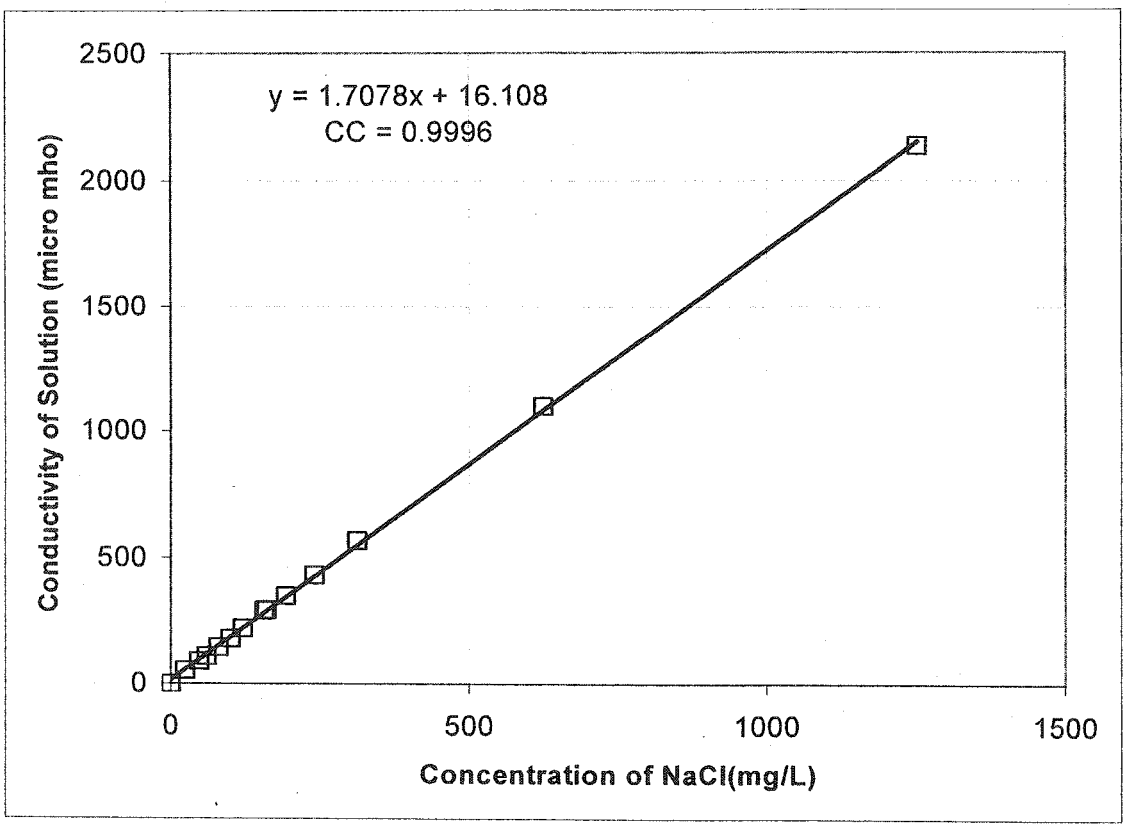

Figure 7-2 Calibration data for conductivity meter for the samples range.

To verify the steady state of the mixing condition, jet concentration, and accuracy of results, a mass balance test was performed on all samples. The rate of salt injected was measured and compared to the mean salt passing at the three

downstream sections. Also, the total mass measured in three sections downstream of jet was balanced.

According to Lam (1997), Chu (1999), and the present study (Chapter 4) the velocity distribution across the test section is essentially axisymmetric. The axial velocity in the short distance between the three sampling sections, less than 2W, on the same horizontal line is constant, therefore, concentration times the related area (Figure 7-3) can be accepted as the total mass of NaCl in the area.

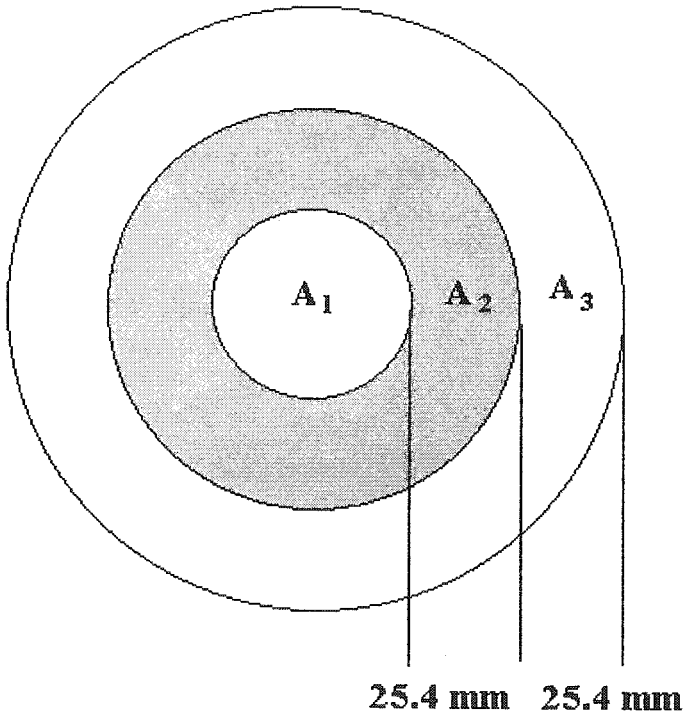

Figure 7-3 The area used for mass balance.

The total mass at each section was calculated and by averaging the three sections in each test, the error was calculated by the maximum value of error ε_i :

$$\varepsilon_i = \left| \frac{\text{saltmass}_i - \text{saltmass}_{avg}}{\text{saltmass}_{avg}} \right| \times 100 \qquad [7\text{-}1]$$

Here, saltmass_i (i=1, 2,and 3 indicates X/W=-2, -3, and –3.7 respectively) is the concentration times area and saltmass_{avg} stands for average of mass or $\text{mass}_{avg} = \sum_{i=1}^{3} \text{mass}_i$. The errors are shown in Figure 7-4.

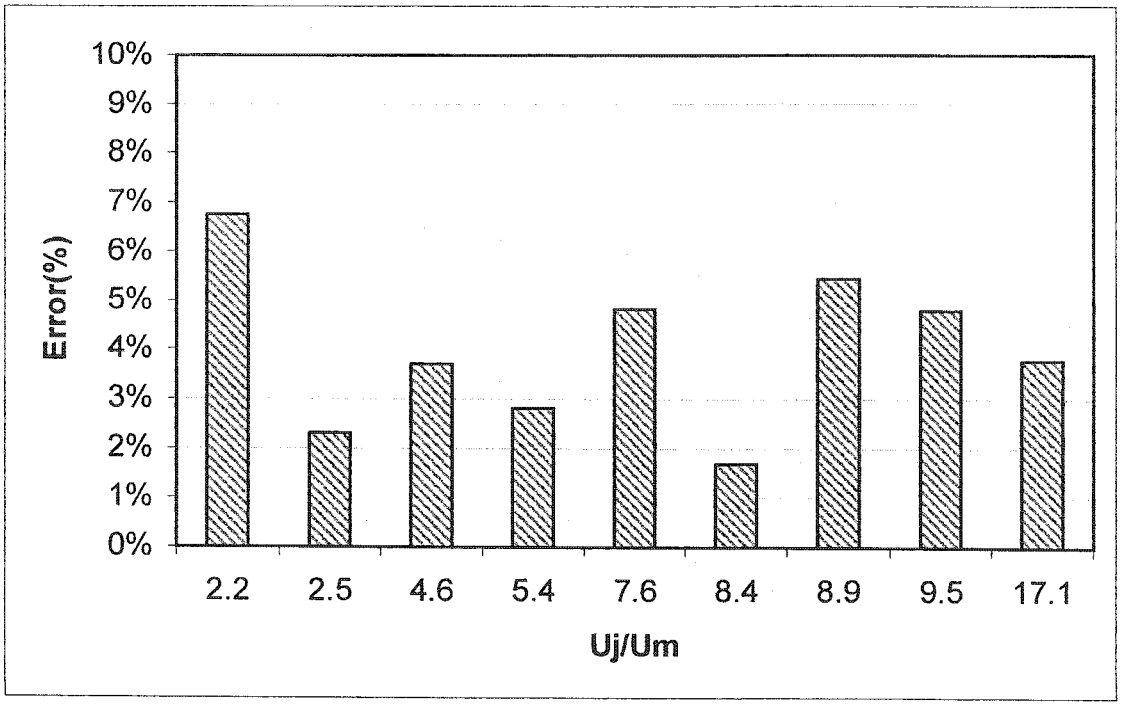

Figure 7-4 Error in mass balance.

Figures 7-5 to 7-8 show the relation between concentration across the test section with the dimensionless distance. As these figures show, concentration at the centerline is maximum for all cases that are not unexpected. Another property of concentration distribution across the test section is the common shape of these curves. Fitting curves to the points close to the centerline show the best fit is a 2nd degree parabola. All of them have a maximum in x=-2W higher than the maximum at x=-3.7W. It means the near wake turbulence contributes to the mixing.

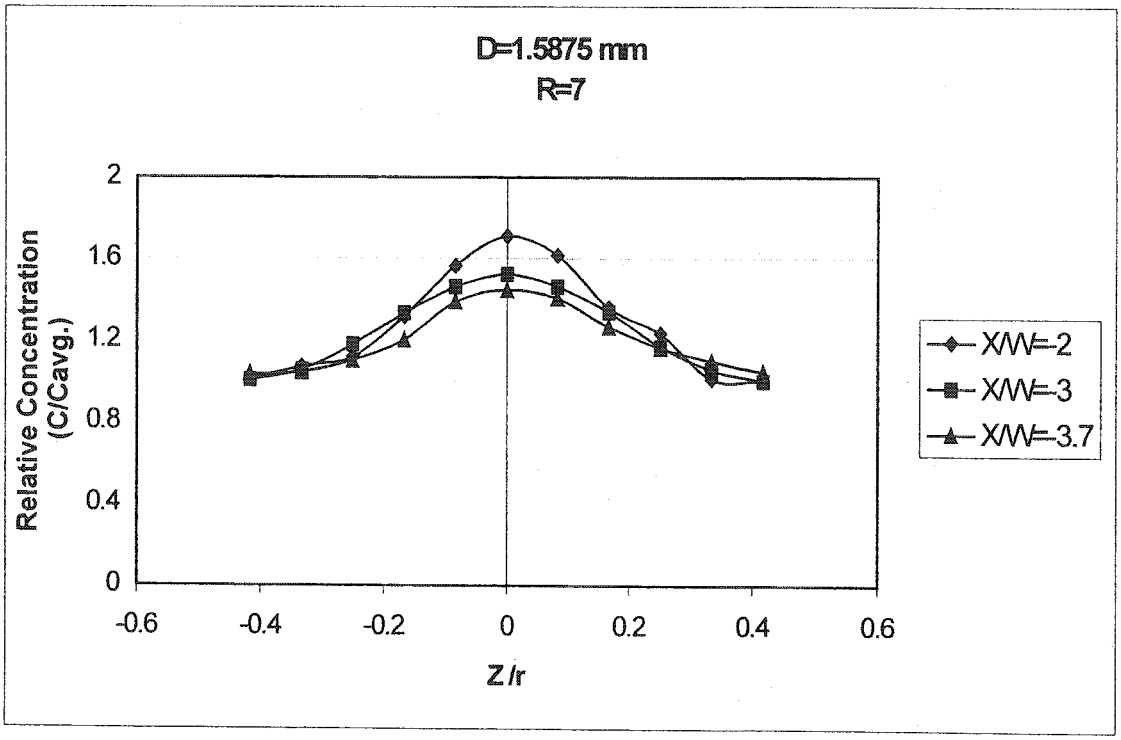

Figure 7-5 Relation between radial distance and concentration

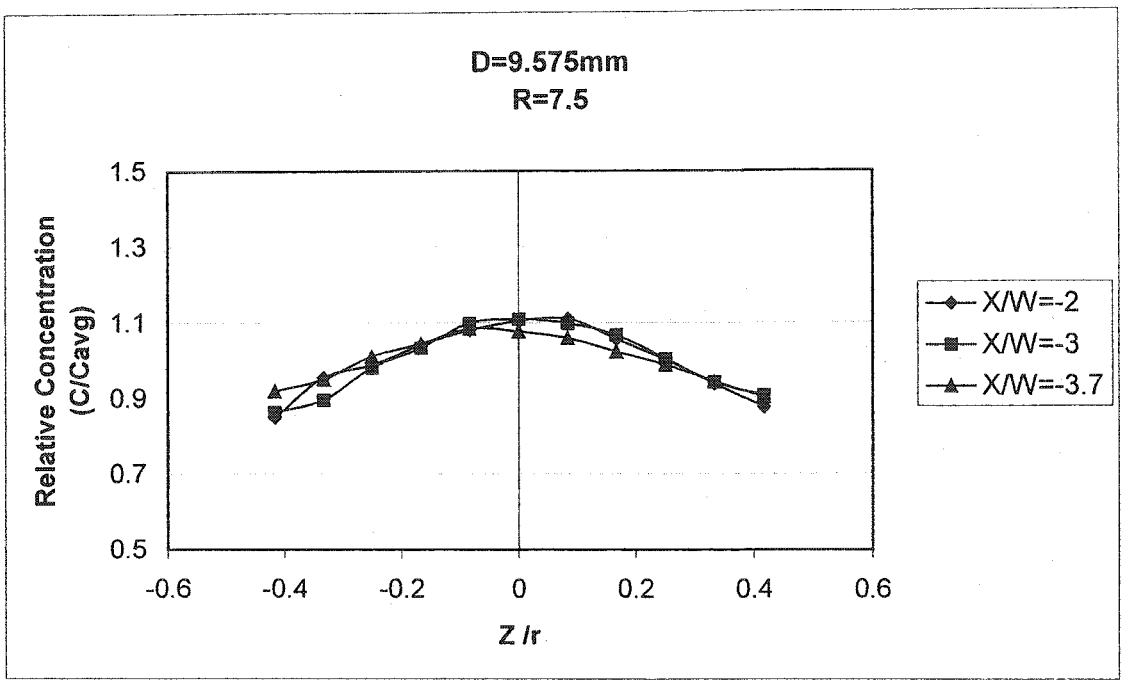

Figure 7-6 Relation between radial distance and concentration

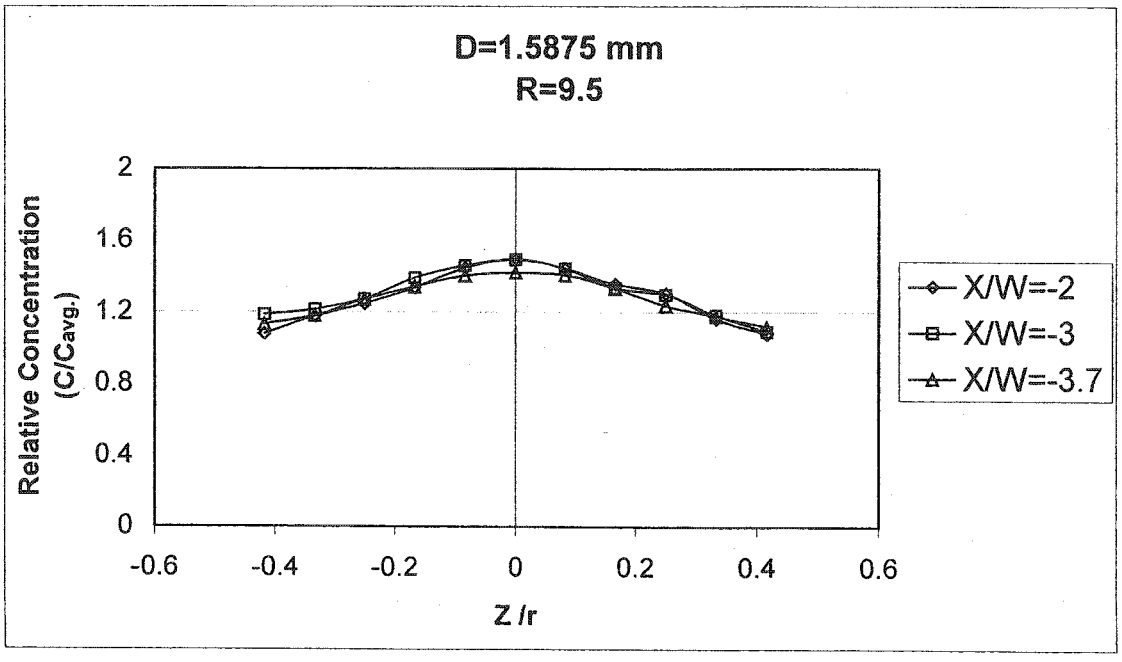

Figure 7-7 Relation between radial distance and concentration

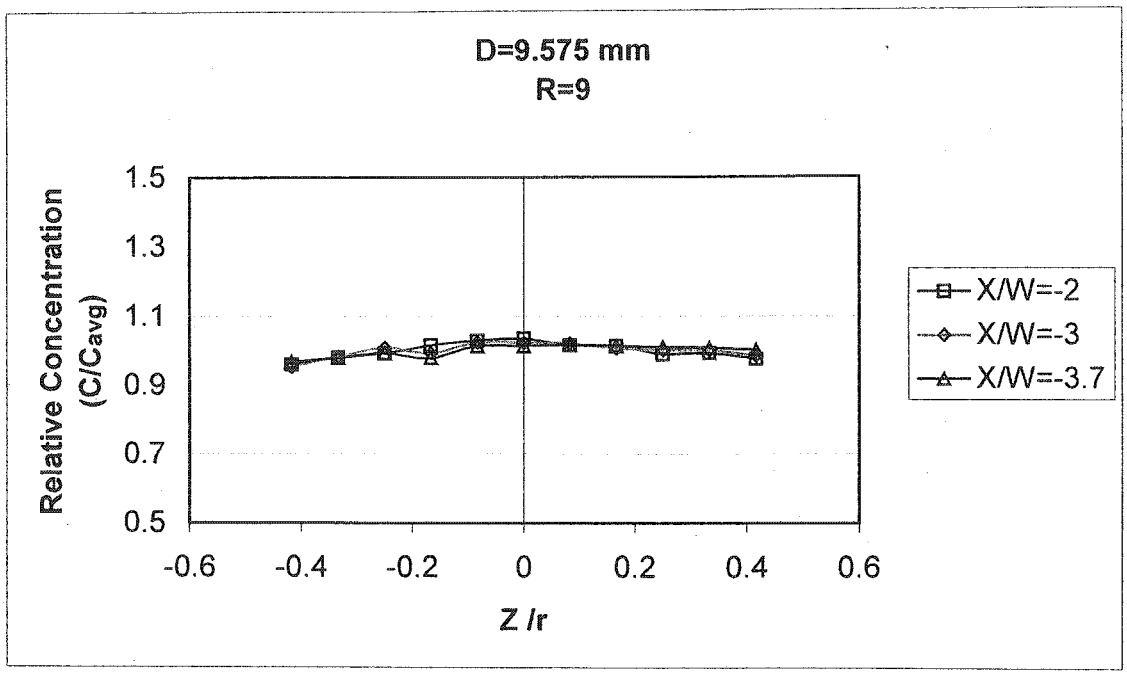

Figure 7-8 Relation between radial distance and concentration

A comparison between Figures 7-5 and 7-7 with 7-6 and 7-8 shows the diameter of the jet is another parameter in concentration diffusion. According to these figures, the bigger jet diameter leads to a better mixing. This improvement in mixing may be the effect of a longer penetration length as it changes with diameter too. Figure 7-9 is to show how velocity ratio can affect the mixing.

To have a scale for mixing, a statistical method was chosen. In this method, the standard deviation of concentration in the samples across the test section was calculated:

$$\text{Std.} = \sqrt{\frac{n\sum x^2 - \left(\sum x\right)^2}{n(n-1)}} \qquad [7\text{-}2]$$

where X=concentration.

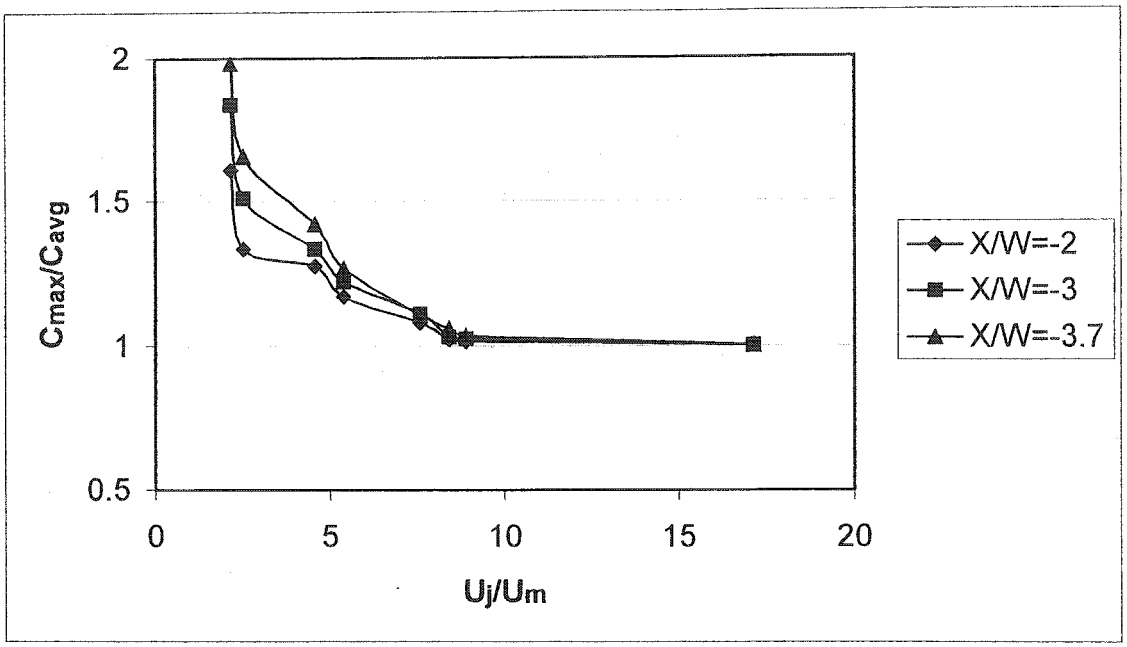

Figure 7-9 Relation between concentration at the centerline (worst cases) and jet velocity ratio.

Figure 7-10 shows the variation of standard deviation of concentration with the velocity ratio. By definition, the higher standard deviation means less homogenous samples. According to this figure, standard deviation is proportionally linear with 1/R or U_m/U_j this means a higher velocity ratio gives better mixing.

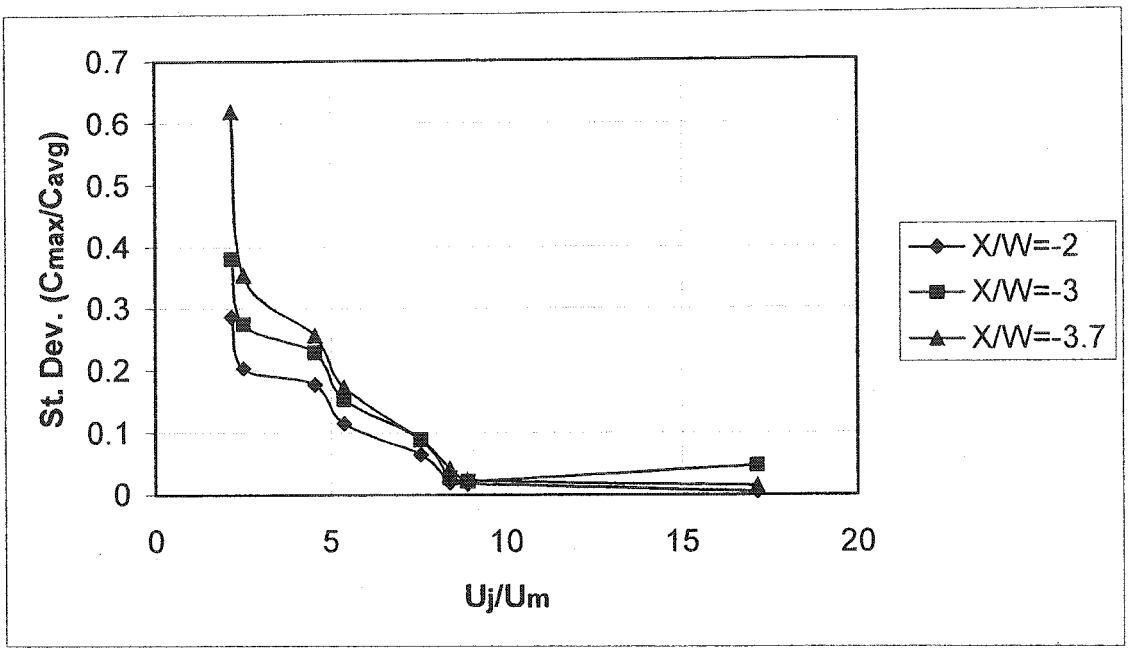

Figure 7-10 Relationship between standard deviations of relative concentration across the cross section and jet velocity ratio.

Chapter 8

Summary and conclusions

8.1 Conclusions of the thesis

This research was performed to investigate the turbulence and mixing characteristics of counter flowing free jets. The tests were conducted to measure axial and radial velocities by LDA techniques using a 2-D laser probe in a square test section with different size of nozzles.

Establishment of a criterion for prediction of the penetration length of the jet was the first part of the study. Covering a wide range of jet velocities to main flow velocity ratio and nozzles size, penetration length comprehensively was investigated and by defining critical velocity ratio R_c the differences in results of the previous studies were explained. According to this study, walls affect the penetration length and after a certain value of the velocity ratio which varies with the ratio of jet diameter to the test section width (Chapter 3).

Measurement of turbulence and centerline velocity decay rate were presented in Chapter 4. These measurements show velocity of jet decays along its axis inversely with the distance to the jet exit that is similar to the decay rate of the velocity of submerged free jet but more rapidly.

For evaluating the balance of turbulence kinetic energy inside the jet region and also in the mixing layer a dimensionless form the equation of the energy was used. All terms except the pressure diffusion were calculated using the data from measurement. The term including pressure was used as closure to the equation of turbulent kinetic energy (Chapter 5).

A small part of the study was devoted to numerical tests using Phoenics™. According to the present study, a k-e model can predict the penetration length that lies in the acceptable range recommended by previous researchers and linearly related to the result of the measurements during the present study (Chapter 6).

Mixing property of counter flowing free jets in its wake was investigated using direct measurement of concentration in different locations in the wake of the jet. The results are presented in Chapter 7. Since the velocity ratio is the major parameter of the jet, it was chosen as the changing factor in the tests. The efficiency of the mixing was characterized by the standard deviation of the

concentration along the radial axis. The results show the mixing can be considered completed when the velocity ratio reaches the R_c.

8.2 Contribution to knowledge

i. The critical velocity ratio was introduced to explain the behavior of the dimensionless penetration length in different dimensionless jet diameters.

ii. Measurement was made to find turbulent intensities and also the expansion of the jet was investigated.

iii. Balance of turbulence kinetic energy was investigated for the jet and mixing layer.

iv. Three turbulence models, mixing length, k-ε, and k-ω were tested and only the standard k-ε model came out successfully.

v. Mixing of a tracer injected by the jet in the wake flow was investigated and a relationship between the mixing and velocity ratio R was established.

8.3 Suggestions for further studies

The statistical characteristics of turbulence such as correlation and the scale of turbulence can be a subject for further studies.

Effects of an inclined jet can also be studied to investigate the behavior of the jet in a main stream with a degree of approach close to 180^{o}.

The mixing in the wake of the jet needs more investigation with a variety of nozzles.

References

Abramovich, (1963) " The Theory of Turbulent Jets" MIT Press, Cambridge, Mass., USA.

Abramovich G N, (1969) "The propagation of a turbulent jet in an opposing stream" in "Turbulent Jets of Air, Plasma, and Real Gas", Consultant Bureau, New York, USA.

Albertson M L, Dai Y B, Jensen R A, Rose H, (1950) " Diffusion of submerged Jets" Transactions ASCE, Volume 115.

Arendt J, Bobcock H A, Schuster J C, (1956) " Penetration of a jet into counter flow" Journal of Hydraulic Division Proceedings of ASCE, August 1956,1038-8-11.

Beltaos S, (1999) "Discussion on 'Round jet in ambient counter flowing stream' paper by Lam K M and Chan H C" Journal of Hydraulic Engineering, (125) 428-430.

Beltaos S, Rajaratnam N, (1973)" Circular turbulent jet in an opposing infinite stream", Proceedings of 1st Canadian Hydrotechnical Conference, 1-17.

Bradbury L J S, (1967) " The structure of a self-preserving turbulent plane jet" Journal of Fluid Mechanics (23) 1, 31-64.

Bradshaw P, (1967) " The turbulence structure of equilibrium boundary layers" Journal of Fluid Mechanics, (29) 625-645.

Bradshaw P, (1971) "An Introduction to Turbulence and its Measurements" Pergamon Press, Germany.

Capp S P, (1983) "Experimental Investigation of the Turbulent Axisymmetric Jet" Ph.D. Thesis, Graduate School, State University of New York at Buffalo.

Cebeci T, Cousteix J (1999) " Modeling and Computation of boundary- Layer Flows" Springer and Horizons Publishing, Heidelberg, Germany.

Chandrsuda C, Bradshaw P, (1981) " Turbulence structure of a reattaching mixing layer" Journal of Fluid Mechanics (110) 171-194.

Chu P C K, Lee J H, Chu V H (1999) " Spreading of turbulent round jet in coflow" Journal of Hydraulic Engineering ASCE (125) 193-204.

Daily J W, Harleman D R F (1966)" Fluid Dynamics" Addison-Wesley, USA.

Dryden H L, Kuethe A M, (1930)"The measurement of fluctuations of air speed by the hot-wire anemometer" NACA Report 320.

Evans G V, (1967) " A study of diffusion in turbulent pipe flow" Transactions of the ASME, Journal of Basic Engineering (89) 624-632.

Hill P G, (1965) " Turbulent jets in ducted stream" Journal of Fluid Mechanics (22) 161-186.

Hinze J O, (1975) " Turbulence" 2nd Ed., McGraw-Hill, USA.

Holly F M Jr., Grace L Jr., (1972) "Model study of dense jet in flowing fluid" Journal of the Hydraulics Division, Proceeding of the ASCE (98) 1921-1933.

Konig O, Fiedler H E, (1991)" The structure of round turbulent jets in counterflow: a visualisation study" in "Advances in Turbulence" Johansson A V, Alfredsson P H (Eds.) Proceedings of the Third European Turbulence Conference Stockholm 1990, Springer-Verlag, Berlin, Germany.

Lam K M, (1991) " Penetration of a submerged round jet into a counter-flowing current ", Environmental Hydraulics, Proceeding of International Symposium on

Environmental Hydraulics, Lee and Cheung (Eds.), A. A. Balkema Publishers, Rotterdam, The Netherlands, 115-120.

Lam K M, Chan H C, (1995) " Investigation of turbulent jets issuing into a counter-flowing stream using digital image processing" Experiments in Fluids, 18(3), 210-212.

Lam K M, Chan H C, (1997) " Round jet in ambient counterflowing stream" Journal of Hydraulic Engineering 123, 895-902.

Laufer J, (1950) " Investigation of turbulent flow in a two - dimensional channel", NACA Technical Report No. 1053.

Laufer J, (1954) " The structure of turbulence in fully developed pipe flow" NACA Report No. 1174.

Morgan W D, Brinkworth B J, Evans G V, (1976)" Upstream penetration of an enclosed counterflowing jet" Ind. Eng. Chem., Fundam. (15) 2, 125-127.

Rajaratnam N, (1976) " Turbulent Jets" Elsevier Scientific Publishing Co., Amsterdam, The Netherlands.

Ramaprian B R, Chandrasekhara M S (1989) " Measurements in vertical plane turbulent plumes" Journal of Fluid Engineering Transaction of ASME (111) 69-77.

Robillard L, Ramamurthy A S, (1974) " Experimental investigation of the vortex street generated by a plane jet in counter flow" Journal of Fluid Engineering, ASME (96) 43-48.

Rodi W, Spalding D B, (1970) " A two-parameter model of turbulence and its application to free jets" Warme und Stoffubertragung (3) 85-95, Reprinted in " Numerical Prediction of Flow, Heat Transfer, Turbulence, and Combustion Selected Works of Professor D. Brian Spalding", (1983) Patankar S V, Pollard A, Singhal A K, Vanka S P EDs. 22-32, Pergamon Press, USA.

Schlichting H, Gersten K, (2000) " Boundary Layer Theory" Mayes K, Trans., Springer, Germany.

Sekundov A. N., (1969) "The propagation of a turbulent jet in an opposing stream" in "Turbulent Jets of Air, Plasma, and Real Gas" Abramovich G N (Ed.), Consultant Bureau, New York, USA.

Spalding D B, (1971) " Concentration fluctuation in a round turbulent free jet" Chemical engineering Science (26) 95-107, reprinted in " Numerical Prediction of Flow, Heat Transfer, Turbulence, and Combustion Selected Works of

Professor D. Brian Spalding", (1983) Patankar S V, Pollard A, Singhal A K, Vanka S P Eds. 41-53, Pergamon Press, USA.

Wilcox D C (1993)" Turbulence Modeling for CFD" DCW Industries Inc., La Canada, California, USA.

Wygnanski I, Fiedler H, (1969)"Some measurements in the self-preserving jet" Journal of Fluid Mechanics (38) 577-612.

Yoda M, Fiedler H E, (1996) "The round jet in a uniform counterflow: flow visualization and mean concentration measurement" Experiment in Fluids (21) 427-436.